Part 8
Appendices

Appendix A: Supplementary Material

A.1 Euler Angles and Frame Transformations

The orientation of a rigid object in three-dimensional space may be specified using three angles. There are different systems for defining the three orientational angles, which have advantages in different circumstances. The *Euler angles* are particularly useful in many NMR contexts.

A.1.1 Definition of the Euler angles

In this book I use the *zyz-convention* for the Euler angles. In this system, a general rotation in three-dimensional space is expressed as the product of three rotations: a rotation by an angle γ about the z-axis, a rotation by an angle β about the y-axis, and a rotation by an angle α about the z-axis again:

$$\widehat{R}(\alpha, \beta, \gamma) = \widehat{R}_z(\alpha)\widehat{R}_y(\beta)\widehat{R}_z(\gamma) \tag{A.1}$$

Note the right-to-left chronological order of the rotations on the right-hand side.

In this appendix, the symbol Ω denotes a set of three Euler angles: $\Omega = \{\alpha, \beta, \gamma\}$. A modified font distinguishes Ω from the frequency symbol Ω.

A.1.2 Euler rotations: first scheme

To see how the Euler angles are used, consider the L-shaped object shown below, which has an arbitrary orientation with respect to a Cartesian reference frame:

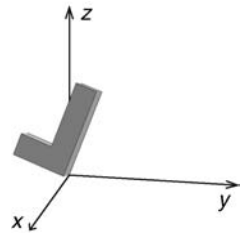

Figure A.1
An L-shaped object.

Spin Dynamics: Basics of Nuclear Magnetic Resonance, Second Edition Malcolm H. Levitt

The orientation of the object may be specified by providing the rotation $\widehat{R}(\alpha, \beta, \gamma)$ which turns the object so that its edges become parallel with the defined axis system. In the case above, the angles are $\alpha = \pi/5$, $\beta = \pi/8$, and $\gamma = \pi/3$. Figure A.2 shows how the object may be turned in three stages so that it becomes aligned with the reference frame:

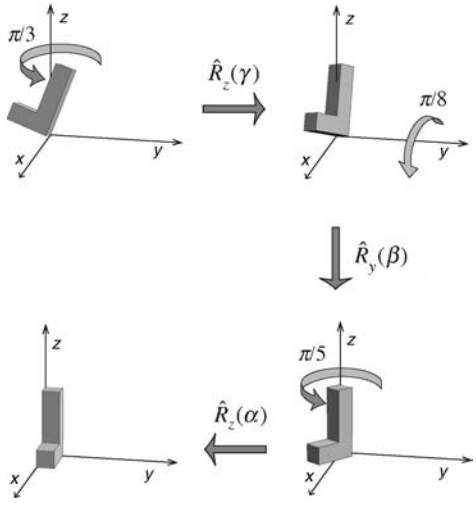

Figure A.2
Rotations around the reference frame axes.

Note the order of the rotations: since the rotation operator in Equation A.1 is applied from the *left*, the γ-rotation comes *first*.

A.1.3 Euler rotations: second scheme

The Euler rotations may also be formulated in a different way. Attach an axis system to the object, parallel to its edges:

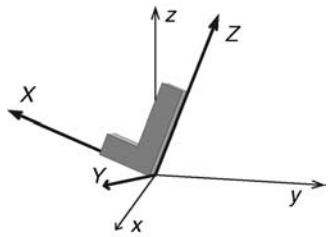

Figure A.3
An L-shaped object with a local axis system.

The attached axis system is shown in bold, and annotated by the upper-case letters $\{X, Y, Z\}$. Now execute the Euler rotations again, but this time (i) rotate *about the axes that are attached to the object itself* (instead of the reference-frame axes) and (ii) use the *opposite* order, i.e. first α, then β, then γ. The sequence of rotations is as follows:

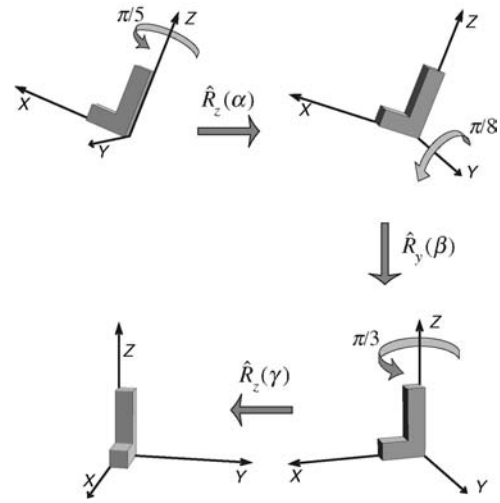

Figure A.4
Rotations around the local axes.

The final orientations in Figures A.2 and A.4 are identical, even though the intermediate positions are different! This equivalence may be expressed by the following equation:

$$\widehat{R}_z(\alpha)\widehat{R}_y(\beta)\widehat{R}_z(\gamma) = \widehat{R}_{Z''}(\gamma)\widehat{R}_{Y'}(\beta)\widehat{R}_Z(\alpha) \tag{A.2}$$

Here, $\widehat{R}_Z(\alpha)$ is a rotation around the Z-axis of the attached system, and $\widehat{R}_{Y'}(\beta)$ is a rotation around the Y-axis of the attached system, etc. The 'primed' notation $\widehat{R}_{Y'}(\beta)$ indicates that the central rotation occurs about a 'new' Y-axis that has *already* been transformed by the first $\widehat{R}_Z(\alpha)$ rotation. Similarly, the final $\widehat{R}_{Z''}(\gamma)$ rotation occurs about a 'new' Z-axis that has already been transformed by the first $\widehat{R}_Z(\alpha)$ rotation, and then by the second $\widehat{R}_{Y'}(\beta)$ rotation. As shown in Figure A.4, the rotation axes follow the object as it is rotated. The Euler angle β represents the angle between the initial and final z-axes.

Equation A.2 is a general result, independent of the values of the angles $\{\alpha, \beta, \gamma\}$.

The two different methods of performing the Euler rotations are equally valid, but the second way is often easier to visualize.

A.1.4 Euler rotation matrices

The Cartesian rotation matrix, written in terms of Euler angles, is as follows:

$$\mathcal{R}(\alpha, \beta, \gamma) = \begin{pmatrix} \cos\alpha\cos\beta\cos\gamma - \sin\alpha\sin\gamma & -\sin\alpha\cos\gamma - \cos\alpha\cos\beta\sin\gamma & \cos\alpha\sin\beta \\ \sin\alpha\cos\beta\cos\gamma + \cos\alpha\sin\gamma & \cos\alpha\cos\gamma - \sin\alpha\cos\beta\sin\gamma & \sin\alpha\sin\beta \\ -\sin\beta\cos\gamma & \sin\beta\sin\gamma & \cos\beta \end{pmatrix} \tag{A.3}$$

The inverse of $\mathcal{R}(\alpha, \beta, \gamma)$ is $\mathcal{R}(-\gamma, -\beta, -\alpha)$.

A.1.5 Reference-frame orientations

The Euler angles are particularly useful for defining the relative orientations of two different orthogonal axis systems. For example, consider two different orthogonal reference frames, A and B, defined by the sets of unit vectors $\{\mathbf{e}_x^{\mathrm{A}}, \mathbf{e}_y^{\mathrm{A}}, \mathbf{e}_z^{\mathrm{A}}\}$ and $\{\mathbf{e}_x^{\mathrm{B}}, \mathbf{e}_y^{\mathrm{B}}, \mathbf{e}_z^{\mathrm{B}}\}$. The set of Euler angles $\Omega^{\mathrm{BA}} = \{\alpha^{\mathrm{BA}}, \beta^{\mathrm{BA}}, \gamma^{\mathrm{BA}}\}$ may be used to specify the relative orientation of these two axis systems. The angles are defined in such a way that the

matrix $\mathcal{R}(\Omega^{BA}) = \mathcal{R}(\alpha^{BA}, \beta^{BA}, \gamma^{BA})$ transforms each of the A-system vectors into the corresponding B-system vector:

$$\mathcal{R}(\Omega^{BA}) \cdot \mathbf{e}_x^A = \mathbf{e}_x^B$$
$$\mathcal{R}(\Omega^{BA}) \cdot \mathbf{e}_y^A = \mathbf{e}_y^B$$
$$\mathcal{R}(\Omega^{BA}) \cdot \mathbf{e}_z^A = \mathbf{e}_z^B$$

where $\mathcal{R}$ is given in Equation A.3. For example, suppose that the 'B' axis system is the one in Figure A.1, and the 'A' axis system is the bold one in Figure A.3. In this case, the relative orientation of the two axis systems is described by the Euler angles $\Omega^{BA} = \{\alpha^{BA}, \beta^{BA}, \gamma^{BA}\} = \{\pi/5, \pi/8, \pi/3\}$. Figure A.2 and Figure A.4 show how the Euler rotations bring the two systems into coincidence.

The frame transformation may be performed the other way using:

$$\mathcal{R}(\Omega^{AB}) \cdot \mathbf{e}_x^B = \mathbf{e}_x^A$$
$$\mathcal{R}(\Omega^{AB}) \cdot \mathbf{e}_y^B = \mathbf{e}_y^A$$
$$\mathcal{R}(\Omega^{AB}) \cdot \mathbf{e}_z^B = \mathbf{e}_z^A$$

which implies $\mathcal{R}(\Omega^{AB}) = \mathcal{R}(\Omega^{BA})^{-1}$ and hence $\alpha^{AB} = -\gamma^{BA}$, $\beta^{AB} = -\beta^{BA}$ and $\gamma^{AB} = -\alpha^{BA}$.

A.1.6 Consecutive reference-frame transformations

The Euler angles are particularly powerful for handling consecutive reference-frame rotations. For example, consider a third reference frame C, defined by the set of unit vectors $\{\mathbf{e}_x^C, \mathbf{e}_y^C, \mathbf{e}_z^C\}$. If the relative orientation of C and B is specified by the Euler angles $\Omega^{CB} = \{\alpha^{CB}, \beta^{CB}, \gamma^{CB}\}$, and the relative orientation of B and A is specified by the Euler angles $\Omega^{BA} = \{\alpha^{BA}, \beta^{BA}, \gamma^{BA}\}$, then the relative orientation of C and A is specified by the Euler angles $\Omega^{CA} = \{\alpha^{CA}, \beta^{CA}, \gamma^{CA}\}$, where

$$\mathcal{R}(\Omega^{CA}) = \mathcal{R}(\Omega^{CB})\mathcal{R}(\Omega^{BA})$$

Note the 'chain rule' for the frame superscripts, which may be continued as desired:

$$\mathcal{R}(\Omega^{DA}) = \mathcal{R}(\Omega^{DC})\mathcal{R}(\Omega^{CB})\mathcal{R}(\Omega^{BA})$$

A.1.7 Passive rotations

The discussion above concentrated on the *active* manipulation of objects (including reference frames) by a series of Euler rotations. In the theory of NMR, it is often relevant to consider the *representations* of objects (such as vectors, tensors, etc.) *as seen from* different reference frames, which are themselves related by Euler rotations. This *passive* perspective is indicated by a subtle change of notation. The frame indices are reversed, and superscripts are changed into subscripts, i.e. $\Omega_{AB} = \Omega^{BA}$, implying $\alpha_{AB} = \alpha^{BA}$, $\beta_{AB} = \beta^{BA}$ and $\gamma_{AB} = \gamma^{BA}$.

For example, the matrix representations of the same tensor $\mathbf{T}$ in two different reference systems are related by

$$[\mathbf{T}]^B = \mathcal{R}(\Omega_{BA})\,[\mathbf{T}]^A\,\mathcal{R}(\Omega_{AB})$$

where

$$\mathcal{R}(\Omega_{BA}) = \mathcal{R}(\Omega_{AB})^{\dagger}$$

The arrangement of the 'passive subscripts' allows use of the chain rule for consecutive transformations; for example:

$$[\mathbf{T}]^C = \mathcal{R}(\Omega_{\mathrm{CB}})\mathcal{R}(\Omega_{\mathrm{BA}})\,[\mathbf{T}]^A\,\mathcal{R}(\Omega_{\mathrm{AB}})\mathcal{R}(\Omega_{\mathrm{BC}}) \tag{A.4}$$

The chains of frame labels may readily be followed inwards, allowing the transformations to be written down by inspection. The convenience of this chain property is lost if active notation is used in this context.

Note that an 'active' angle such as α^{BA} has exactly the same meaning as the 'passive' angle α_{AB} – the different notations are used purely for orthographic convenience, depending on whether the calculation involves the rotation of an object with respect to a fixed reference frame, or the appearance of a fixed object as seen from a rotated reference frame.

A.1.8 Tensor transformations

As one example of this technique, consider a chemical shift tensor $\boldsymbol{\delta}^j$ with principal components $\{\delta^j_{XX}, \delta^j_{YY}, \delta^j_{ZZ}\}$. When written in its principal axis frame, this tensor has a diagonal representation:

$$\left[\boldsymbol{\delta}^j\right]^P = \begin{pmatrix} \delta^j_{XX} & 0 & 0 \\ 0 & \delta^j_{YY} & 0 \\ 0 & 0 & \delta^j_{ZZ} \end{pmatrix}$$

Suppose, now, that a laboratory reference frame L is defined with the z-axis along the static magnetic field direction. The relative orientation of the principal axis frame of the chemical shift tensor at site I_j with respect to the laboratory frame L is specified using the Euler angle set $\Omega^{\mathrm{LP}}_{\mathrm{j}} = \{\alpha^{\mathrm{LP}}_{\mathrm{j}}, \beta^{\mathrm{LP}}_{\mathrm{j}}, \gamma^{\mathrm{LP}}_{\mathrm{j}}\}$ in active notation, or equivalently $\Omega^{\mathrm{j}}_{\mathrm{PL}} = \{\alpha^{\mathrm{j}}_{\mathrm{PL}}, \beta^{\mathrm{j}}_{\mathrm{PL}}, \gamma^{\mathrm{j}}_{\mathrm{PL}}\}$ in passive notation. The matrix representation of the tensor in the laboratory frame may be derived as follows:

$$\left[\boldsymbol{\delta}^j\right]^L = \mathcal{R}(\Omega^j_{\mathrm{LP}}) \cdot \left[\boldsymbol{\delta}^j\right]^P \cdot \mathcal{R}(\Omega^{\mathrm{j}}_{\mathrm{PL}}) \tag{A.5}$$

Note, again, the chaining of the frame labels in the passive convention.

Consider, now, the common situation in which the chemical shift tensor has a fixed orientation with respect to a molecule reference frame M, while the orientation of the molecule changes, relative to the external magnetic field. If the orientation of the chemical shift tensor principal axis system at site I_j with respect to the molecular reference frame is specified using the Euler angles $\Omega^{\mathrm{j}}_{\mathrm{PM}}$, and the orientation of the molecule with respect to the laboratory frame L is specified using the Euler angles Ω_{ML}, then the matrix $\mathcal{R}(\Omega^{\mathrm{j}}_{\mathrm{PL}})$ in Equation A.5 is given by

$$\mathcal{R}(\Omega^{\mathrm{j}}_{\mathrm{PL}}) = \mathcal{R}(\Omega^{\mathrm{j}}_{\mathrm{PM}})\mathcal{R}(\Omega_{\mathrm{ML}}) \tag{A.6}$$

The matrix $\mathcal{R}^j(\Theta)$ used in Section 9.1 should be identified with $\mathcal{R}(\Omega^{\mathrm{j}}_{\mathrm{PL}})$ in Equation A.6. The generic symbol Θ for the molecular orientation with respect to the static magnetic field, which is used throughout the book, should be identified with the Euler angle set Ω_{ML}.

For example, the term $R^j_{zX}(\Theta)$ in Equation 9.12 should be interpreted as follows:

$$\begin{aligned} R^j_{zX}(\Theta) &= R_{zx}(\Omega^{\mathrm{j}}_{\mathrm{PL}}) \\ &= R_{zx}(\Omega^{\mathrm{j}}_{\mathrm{PM}})R_{xx}(\Omega_{\mathrm{ML}}) + R_{zy}(\Omega^{\mathrm{j}}_{\mathrm{PM}})R_{yx}(\Omega_{\mathrm{ML}}) + R_{zz}(\Omega^{\mathrm{j}}_{\mathrm{PM}})R_{zx}(\Omega_{\mathrm{ML}}) \end{aligned}$$

where the rotation matrix elements are specified in terms of the Euler angles in Equation A.3.

A.1.9 Intermediate reference frames

The chain rule (Equation A.4) makes it straightforward to incorporate any number of intermediate reference frames between the principal axis system of a tensor and the laboratory frame. Multiple reference frames are often used in solid-state NMR. For example, in a rotating sample, it is often useful to define a reference frame R that is fixed to the sample holder and which rotates with respect to the laboratory frame. In this case, the transformation in Equation A.6 reads as follows:

$$\mathcal{R}(\Omega^{\mathrm{j}}_{\mathrm{PL}}(t)) = \mathcal{R}(\Omega^{\mathrm{j}}_{\mathrm{PM}})\mathcal{R}(\Omega_{\mathrm{MR}})\mathcal{R}(\Omega_{\mathrm{RL}}(t))$$

where $\Omega^{\mathrm{j}}_{\mathrm{PM}}$ defines the orientation of the CSA principal axis system with respect to the molecular reference frame, Ω_{MR} defines the orientation of the molecular reference frame with respect to the sample holder, and $\Omega_{\mathrm{RL}}(t)$ defines the orientation of the sample holder with respect to the magnetic field. In a rotating sample, the Euler angle α_{RL} is time dependent.

Any number of intermediate reference frames may be introduced this way, always chaining the frame labels to keep track of the successive rotations.

Further discussion is beyond the scope of this book, but the literature contains many examples of this technique. See, for example, A. Brinkmann and M. H. Levitt, *J. Chem. Phys.* **115**, 357–384 (2001).

A.2 Rotations and Cyclic Commutation

In this appendix, I prove that the cyclic commutation:

$$\left[\widehat{A}, \widehat{B}\right] = \mathrm{i}\widehat{C} \qquad \circlearrowleft \tag{A.7}$$

implies the property

$$\exp\{-\mathrm{i}\theta\widehat{A}\}\widehat{B}\exp\{+\mathrm{i}\theta\widehat{A}\} = \widehat{B}\cos\theta + \widehat{C}\sin\theta \tag{A.8}$$

which may be interpreted as a rotation of operator $\widehat{B}$ towards the operator $\widehat{C}$, around the $\widehat{A}$ axis, as discussed in Section 6.6.2.

For clarity, the following proof is conducted in terms of the specific case $\widehat{A} = \hat{I}_z$, $\widehat{B} = \hat{I}_x$, $\widehat{C} = \hat{I}_y$, which corresponds to the identity

$$\widehat{R}_z(\theta)\hat{I}_x\widehat{R}_z(-\theta) = \hat{I}_x\cos\theta + \hat{I}_y\sin\theta \tag{A.9}$$

However, since only cyclic commutation is used, the result applies to any three operators satisfying Equation A.7.

A number of proofs of Equation A.9 exist.[1] My personal favourite runs as follows. Consider the operator $\hat{I}^-$, defined as usual:

$$\hat{I}^- = \hat{I}_x - \mathrm{i}\hat{I}_y$$

From the cyclic commutation relationships, the commutator of $\hat{I}_z$ and $\hat{I}^-$ is given by

$$\left[\hat{I}_z, \hat{I}^-\right] = \left[\hat{I}_z, \hat{I}_x\right] - \mathrm{i}\left[\hat{I}_z, \hat{I}_y\right] = \mathrm{i}\hat{I}_y - \mathrm{i}(-\mathrm{i}\hat{I}_x) = -\hat{I}^-$$

Hence, we have

$$\hat{I}_z\hat{I}^- - \hat{I}^-\hat{I}_z = -\hat{I}^-$$

or equivalently

$$\hat{I}_z\hat{I}^- = \hat{I}^-\hat{I}_z - \hat{I}^- = \hat{I}^-(\hat{I}_z - \widehat{1}) \tag{A.10}$$

Now multiply both sides of this equation on the left by $\hat{I}_z$. We get

$$\hat{I}_z^2\hat{I}^- = \hat{I}_z\hat{I}^-(\hat{I}_z - \widehat{1})$$

If the identity shown in Equation A.10 is substituted in on the right-hand side, we get

$$\hat{I}_z^2\hat{I}^- = \hat{I}^-(\hat{I}_z - \widehat{1})(\hat{I}_z - \widehat{1}) = \hat{I}^-(\hat{I}_z - \widehat{1})^2$$

This may be repeated any number of times to generate the relationship

$$\hat{I}_z^n\hat{I}^- = \hat{I}^-(\hat{I}_z - \widehat{1})^n$$

where n is a positive integer. The following result may, therefore, be established:

$$\begin{aligned}\exp\{-\mathrm{i}\theta\hat{I}_z\}\hat{I}^- &= \sum_{n=0}^{\infty}\frac{(-\mathrm{i}\theta)^n}{n!}\hat{I}_z^n\hat{I}^- \\ &= \hat{I}^-\sum_{n=0}^{\infty}\frac{(-\mathrm{i}\theta)^n}{n!}(\hat{I}_z - \widehat{1})^n \\ &= \hat{I}^-\exp\{-\mathrm{i}\theta(\hat{I}_z - \widehat{1})\}\end{aligned}$$

Since the unity operator commutes with all other operators, this may be written as

$$\exp\{-\mathrm{i}\theta\hat{I}_z\}\hat{I}^- = \hat{I}^-\exp\{-\mathrm{i}\theta\hat{I}_z\}\exp\{\mathrm{i}\theta\widehat{1}\}$$

Now, since $\widehat{1}^n = \widehat{1}$ for all n, we have

$$\exp\{\mathrm{i}\theta\widehat{1}\} = \mathrm{e}^{\mathrm{i}\theta}\widehat{1}$$

Therefore:

$$\exp\{-\mathrm{i}\theta\hat{I}_z\}\hat{I}^- = \mathrm{e}^{\mathrm{i}\theta}\hat{I}^-\exp\{-\mathrm{i}\theta\hat{I}_z\}$$

This equation may be multiplied from the right by $\exp\{+\mathrm{i}\theta\hat{I}_z\}$ to get

$$\exp\{-\mathrm{i}\theta\hat{I}_z\}\hat{I}^-\exp\{+\mathrm{i}\theta\hat{I}_z\} = \mathrm{e}^{\mathrm{i}\theta}\hat{I}^-$$

Similar arguments may be used to derive an analogous relationship for $\hat{I}^+$:

$$\exp\{-\mathrm{i}\theta\hat{I}_z\}\hat{I}^+\exp\{+\mathrm{i}\theta\hat{I}_z\} = \mathrm{e}^{-\mathrm{i}\theta}\hat{I}^+$$

These two equations may be added together to generate the desired result:

$$\exp\{-\mathrm{i}\theta\hat{I}_z\}\hat{I}_x\exp\{+\mathrm{i}\theta\hat{I}_z\} = \frac{1}{2}\mathrm{e}^{\mathrm{i}\theta}\hat{I}^- + \frac{1}{2}\mathrm{e}^{-\mathrm{i}\theta}\hat{I}^+ = \hat{I}_x\cos\theta + \hat{I}_y\sin\theta$$

A.3 Rotation Sandwiches

In this appendix, I prove the rotation sandwich property:

$$\widehat{R}_x(\theta)\widehat{R}_y(\beta)\widehat{R}_x(-\theta) = \exp\{-\mathrm{i}\beta\left(\hat{I}_y\cos\theta + \hat{I}_z\sin\theta\right)\} \qquad \text{(A.11)}$$

For clarity, the equations are written using spin angular momentum operators, but the properties are general for any set of three cyclically commuting operators.

The sandwich relationship for angular momentum operators (Equation A.8) may be used to write the right-hand side of Equation A.11 as

$$\exp\{-\mathrm{i}\beta\left(\hat{I}_y\cos\theta+\hat{I}_z\sin\theta\right)\}=\exp\{-\mathrm{i}\beta\widehat{R}_x(\theta)\hat{I}_y\widehat{R}_x(-\theta)\}$$

The exponential may be expanded as an infinite series:

$$\exp\{-\mathrm{i}\beta\widehat{R}_x(\theta)\hat{I}_y\widehat{R}_x(-\theta)\}=\widehat{1}+(-\mathrm{i}\beta\widehat{R}_x(\theta)\hat{I}_y\widehat{R}_x(-\theta))+\frac{(-\mathrm{i}\beta)^2}{2!}[\widehat{R}_x(\theta)\hat{I}_y\widehat{R}_x(-\theta)]^2+\frac{(-\mathrm{i}\beta)^3}{3!}[\widehat{R}_x(\theta)\hat{I}_y\widehat{R}_x(-\theta)]^3+\ldots$$

Consider the third term. We find

$$[\widehat{R}_x(\theta)\hat{I}_y\widehat{R}_x(-\theta)]^2=\widehat{R}_x(\theta)\hat{I}_y\widehat{R}_x(-\theta)\widehat{R}_x(\theta)\hat{I}_y\widehat{R}_x(-\theta)=\widehat{R}_x(\theta)\hat{I}_y\hat{I}_y\widehat{R}_x(-\theta)$$

since the opposite rotation operators in the middle of the expression annihilate. The same happens for all the other terms. Even the unity operator at the beginning of the series may be written as

$$\widehat{1}=\widehat{R}_x(\theta)\widehat{1}\widehat{R}_x(-\theta)$$

The whole expression is therefore

$$\begin{aligned}\exp\{-\mathrm{i}\beta\widehat{R}_x(\theta)\hat{I}_y\widehat{R}_x(-\theta)\}&=\widehat{R}_x(\theta)\left\{\widehat{1}+(-\mathrm{i}\beta\hat{I}_y)+\frac{(-\mathrm{i}\beta)^2}{2!}\hat{I}_y\hat{I}_y+\ldots\right\}\widehat{R}_x(-\theta)\\&=\widehat{R}_x(\theta)\exp\{-\mathrm{i}\beta\hat{I}_y\}\widehat{R}_x(-\theta)\\&=\widehat{R}_x(\theta)\widehat{R}_y(\beta)\widehat{R}_x(-\theta)\end{aligned}$$

which corresponds to the left-hand side of Equation A.11.

Numerous other rotation sandwich relationships may be generated by cyclically permuting the operators.

A.4 Spin-1/2 Rotation Operators

The operator for a rotation about the x-axis through the angle β is given by

$$\widehat{R}_x(\beta)=\exp\{-\mathrm{i}\beta\hat{I}_x\}$$

The matrix representation of this operator is not easy to calculate, since $\hat{I}_x$ is not diagonal. One way is to use the techniques in Section 6.5.8. An alternative method is given here.

The operator $\exp\{-\mathrm{i}\beta\hat{I}_x\}$ may be understood as the infinite series

$$\exp\{-\mathrm{i}\beta\hat{I}_x\}=\widehat{1}+(-\mathrm{i}\beta\hat{I}_x)+\frac{(-\mathrm{i}\beta)^2}{2!}\hat{I}_x\hat{I}_x+\frac{(-\mathrm{i}\beta)^3}{3!}\hat{I}_x\hat{I}_x\hat{I}_x+\ldots \tag{A.12}$$

The sum in Equation A.12 may be sorted into two 'sub-sums', one involving even powers and one involving odd powers of $2\hat{I}_x$ (we will see why we need the factor of two in a moment):

$$\exp\{-\mathrm{i}\beta\hat{I}_x\}=\widehat{1}-\frac{1}{2!}\left(\frac{1}{2}\beta\right)^2(2\hat{I}_x)^2+\frac{1}{4!}\left(\frac{1}{2}\beta\right)^4(2\hat{I}_x)^4+\ldots-\mathrm{i}\left\{\left(\frac{1}{2}\beta\right)(2\hat{I}_x)-\frac{1}{3!}\left(\frac{1}{2}\beta\right)^3(2\hat{I}_x)^3+\frac{1}{5!}\left(\frac{1}{2}\beta\right)^5(2\hat{I}_x)^5+\ldots\right\}$$

Now note the following property of the spin-1/2 matrix representation of $2\hat{I}_x$:

$$(2\hat{I}_x)^2 = \left\{2\frac{1}{2}\begin{pmatrix}0&1\\1&0\end{pmatrix}\right\}^2 = \begin{pmatrix}0&1\\1&0\end{pmatrix}\begin{pmatrix}0&1\\1&0\end{pmatrix} = \begin{pmatrix}1&0\\0&1\end{pmatrix} = \widehat{1}$$

This means that any *even* power of $2\hat{I}_x$ has the same spin-1/2 matrix representation as unity, and any *odd* power of $2\hat{I}_x$ has the same spin-1/2 matrix representation as $2\hat{I}_x$ itself. The series, therefore, may be written as

$$\exp\{-\mathrm{i}\beta\hat{I}_x\} = \widehat{1}\left\{1 - \frac{1}{2!}\left(\frac{1}{2}\beta\right)^2 + \frac{1}{4!}\left(\frac{1}{2}\beta\right)^4 + \ldots\right\} - \mathrm{i}2\hat{I}_x\left\{\left(\frac{1}{2}\beta\right) - \frac{1}{3!}\left(\frac{1}{2}\beta\right)^3 + \frac{1}{5!}\left(\frac{1}{2}\beta\right)^5 + \ldots\right\}$$

The individual series expansions may be identified as equal to the sine and cosine of half the angle; so, we can write

$$\widehat{R}_x(\beta) = \exp\{-\mathrm{i}\beta\hat{I}_x\} = \widehat{1}\cos\frac{1}{2}\beta - \mathrm{i}2\hat{I}_x\sin\frac{1}{2}\beta \qquad (\text{for } I = 1/2) \tag{A.13}$$

⚠This relationship applies only to the spin-1/2 matrix representations of $\widehat{R}_x(\beta)$ and $\hat{I}_x$, and not to the operators themselves.

The spin-1/2 matrix representation of the operator $\widehat{R}_x(\beta)$ is therefore

$$\widehat{R}_x(\beta) = \begin{pmatrix}\cos\frac{1}{2}\beta & -\mathrm{i}\sin\frac{1}{2}\beta\\ -\mathrm{i}\sin\frac{1}{2}\beta & \cos\frac{1}{2}\beta\end{pmatrix} \tag{A.14}$$

Similar arguments may be used to obtain the spin-1/2 matrix representation of the operator $\widehat{R}_y(\beta)$:

$$\widehat{R}_y(\beta) = \begin{pmatrix}\cos\frac{1}{2}\beta & -\sin\frac{1}{2}\beta\\ \sin\frac{1}{2}\beta & \cos\frac{1}{2}\beta\end{pmatrix} \tag{A.15}$$

The matrix representation of the operator $\widehat{R}_z(\beta)$ is obtained more easily, since $\hat{I}_z$ is diagonal in the Zeeman basis:

$$\widehat{R}_z(\beta) = \begin{pmatrix}\exp\{-\mathrm{i}\frac{1}{2}\beta\} & 0\\ 0 & \exp\{+\mathrm{i}\frac{1}{2}\beta\}\end{pmatrix} \tag{A.16}$$

A.5 Quadrature Detection and Spin Coherences

The NMR signal is generated by electromagnetic induction of a current in the coil, produced by the precessing nuclear spin magnetization.

In this appendix, I use a notational distinction between the laboratory frame and the rotating-frame coherences. Rotating-frame coherences are denoted by a tilde.

Suppose that the coil is aligned along the x-axis of the laboratory frame. The nuclear spin magnetization along this axis is given by

$$M_x \sim \langle \hat{I}_x \rangle = \mathrm{Tr}\{\hat{\rho}\hat{I}_x\} \sim \rho_{\boxed{-}} + \rho_{\boxed{+}} \tag{A.17}$$

where $\rho_{\boxed{-}}$ and $\rho_{\boxed{+}}$ are laboratory-frame (± 1)-quantum coherences. Both the ($+1$)- and (-1)-quantum coherences in the laboratory frame contribute to the transverse nuclear spin magnetization.

The voltage generated in the coil is proportional to the time derivative of the nuclear spin magnetization in the coil direction. Assuming that the FID is simply proportional to this voltage, and ignoring constant instrumental phase shifts, we obtain the following:

$$s_{\mathrm{FID}}(t) \sim \frac{\mathrm{d}}{\mathrm{d}t}\rho_{\boxed{-}}(t) + \frac{\mathrm{d}}{\mathrm{d}t}\rho_{\boxed{+}}(t)$$

The coherences are time dependent through the Schrödinger equation. Their equation of motion in the laboratory frame is

$$\rho_{\boxed{-}}(t) = \rho_{\boxed{-}}(0)\exp\{(\mathrm{i}\omega^0 - \lambda)t\}$$
$$\rho_{\boxed{+}}(t) = \rho_{\boxed{+}}(0)\exp\{(-\mathrm{i}\omega^0 - \lambda)t\}$$

and hence the FID is given by

$$s_{\mathrm{FID}}(t) \sim \mathrm{i}\omega^0\rho_{\boxed{-}}(t) - \mathrm{i}\omega^0\rho_{\boxed{+}}(t)$$

since ω^0 is much larger than λ. The constant factor ω^0 is now omitted, after noting that the amplitude of the signal is proportional to the Larmor frequency (this is one of the reasons that high fields and large gyromagnetic ratios are favourable for NMR experiments; see Section 16.3.1).

We now assume that this signal is amplified and passed into the quadrature receiver without any substantial change.

A block diagram of a traditional quadrature receiver is shown below:

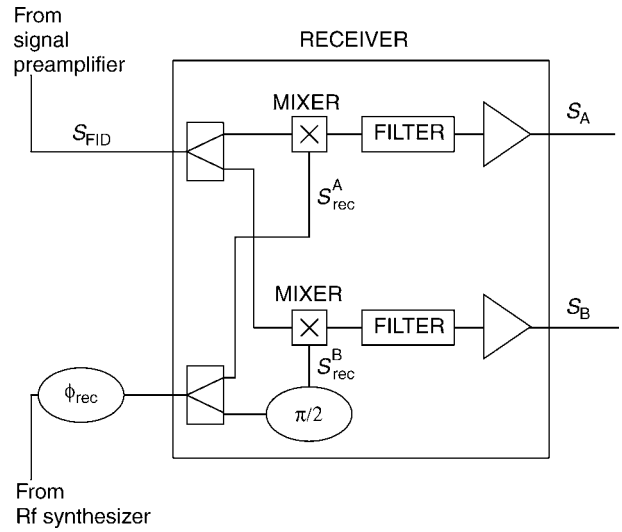

Figure A.5
Schematic of a quadrature receiver.

Modern equipment often uses a more sophisticated handling of the signal, but the basic principles are the same.

The NMR signal enters from the top left, whereas the receiver reference signal, given by

$$s_{\text{rec}}(t) \sim \cos(\omega_{\text{ref}} t + \phi^{\text{rf}}_{\text{rec}})$$

enters from the bottom left. The round symbol indicates the possibility of giving this reference signal an r.f. phase shift $\phi^{\text{rf}}_{\text{rec}}$.

The receiver reference signal is split into two paths. In the top path, the reference signal is unchanged:

$$s^{\text{A}}_{\text{rec}}(t) \sim \cos(\omega_{\text{ref}} t + \phi^{\text{rf}}_{\text{rec}})$$

In the lower path, the reference signal is given an additional phase shift of $\pi/2$:

$$s^{\text{B}}_{\text{rec}}(t) \sim \cos(\omega_{\text{ref}} t + \phi^{\text{rf}}_{\text{rec}} + \pi/2)$$

The NMR signal is also split into two paths. Consider the upper path first.

The NMR signal s_{FID} and the reference signal $s^{\text{A}}_{\text{rec}}$ both enter an electronic device called a *mixer*. This simply multiplies the two signals together. The signal exiting the upper mixer is therefore

$$s_{\text{FID}}(t) s^{\text{A}}_{\text{rec}}(t) \sim \text{i}\left(\rho_{\boxed{-}}(t) - \rho_{\boxed{+}}(t)\right) \cos(\omega_{\text{ref}} t + \phi^{\text{rf}}_{\text{rec}})$$

which evaluates to

$$\begin{aligned} s_{\text{FID}}(t) s^{\text{A}}_{\text{rec}}(t) \sim\ & \frac{1}{2}\text{i}\rho_{\boxed{-}}(0) \exp\{\text{i}[(\omega^0 + \omega_{\text{ref}})t + \phi^{\text{rf}}_{\text{rec}}]\}\, \text{e}^{-\lambda t} \\ & + \frac{1}{2}\text{i}\rho_{\boxed{-}}(0) \exp\{\text{i}[(\omega^0 - \omega_{\text{ref}})t - \phi^{\text{rf}}_{\text{rec}}]\}\, \text{e}^{-\lambda t} \\ & - \frac{1}{2}\text{i}\rho_{\boxed{+}}(0) \exp\{\text{i}[-(\omega^0 - \omega_{\text{ref}})t + \phi^{\text{rf}}_{\text{rec}}]\}\, \text{e}^{-\lambda t} \\ & - \frac{1}{2}\text{i}\rho_{\boxed{+}}(0) \exp\{\text{i}[-(\omega^0 + \omega_{\text{ref}})t - \phi^{\text{rf}}_{\text{rec}}]\}\, \text{e}^{-\lambda t} \end{aligned}$$

This signal now passes into a low-pass r.f. filter, which removes the high-frequency components. In the present case, the filter removes the components oscillating at $\omega^0 + \omega_{\text{ref}}$, and it retains those components

oscillating at the low frequency $\Omega^0 = \omega^0 - \omega_{\mathrm{ref}}$. The signal s_{A} emerging from the filter is therefore

$$\begin{aligned} s_{\mathrm{A}}(t) \;\sim\; & \frac{1}{2}\mathrm{i}\rho_{\boxed{-}}(0)\exp\{\mathrm{i}(\Omega^0 t - \phi_{\mathrm{rec}}^{\mathrm{rf}})\}\,\mathrm{e}^{-\lambda t} \\ & -\frac{1}{2}\mathrm{i}\rho_{\boxed{+}}(0)\exp\{\mathrm{i}(-\Omega^0 t + \phi_{\mathrm{rec}}^{\mathrm{rf}})\}\,\mathrm{e}^{-\lambda t} \end{aligned}$$

From the relationship between laboratory frame and rotating-frame coherences (Equation 11.21), this equation may be written as

$$\begin{aligned} s_{\mathrm{A}}(t) \;\sim\; & \frac{1}{2}\mathrm{i}\tilde{\rho}_{\boxed{-}}(0)\exp\{\mathrm{i}(\Omega^0 t - \phi_{\mathrm{rec}}^{\mathrm{rf}} + \phi_{\mathrm{ref}})\}\,\mathrm{e}^{-\lambda t} \\ & -\frac{1}{2}\mathrm{i}\tilde{\rho}_{\boxed{+}}(0)\exp\{\mathrm{i}(-\Omega^0 t + \phi_{\mathrm{rec}}^{\mathrm{rf}} - \phi_{\mathrm{ref}})\}\,\mathrm{e}^{-\lambda t} \end{aligned} \tag{A.18}$$

The term ϕ_{ref} represents the angle of the rotating frame with respect to the laboratory frame at the time origin $t = 0$ (see Section 10.6).

The equation for the precession of the rotating-frame coherences (Equation 11.39) allows the above equation to be simplified:

$$s_{\mathrm{A}}(t) \sim \frac{1}{2}\mathrm{i}\tilde{\rho}_{\boxed{-}}(t)\exp\{-\mathrm{i}(\phi_{\mathrm{rec}}^{\mathrm{rf}} - \phi_{\mathrm{ref}})\} - \frac{1}{2}\mathrm{i}\tilde{\rho}_{\boxed{+}}(t)\exp\{\mathrm{i}(\phi_{\mathrm{rec}}^{\mathrm{rf}} - \phi_{\mathrm{ref}})\}$$

The same arguments may be repeated to obtain the filtered signal emerging from the second signal path in the receiver:

$$s_{\mathrm{B}}(t) \sim \frac{1}{2}\tilde{\rho}_{\boxed{-}}(t)\exp\{-\mathrm{i}(\phi_{\mathrm{rec}}^{\mathrm{rf}} - \phi_{\mathrm{ref}})\} + \frac{1}{2}\tilde{\rho}_{\boxed{+}}(t)\exp\{\mathrm{i}(\phi_{\mathrm{rec}}^{\mathrm{rf}} - \phi_{\mathrm{ref}})\}$$

These signals are treated as two components of one complex signal:

$$s(t) = s_{\mathrm{A}}(t) + \mathrm{i}s_{\mathrm{B}}(t)$$

This evaluates to

$$s(t) \sim \mathrm{i}\tilde{\rho}_{\boxed{-}}(t)\exp\{-\mathrm{i}(\phi_{\mathrm{rec}}^{\mathrm{rf}} - \phi_{\mathrm{ref}})\}$$

which only contains contributions from the rotating-frame (-1)-quantum coherence. The $(+1)$-quantum coherence contribution has disappeared.

In addition, a phase shift ϕ_{dig} is sometimes imposed after digitization of the signal. If this is included, we get

$$s(t) \sim \mathrm{i}\tilde{\rho}_{\boxed{-}}(t)\exp\{-\mathrm{i}(\phi_{\mathrm{rec}}^{\mathrm{rf}} + \phi_{\mathrm{dig}} - \phi_{\mathrm{ref}})\}$$

It is possible to ignore the constant phase ϕ_{ref}, since there are many other instrumental sources of a constant phase shift, and the spectral phase is adjusted anyway after FT using the phase correction parameter $\phi_{\mathrm{corr}}^{(0)}$ (see Section 5.8.5). If the frame phase shift ϕ_{ref} is removed, and numerical factors adjusted for convenience, then we get

$$s(t) \sim 2\mathrm{i}\tilde{\rho}_{\boxed{-}}(t)\exp\{-\mathrm{i}(\phi_{\mathrm{rec}}^{\mathrm{rf}} + \phi_{\mathrm{dig}})\}$$

The r.f. receiver reference phase and post-digitization phase shift may be combined to give an overall receiver phase:

$$\phi_{\mathrm{rec}} = \phi_{\mathrm{rec}}^{\mathrm{rf}} + \phi_{\mathrm{dig}}$$

This gives the following expression for the quadrature signal:

$$s(t) \sim 2\mathrm{i}\tilde{\rho}_{\boxed{-}}(t)\exp\{-\mathrm{i}\phi_{\mathrm{rec}}\}$$

which is used in the main text.

A.6 Secular Approximation

The secular approximation concerns the case where the Hamiltonian is the sum of two terms:

$$\widehat{\mathcal{H}} = \widehat{A} + \widehat{B}$$

where $\widehat{A}$ is a 'large' operator and $\widehat{B}$ is a 'small' operator. In the following discussion, both $\widehat{A}$ and $\widehat{B}$ are considered to be hermitian.

Since $\widehat{A}$ is hermitian, it is possible to form an orthogonal basis set from the eigenvectors $|n\rangle$ of $\widehat{A}$:

$$\widehat{A}|n\rangle = a_n|n\rangle$$

where a_n are the eigenvalues. Suppose that the eigenvalues of $\widehat{A}$ form the following pattern:

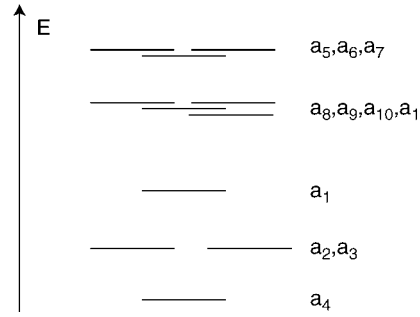

Figure A.6
Eigenvalues of the operator $\widehat{A}$.

The second and third eigenvalues are degenerate, the fifth, sixth and seventh eigenvalues form one near-degenerate group, and the eighth, ninth, tenth and eleventh eigenvalues form a second near-degenerate group.

If $\widehat{B}$ does not commute with $\widehat{A}$, then the matrix representation of $\widehat{B}$ in the eigenbasis of $\widehat{A}$ has finite elements everywhere, in general:

$$\begin{pmatrix}
\bullet & \bullet & \bullet & \bullet & \bullet & \bullet & \bullet & \bullet & \bullet & \bullet & \bullet & \cdots \\
\bullet & \bullet & \bullet & \bullet & \bullet & \bullet & \bullet & \bullet & \bullet & \bullet & \bullet & \cdots \\
\bullet & \bullet & \bullet & \bullet & \bullet & \bullet & \bullet & \bullet & \bullet & \bullet & \bullet & \cdots \\
\bullet & \bullet & \bullet & \bullet & \bullet & \bullet & \bullet & \bullet & \bullet & \bullet & \bullet & \cdots \\
\bullet & \bullet & \bullet & \bullet & \bullet & \bullet & \bullet & \bullet & \bullet & \bullet & \bullet & \cdots \\
\bullet & \bullet & \bullet & \bullet & \bullet & \bullet & \bullet & \bullet & \bullet & \bullet & \bullet & \cdots \\
\bullet & \bullet & \bullet & \bullet & \bullet & \bullet & \bullet & \bullet & \bullet & \bullet & \bullet & \cdots \\
\bullet & \bullet & \bullet & \bullet & \bullet & \bullet & \bullet & \bullet & \bullet & \bullet & \bullet & \cdots \\
\bullet & \bullet & \bullet & \bullet & \bullet & \bullet & \bullet & \bullet & \bullet & \bullet & \bullet & \cdots \\
\bullet & \bullet & \bullet & \bullet & \bullet & \bullet & \bullet & \bullet & \bullet & \bullet & \bullet & \cdots \\
\bullet & \bullet & \bullet & \bullet & \bullet & \bullet & \bullet & \bullet & \bullet & \bullet & \bullet & \cdots \\
\vdots & \vdots & \vdots & \vdots & \vdots & \vdots & \vdots & \vdots & \vdots & \vdots & \vdots & \ddots
\end{pmatrix}$$

The *secular approximation* for $\widehat{B}$ takes only the *block diagonal* form of this matrix:

$$\widehat{B}^0 = \begin{pmatrix} \bullet & 0 & 0 & 0 & 0 & 0 & 0 & 0 & 0 & 0 & 0 & \cdots \\ 0 & \bullet & \bullet & 0 & 0 & 0 & 0 & 0 & 0 & 0 & 0 & \cdots \\ 0 & \bullet & \bullet & 0 & 0 & 0 & 0 & 0 & 0 & 0 & 0 & \cdots \\ 0 & 0 & 0 & \bullet & 0 & 0 & 0 & 0 & 0 & 0 & 0 & \cdots \\ 0 & 0 & 0 & 0 & \bullet & \bullet & \bullet & 0 & 0 & 0 & 0 & \cdots \\ 0 & 0 & 0 & 0 & \bullet & \bullet & \bullet & 0 & 0 & 0 & 0 & \cdots \\ 0 & 0 & 0 & 0 & \bullet & \bullet & \bullet & 0 & 0 & 0 & 0 & \cdots \\ 0 & 0 & 0 & 0 & 0 & 0 & 0 & \bullet & \bullet & \bullet & \bullet & \cdots \\ 0 & 0 & 0 & 0 & 0 & 0 & 0 & \bullet & \bullet & \bullet & \bullet & \cdots \\ 0 & 0 & 0 & 0 & 0 & 0 & 0 & \bullet & \bullet & \bullet & \bullet & \cdots \\ 0 & 0 & 0 & 0 & 0 & 0 & 0 & \bullet & \bullet & \bullet & \bullet & \cdots \\ \vdots & \vdots & \vdots & \vdots & \vdots & \vdots & \vdots & \vdots & \vdots & \vdots & \vdots & \ddots \end{pmatrix} \tag{A.19}$$

where the blocks are formed by the pattern of degenerate or near-degenerate eigenvalues of $\widehat{A}$.

Another way of writing the secular approximation for $\widehat{B}$ is

$$\widehat{B}^0 = \sum_n b_{nn}|n\rangle\langle n| + {\sum_{m\neq n}}' b_{mn}|m\rangle\langle n| \tag{A.20}$$

where $|n\rangle$ are the eigenfunctions of $\widehat{A}$ and $b_{mn} = \langle m|\widehat{B}|n\rangle$ is a matrix element of $\widehat{B}$ in the eigenbase of $\widehat{A}$. The 'primed' summation only includes terms that 'connect' degenerate or near-degenerate eigenstates of $\widehat{A}$.

How 'near' does 'near-degenerate' have to be? Strictly, the summation in Equation A.20 omits terms for which the following inequality holds:

$$|b_{mn}| << |a_m - a_n| \tag{A.21}$$

A matrix element of $\widehat{B}$ may be dropped if its magnitude is small compared with the corresponding difference in the eigenvalues of $\widehat{A}$.

The secular Hamiltonian $\widehat{B}^0$ has the block-diagonal matrix representation given in Equation A.19. In general, $\widehat{B}^0$ does not commute with $\widehat{A}$, since the matrix representation in Equation A.19 may have off-diagonal elements connecting eigenstates of $\widehat{A}$ that are not *exactly* degenerate (contrast the discussion in Section 6.3.6).

The consequences of the secular approximation are best illustrated by specific examples.

Example 1. Chemical shift interaction of spin-1/2

Consider a single spin-1/2, with the following Hamiltonian terms:

$$\widehat{A} = \omega^0 \hat{I}_z$$
$$\widehat{B} = \omega_x \hat{I}_x + \omega_z \hat{I}_z$$

The term $\widehat{A}$ represents the interaction of the spin with a field along the z-axis, and $\widehat{B}$ represents the interaction of the spin with a small additional field, with a longitudinal component proportional to ω_z and a transverse component proportional to ω_x. The terms ω_x and ω_z are assumed to be much smaller than ω^0. This situation resembles the full form of the chemical shift interaction, given in Equation 9.11.

The eigenbasis of $\widehat{A}$ is defined by the two kets $|1\rangle = |+1/2\rangle$ and $|2\rangle = |-1/2\rangle$:

$$\widehat{A}|1\rangle = a_1|1\rangle \qquad \widehat{A}|2\rangle = a_2|2\rangle$$

with eigenvalues

$$a_1 = +\frac{1}{2}\omega^0 \qquad a_2 = -\frac{1}{2}\omega^0$$

The matrix representation of $\widehat{B}$ in this basis is

$$\widehat{B} = \frac{1}{2}\begin{pmatrix} \omega_z & \omega_x \\ \omega_x & -\omega_z \end{pmatrix}$$

The secular approximation for $\widehat{B}$, therefore, has a matrix representation given by

$$\widehat{B}^0 = \frac{1}{2}\begin{pmatrix} \omega_z & 0 \\ 0 & -\omega_z \end{pmatrix}$$

since the 'off-diagonal' elements ω_x connect eigenstates of $\widehat{A}$ with non-degenerate eigenvalues $\pm\frac{1}{2}\omega^0$. The secular approximation for $\widehat{B}$ is therefore

$$\widehat{B}^0 = \omega_z \hat{I}_z$$

which represents the interaction of the spin with only the longitudinal part of the additional field, as in Equation 9.13.

Example 2. Two spins-1/2

In a second example, consider the case of two spins-1/2 I_1 and I_2, with Larmor frequencies ω_1^0 and ω_2^0, a J-coupling J_{12}, and a secular dipole–dipole coupling d_{12}, as discussed in Chapter 14. The spin Hamiltonian may be written as $\widehat{\mathcal{H}} = \widehat{\mathcal{H}}_{\mathrm{A}}^0 + \widehat{\mathcal{H}}_{\mathrm{B}}^0$, where the matrix representations of the two parts of the Hamiltonian are given by Equations 14.7 and 14.8, in the Zeeman product basis.

The Hamiltonian $\widehat{\mathcal{H}}_{\mathrm{B}}^0$ is off-diagonal in the Zeeman product basis. The secular approximation allows $\widehat{\mathcal{H}}_{\mathrm{B}}^0$ to be omitted, providing that the off-diagonal elements of $\widehat{\mathcal{H}}_{\mathrm{B}}^0$ are much smaller than the differences in the connected diagonal elements of $\widehat{\mathcal{H}}_{\mathrm{A}}^0$.

Since the difference between the diagonal eigenvalues in rows 2 and 3 is equal to $\omega_1^0 - \omega_2^0$, and the off-diagonal elements are both equal to $\frac{1}{2}\omega_{12}^{\mathrm{B}} = \pi J_{12} - \frac{1}{2}d_{12}$, the off-diagonal part of $\widehat{B}$ may be ignored if the condition

$$|\omega_1^0 - \omega_2^0| >> |\pi J_{12} - \frac{1}{2}d_{12}| \tag{A.22}$$

is satisfied. In an isotropic phase, this reduces to the condition in Equation 14.19.

Equation A.22 is always valid for the coupling between nuclei of different isotopic types, since the difference in Larmor frequency is very large in that case.

⚠ The secular approximation shown in Equation A.20 is a result of *time-independent* perturbation theory. It must, therefore, be applied with caution to *time-dependent* situations, which are common in NMR. In general, the off-diagonal element b_{mn} may be ignored only if Equation A.21 is satisfied *and* if b_{mn} has a time dependence that is slow compared with the difference in eigenvalues $|a_m - a_n|$. For example, the homonuclear weak-coupling approximation breaks down if sufficiently rapid r.f. pulse sequences are applied (see Section 18.14 and Appendix A.10).

A.7 Quadrupolar Interaction

A.7.1 Full quadrupolar interaction

The spin Hamiltonian for the full electric quadrupolar interaction of spin I is given by (see *Further Reading*)

$$\widehat{\mathcal{H}}_Q^{\text{full}} = \frac{eQ}{2I(2I-1)\hbar}\hat{\mathbf{I}}.\mathbf{V}.\hat{\mathbf{I}} \tag{A.23}$$

where the tensor $\mathbf{V}$ represents the electric field gradient at the site of the nucleus:

$$\mathbf{V} = \begin{pmatrix} V_{xx} & V_{xy} & V_{xz} \\ V_{yx} & V_{yy} & V_{yz} \\ V_{zx} & V_{zy} & V_{zz} \end{pmatrix} \tag{A.24}$$

and Q is the nuclear electric quadrupole moment. The elements of $\mathbf{V}$ are given by the second derivatives of the electric potential V:

$$V_{xy} = \left.\frac{\partial^2 V}{\partial x \partial y}\right|_{\text{at nucleus}}$$

and similarly for the terms V_{zz}, V_{zx}, and so on. By definition, $\mathbf{V}$ is symmetric, i.e. $V_{xy} = V_{yx}$, etc. In addition, electromagnetic theory constrains $\mathbf{V}$ to be traceless, i.e. $V_{xx} + V_{yy} + V_{zz} = 0$.

The principal values of the electric field gradient tensor are

$$V_{XX} = -\frac{1}{2}eq(1-\eta_{\text{Q}})$$

$$V_{YY} = -\frac{1}{2}eq(1+\eta_{\text{Q}})$$

$$V_{XX} = eq$$

where η is the biaxiality. The representation of the electric field gradient tensor in the laboratory frame is given by

$$\mathbf{V} = \mathcal{R}(\Omega_{\text{LP}}^{\text{Q}}) \cdot \begin{pmatrix} V_{XX} & 0 & 0 \\ 0 & V_{YY} & 0 \\ 0 & 0 & V_{ZZ} \end{pmatrix} \cdot \mathcal{R}(\Omega_{\text{PL}}^{\text{Q}}) \tag{A.25}$$

Here, $\mathcal{R}(\Omega_{\text{PL}}^{\text{Q}})$ defines the relative orientation of the electric field gradient principal axis system and the laboratory frame:

$$\mathcal{R}(\Omega_{\text{PL}}^{\text{Q}}) = \mathcal{R}(\Omega_{\text{PM}}^{\text{Q}})\mathcal{R}(\Omega_{\text{ML}})$$

The Euler angle set $\Omega_{\text{PM}}^{\text{Q}}$ defines the orientation of the electric field gradient tensor in the molecular frame (compare with Equation A.6).

A.7.2 First-order quadrupolar interaction

The secular part of the quadrupolar Hamiltonian in Equation A.23 is given in the general case by

$$\widehat{\mathcal{H}}_Q^{(1)} = \omega_Q^{(1)} \times \frac{1}{6}\left(3\hat{I}_z^2 - I(I+1)\widehat{1}\right) \tag{A.26}$$

where the first-order quadrupolar coupling is given by

$$\omega_{\mathrm{Q}}^{(1)} = \frac{3eQ}{2I(2I-1)\hbar} V_{zz} \tag{A.27}$$

Here, V_{zz} is a component of the electric field gradient tensor in the laboratory frame (Equation A.25).

In the case of a uniaxial electric field gradient tensor ($\eta_Q = 0$), this component is given by

$$V_{zz} = V_{ZZ} \frac{1}{2}(3\cos^2\theta_Q - 1)$$

where θ_{Q} is the angle between the unique principal axis of the electric field gradient tensor and the magnetic field (θ_{Q} corresponds to the Euler angle $\beta_{\mathrm{PL}}^{\mathrm{Q}}$). In the uniaxial case, Equation A.27 reduces to

$$\begin{aligned} \omega_Q^{(1)} &= \frac{3e^2Qq}{2I(2I-1)\hbar} \times \frac{1}{2}(3\cos^2\theta_Q - 1) \\ &= \frac{3\pi C_{\mathrm{Q}}}{I(2I-1)} \times \frac{1}{2}(3\cos^2\theta_Q - 1) \end{aligned} \tag{A.28}$$

as in Equation 9.30.

A.7.3 Higher-order quadrupolar interactions

The second-order quadrupolar interaction is best described using the technique of *irreducible spherical tensor operators* and is given explicitly elsewhere (e.g. see A. Jerschow, *Prog. NMR Spectrosc.* **46**, 63–78 (2005)).

For nuclei with spin $I \geq 2$, there are additional electric and magnetic interactions. For example, the $E_{\mathrm{elec}}^{(4)}$ term represents the interaction of the $\mathbb{C}^{(4)}$ part of the electric charge distribution (the 'electric hexadecapole moment') with the fourth derivative of the electric potential. There are also high-order magnetic interactions. In practice, all higher-order electromagnetic interactions are weak and unimportant.

A.8 Strong Coupling

A.8.1 Strongly-coupled Spin-1/2 pairs

Chapter 14 considers the dynamics of spin-1/2 pairs in two extreme cases: magnetic equivalence (no difference in chemical shifts) and weak coupling (a large difference in chemical shifts). This appendix considers the general case.

The rotating-frame spin Hamiltonian is given by

$$\widehat{\mathcal{H}}^0 = \Omega_1^0 \hat{I}_{1z} + \Omega_2^0 \hat{I}_{2z} + 2\pi J_{12} \hat{\mathbf{I}}_1 \cdot \hat{\mathbf{I}}_2 + d_{12}(3\hat{I}_{1z}\hat{I}_{2z} - \hat{\mathbf{I}}_1 \cdot \hat{\mathbf{I}}_2)$$

which has the following matrix representation in the Zeeman product basis:

$$\widehat{\mathcal{H}}^0 = \frac{1}{2} \begin{pmatrix} \Omega_\Sigma + \omega_{12}^{\mathrm{A}} & 0 & 0 & 0 \\ 0 & \Omega_\Delta - \omega_{12}^{\mathrm{A}} & \omega_{12}^{\mathrm{B}} & 0 \\ 0 & \omega_{12}^{\mathrm{B}} & -\Omega_\Delta - \omega_{12}^{\mathrm{A}} & 0 \\ 0 & 0 & 0 & -\Omega_\Sigma + \omega_{12}^{\mathrm{A}} \end{pmatrix} \tag{A.29}$$

where the A and B coupling terms are given by

$$\omega_{12}^{\mathrm{A}} = \pi J_{12} + d_{12}$$
$$\omega_{12}^{\mathrm{B}} = 2\pi J_{12} - d_{12}$$

and the sum and difference of the chemical shift frequencies are

$$\Omega_{\Sigma} = \Omega_1^0 + \Omega_2^0$$
$$\Omega_{\Delta} = \Omega_1^0 - \Omega_2^0$$

It is possible to solve for the eigenvalues and eigenvectors of the matrix in Equation A.29 using standard methods.[2] The eigenvectors are given by

$$|1\rangle = \begin{pmatrix} 1 \\ 0 \\ 0 \\ 0 \end{pmatrix} \qquad |2\rangle = \begin{pmatrix} 0 \\ \cos\frac{1}{2}\xi \\ \sin\frac{1}{2}\xi \\ 0 \end{pmatrix}$$

$$|3\rangle = \begin{pmatrix} 0 \\ -\sin\frac{1}{2}\xi \\ \cos\frac{1}{2}\xi \\ 0 \end{pmatrix} \qquad |4\rangle = \begin{pmatrix} 0 \\ 0 \\ 0 \\ 1 \end{pmatrix}$$

and the eigenvalues are given by

$$\Omega_1 = \frac{1}{2}(\Omega_{\Sigma} + \omega_{12}^{\mathrm{A}}) \qquad \Omega_2 = -\frac{1}{2}\omega_{12}^{\mathrm{A}} + \frac{1}{2}\sqrt{(\omega_{12}^{\mathrm{B}})^2 + \Omega_{\Delta}^2}$$
$$\Omega_3 = -\frac{1}{2}\omega_{12}^{\mathrm{A}} - \frac{1}{2}\sqrt{(\omega_{12}^{\mathrm{B}})^2 + \Omega_{\Delta}^2} \qquad \Omega_4 = \frac{1}{2}(-\Omega_{\Sigma} + \omega_{12}^{\mathrm{A}}) \tag{A.30}$$

where the angle ξ is defined by

$$\tan\xi = \frac{\omega_{12}^{\mathrm{B}}}{\Omega_{\Delta}} \tag{A.31}$$

If the angle ξ is small, then the system is weakly coupled. If the angle ξ approaches $\pi/2$, then the system is strongly coupled.

We can use these results to see what happens when an NMR signal is induced by a strong $\pi/2$ pulse.

Take the usual expression for the thermal equilibrium spin density operator:

$$\hat{\rho}_{①} = \hat{\rho}^{\mathrm{eq}} \sim \hat{I}_{1z} + \hat{I}_{2z}$$

omitting the unity operator and the Boltzmann factor. The thermal equilibrium density operator is independent of whether the spin system is weakly or strongly coupled, within the usual approximations of high temperature and high field.

The $(\pi/2)_x$ pulse rotates the spin density operator in the usual way, yielding

$$\hat{\rho}_{②} \sim -\hat{I}_{1y} - \hat{I}_{2y}$$

This transformation is also independent of the coupling state of the spin system.

Now suppose that the system evolves freely, in the absence of r.f. fields. The treatment in Section 15.9 does not apply if the system is strongly coupled. How does one proceed?

The first step is to express the spin density operator in terms of the coherences between the eigenstates of $\widehat{\mathcal{H}}$, defined in Equation A.30. This may be done using

$$\hat{\rho} = \sum_{r=1}^{4} \sum_{s=1}^{4} \rho_{rs} |r\rangle\langle s|$$

where ρ_{rs} is the coherence between eigenstate $|r\rangle$ and eigenstate $|s\rangle$. If the time point $t = 0$ corresponds to the end of the pulse, then the coherence ρ_{rs} at $t = 0$ is given by

$$\rho_{rs}(0) = \langle r|\hat{\rho}_{\textcircled{2}}|s\rangle = -\langle r|(\hat{I}_{1y} + \hat{I}_{2y})|s\rangle$$

The coherences may be evaluated by using the vector representations of $\langle r|$ and $|s\rangle$, and the matrix representation of $\hat{I}_{1y} + \hat{I}_{2y}$. For example, the (-1)-quantum coherence between states $|2\rangle$ and $|1\rangle$ is given by

$$\rho_{21}(0) = -\frac{1}{2\mathrm{i}} \left(0\,, \quad \cos\frac{1}{2}\xi\,, \quad \sin\frac{1}{2}\xi\,, \quad 0 \right) \cdot \begin{pmatrix} 0 & 1 & 1 & 0 \\ -1 & 0 & 0 & 1 \\ -1 & 0 & 0 & 1 \\ 0 & -1 & -1 & 0 \end{pmatrix} \cdot \begin{pmatrix} 1 \\ 0 \\ 0 \\ 0 \end{pmatrix}$$

$$= \frac{1}{2\mathrm{i}} \left(\cos\frac{1}{2}\xi + \sin\frac{1}{2}\xi \right)$$

If the calculation is repeated for the other three (-1)-quantum coherences, we get:

$$\rho_{31}(0) = \frac{1}{2\mathrm{i}}(\cos\frac{1}{2}\xi - \sin\frac{1}{2}\xi)$$

$$\rho_{42}(0) = \frac{1}{2\mathrm{i}}(\cos\frac{1}{2}\xi + \sin\frac{1}{2}\xi)$$

$$\rho_{43}(0) = \frac{1}{2\mathrm{i}}(\cos\frac{1}{2}\xi - \sin\frac{1}{2}\xi)$$

If the angle ξ is equal to zero, all four (-1)-quantum coherences have equal amplitude. This is the weak coupling case. If the angle ξ is equal to $\pi/2$, on the other hand, the coherences ρ_{31} and ρ_{43} are not excited by the pulse at all. This is the case of magnetic equivalence. In the general strong coupling case, all four (-1)-quantum coherences are excited, but with unequal amplitudes.

Now suppose that the system evolves for an interval t. The coherences oscillate as usual according to the difference in energies between the states involved (see Section 15.4). A given coherence, therefore, has the following value at time t:

$$\rho_{rs}(t) = \rho_{rs}(0) \exp\{[-\mathrm{i}(\Omega_r - \Omega_s) - \lambda]t\}$$

where a damping decay constant λ has been included to take into account transverse relaxation (assumed to be the same for all coherences, for the sake of simplicity). The rotating-frame eigenvalues Ω_r and Ω_s are specified in Equation A.30.

Each oscillating (-1)-quantum coherence induces an NMR signal, which therefore has the form

$$s(t) = \sum_{r=1}^{4} \sum_{s=1}^{4} a_{rs} \exp\{[\mathrm{i}\Omega_{rs} - \lambda]t\}$$

The terms a_{rs} are the complex amplitudes of the spectral peaks. The peak frequencies are given by differences in the Hamiltonian eigenvalues:

$$\Omega_{rs} = -\Omega_r + \Omega_s$$

In order to complete the calculation of the NMR signal, we require the signal amplitudes a_{rs}. Here, we must be careful, since in strongly coupled systems the different (-1)-quantum coherences couple to the observable magnetization with different efficiencies. This may be seen by repeating the arguments in Appendix A.5 for the strongly coupled system. For example, Equation A.17 becomes

$$M_x \sim \langle \hat{I}_x \rangle \quad = \mathrm{Tr}\{\hat{\rho}\hat{I}_x\} = \sum_{r=1}^{4}\sum_{s=1}^{4} \langle r|\hat{\rho}|s\rangle\langle s|\hat{I}_x|r\rangle = \sum_{r=1}^{4}\sum_{s=1}^{4} \rho_{rs}\langle s|\hat{I}_x|r\rangle$$

which shows that a coherence ρ_{rs} couples to the observable magnetization with a factor $\langle s|\hat{I}_x|r\rangle$. The signal coupling efficiencies for the four (-1)-quantum coherences in the AB system are readily calculated to be

$$\langle 1|\hat{I}_x|2\rangle = \frac{1}{2}(\cos\frac{1}{2}\xi + \sin\frac{1}{2}\xi) \qquad \langle 1|\hat{I}_x|3\rangle = \frac{1}{2}(\cos\frac{1}{2}\xi - \sin\frac{1}{2}\xi)$$
$$\langle 2|\hat{I}_x|4\rangle = \frac{1}{2}(\cos\frac{1}{2}\xi + \sin\frac{1}{2}\xi) \qquad \langle 3|\hat{I}_x|4\rangle = \frac{1}{2}(\cos\frac{1}{2}\xi - \sin\frac{1}{2}\xi)$$

In general, two of the four coherences provide stronger NMR signals than the other two. In the case of magnetic equivalence ($\xi = \pi/2$), two of the coherences do not induce NMR signals at all.

Taking this into account, we get the following general expression for the quadrature-detected signal amplitude generated by the coherence ρ_{rs}:

$$a_{rs} = 2\mathrm{i}\rho_{rs}(0)\langle r|\hat{I}_x|s\rangle \exp\{-\mathrm{i}\phi_{\mathrm{rec}}\} \tag{A.32}$$

where ϕ_{rec} is the receiver phase. This equation applies to any (-1)-quantum coherence in an arbitrary coupled system.

The above expressions may be combined to obtain the NMR signal obtained by applying a single $\pi/2$ pulse to an ensemble of AB systems:

$$s(t) = a_{21}\exp\{[\mathrm{i}\Omega_{21} - \lambda]t\} + a_{31}\exp\{[\mathrm{i}\Omega_{31} - \lambda]t\}$$
$$+a_{42}\exp\{[\mathrm{i}\Omega_{42} - \lambda]t\} + a_{43}\exp\{[\mathrm{i}\Omega_{43} - \lambda]t\}$$

The signal frequencies are given by

$$\Omega_{21} = \frac{1}{2}\Omega_\Sigma + \omega_{12}^{\mathrm{A}} - \frac{1}{2}\sqrt{(\omega_{12}^{\mathrm{B}})^2 + \Omega_\Delta^2}$$
$$\Omega_{31} = \frac{1}{2}\Omega_\Sigma + \omega_{12}^{\mathrm{A}} + \frac{1}{2}\sqrt{(\omega_{12}^{\mathrm{B}})^2 + \Omega_\Delta^2}$$
$$\Omega_{42} = \frac{1}{2}\Omega_\Sigma - \omega_{12}^{\mathrm{A}} + \frac{1}{2}\sqrt{(\omega_{12}^{\mathrm{B}})^2 + \Omega_\Delta^2}$$
$$\Omega_{43} = \frac{1}{2}\Omega_\Sigma - \omega_{12}^{\mathrm{A}} - \frac{1}{2}\sqrt{(\omega_{12}^{\mathrm{B}})^2 + \Omega_\Delta^2}$$

and the signal amplitudes after a single $\pi/2$ pulse are

$$a_{21} = \frac{1}{2}\left(\cos\frac{1}{2}\xi + \sin\frac{1}{2}\xi\right)^2 = \frac{1}{2}(1+\sin\xi) \qquad a_{31} = \frac{1}{2}\left(\cos\frac{1}{2}\xi - \sin\frac{1}{2}\xi\right)^2 = \frac{1}{2}(1-\sin\xi)$$

$$a_{42} = \frac{1}{2}\left(\cos\frac{1}{2}\xi + \sin\frac{1}{2}\xi\right)^2 = \frac{1}{2}(1+\sin\xi) \qquad a_{43} = \frac{1}{2}\left(\cos\frac{1}{2}\xi - \sin\frac{1}{2}\xi\right)^2 = \frac{1}{2}(1-\sin\xi)$$

assuming $\phi_{\text{rec}} = 0$.

After FT, we get the following expression for the NMR spectrum:

$$S(\Omega) = a_{21}\mathcal{L}(\Omega;\Omega_{21},\lambda) + a_{31}\mathcal{L}(\Omega;\Omega_{31},\lambda) + a_{42}\mathcal{L}(\Omega;\Omega_{42},\lambda) + a_{43}\mathcal{L}(\Omega;\Omega_{43},\lambda)$$

displaying four peaks with different frequencies and amplitudes.

The simulations shown below illustrate the case with $\Omega_\Sigma = 0$, no dipole–dipole coupling ($d_{jk} = 0$), a J-coupling of $J_{jk} = 10\,\text{Hz}$, and different values for the chemical shift frequency difference Ω_Δ:

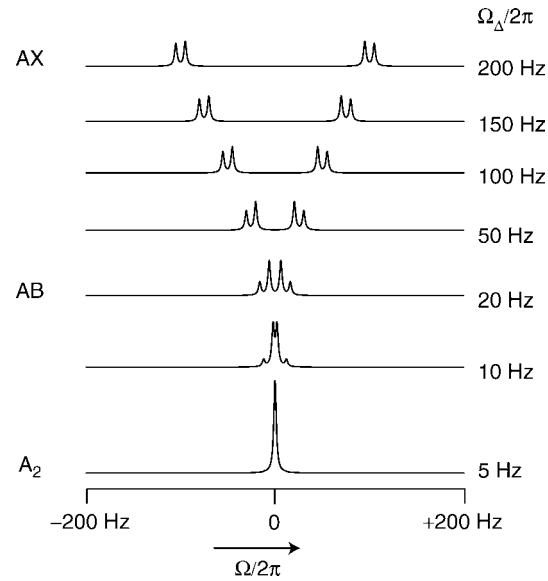

Figure A.7
Spectra of spin-1/2 pairs, in the case of $J_{jk} = 10\,\text{Hz}$ and zero dipole–dipole coupling.

In the limit of a large frequency difference Ω_Δ, the system is weakly coupled, and the spectrum displays the typical four-peak pattern of an AX spin system (although with small residual distortions in the relative peak amplitudes). As Ω_Δ is reduced, the outer peaks lose amplitude (these peaks correspond to the coherences ρ_{31} and ρ_{43}, which are weakly excited by the $\pi/2$ pulse and which also couple poorly to the observable signal). At the same time, the inner peaks gain amplitude. In the case of a very small chemical shift difference, the outer peaks disappear and the inner peaks coalesce. In the limit of a identical chemical shift frequencies, the system displays only a single spectral peak. This is the case of magnetic equivalence in the absence of J-coupling (see Figure 14.6a).

The simulation shown in Figure A.8 illustrates what happens if there is no J-coupling $J_{jk} = 0$, but there is a finite secular dipole–dipole coupling of $d_{jk}/2\pi = 10\,\text{Hz}$. The behaviour of the spin system is similar to the J-coupled case in the limit of large chemical shift difference: a four-peak AX pattern is observed, with a frequency splitting of $2d_{jk}/2\pi = 20\,\text{Hz}$ between the doublet components. However, when Ω_Δ is reduced, it is the central peaks that lose amplitude in the dipolar-coupled case. At very small values of Ω_Δ, the central peaks vanish altogether, leaving a doublet with splitting $3d_{jk}/2\pi = 30\,\text{Hz}$.

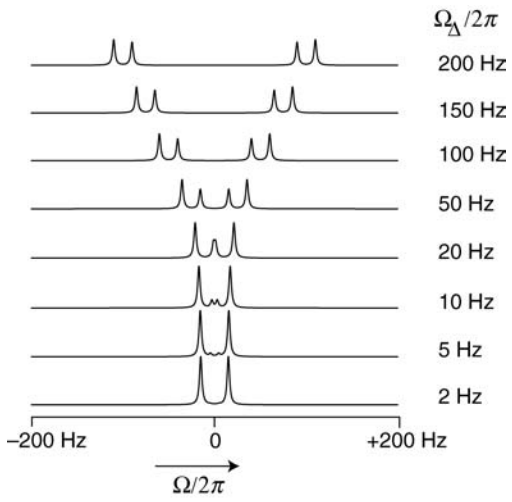

Figure A.8
Spectra of spin-1/2 pairs, in the case $d_{jk} = 10\,\text{Hz}$ and zero J-coupling.

Note carefully that the magnetic equivalence of the two spins in the case $\Omega_\Delta = 0$ does *not* remove the spin–spin splitting, in the case of a dipolar-coupled system (see Figure 14.6b).

The above expressions also apply when both J-couplings and secular dipolar couplings exist at the same time. The following simulation is for the case $\Omega_\Sigma = 0$ and $J_{jk} = d_{jk}/2\pi = 10\,\text{Hz}$:

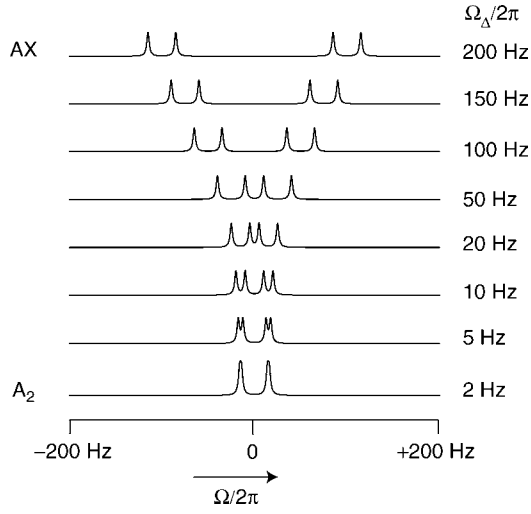

Figure A.9
Spectra of spin-1/2 pairs, in the case of $J_{jk} = d_{jk} = 10\,\text{Hz}$.

Remarkably, all four peak amplitudes remain the same, independent of the shift frequency difference Ω_Δ. Formally, this system is weakly coupled for all values of Ω_Δ ($\xi = 0$ in Equation A.31).

Strongly-coupled spectra are sometimes called "second-order spectra" in the literature, while weakly-coupled spectra are sometimes called "first-order". The meaning of these terms is unclear, and they should be avoided.

A.8.2 General strongly coupled systems

The situation is more complicated when there are more than two coupled spins, but the general principles are the same. The spectrum induced by a single strong $\pi/2$ pulse, applied to a thermal equilibrium spin

ensemble in high magnetic field, may be calculated as follows:

1. Construct the rotating-frame Hamiltonian operator $\widehat{\mathcal{H}}$ for the spin system.

2. Calculate the matrix representation $\mathbf{H}$ of the Hamiltonian $\widehat{\mathcal{H}}$ in a suitable basis (for example the Zeeman product basis). If each spin system contains N coupled spins-1/2, the dimension of the matrix $\mathbf{H}$ is $2^N \times 2^N$.

3. Determine the matrix representation of the operator $\hat{I}^+$ in the same basis. Denote this $\mathbf{I}^+$.

4. Determine the eigenvalues and normalized eigenvectors of $\mathbf{H}$ (see Section 6.4). Each normalized eigenvector $\mathbf{x}_r$ corresponds to a rotating-frame Hamiltonian eigenvalue Ω_r, with the eigenvalue index r taking the values $\{1, 2 \ldots 2^N\}$:

$$\mathbf{H} \cdot \mathbf{x}_r = \Omega_r \mathbf{x}_r$$

   In simple cases, the eigenvalues and eigenvectors may be determined analytically, as in Section A.8. In more complicated cases, numerical methods are available for diagonalizing the matrix.

5. In general, the NMR spectrum consists of 2^{2N} spectral peaks, each corresponding to a coherence between the eigenvectors. The coherence frequencies correspond to differences in Hamiltonian eigenvalues:

$$\Omega_{rs} = -\Omega_r + \Omega_s$$

   The peak amplitudes correspond to the squares of the matrix elements of $\hat{I}^+$:

$$a_{rs} = |\mathbf{x}_r{}^\dagger \cdot \mathbf{I}^+ \cdot \mathbf{x}_s|^2$$

6. The NMR spectrum is a sum of Lorentzians, one for each coherence:

$$S(\Omega) = \sum_{r,s=1}^{2^N} a_{rs} \mathcal{L}(\Omega; \Omega_{rs}, \lambda) \tag{A.33}$$

   where $\lambda = T_2{}^{-1}$.

In practice, the sum in Equation A.33 may be restricted to (-1)-quantum coherences, since the amplitudes a_{rs} vanish in all other cases.

A.9 *J*-Couplings and Magnetic Equivalence

In this appendix, I prove that J-couplings between magnetically equivalent spins may be omitted from the spin Hamiltonian without changing the results of any calculations.

Consider first the following theorem. Suppose that the spin Hamiltonian contains two hermitian terms $\widehat{A}$ and $\widehat{B}$, which mutually commute:

$$\begin{aligned} \widehat{\mathcal{H}} &= \widehat{A} + \widehat{B} \\ \left[\widehat{A}, \widehat{B}\right] &= 0 \end{aligned} \tag{A.34}$$

Suppose also that $\widehat{B}$ commutes with an operator $\widehat{Q}$:

$$\left[\widehat{B}, \widehat{Q}\right] = 0 \tag{A.35}$$

The theorem states that the expectation value of $\widehat{Q}$ may be calculated as a function of time without including the term $\widehat{B}$ in the Hamiltonian.

This may be shown as follows. The Schrödinger equation leads to the following equation of motion for a spin state $|\psi\rangle$:

$$|\psi\rangle(t) = \exp\{-\mathrm{i}\widehat{\mathcal{H}}t\}|\psi\rangle(0)$$

If the Hamiltonian contains two commuting terms, then the exponential operator may be written as

$$\exp\{-\mathrm{i}\widehat{\mathcal{H}}t\} = \exp\{-\mathrm{i}\widehat{B}t\}\exp\{-\mathrm{i}\widehat{A}t\}$$

The equation of motion for the ket and bra states is therefore

$$|\psi\rangle(t) = \exp\{-\mathrm{i}\widehat{B}t\}\exp\{-\mathrm{i}\widehat{A}t\}|\psi\rangle(0)$$

$$\langle\psi|(t) = \langle\psi|(0)\exp\{+\mathrm{i}\widehat{A}t\}\exp\{+\mathrm{i}\widehat{B}t\}$$

The expectation value of the operator $\widehat{Q}$ evolves as follows:

$$\begin{aligned}\langle\widehat{Q}\rangle(t) &= \langle\psi|(t)\,\widehat{Q}\,|\psi\rangle(t)\\ &= \langle\psi|(0)\exp\{+\mathrm{i}\widehat{A}t\}\exp\{+\mathrm{i}\widehat{B}t\}\widehat{Q}\exp\{-\mathrm{i}\widehat{B}t\}\exp\{-\mathrm{i}\widehat{A}t\}|\psi\rangle(0)\end{aligned}$$

Now if the operators $\widehat{Q}$ and $\widehat{B}$ commute, then

$$\exp\{+\mathrm{i}\widehat{B}t\}\widehat{Q}\exp\{-\mathrm{i}\widehat{B}t\} = \widehat{Q}$$

Hence

$$\langle\widehat{Q}\rangle(t) = \langle\psi|(0)\exp\{+\mathrm{i}\widehat{A}t\}\widehat{Q}\exp\{-\mathrm{i}\widehat{A}t\}|\psi\rangle(0)$$

which is independent of $\widehat{B}$.

This theorem may be applied to the problem of magnetic equivalence as follows. Consider a molecular spin system containing three spins I_1, I_2 and I_3, with the following relationships between the chemical shift frequencies and the J-couplings:

$$\begin{aligned}\omega_1^0 &= \omega' & \omega_2^0 &= \omega'\\ \omega_3^0 &= \omega'' & J_{12} &= J'\\ J_{13} &= J'' & J_{23} &= J''\end{aligned}$$

Spins I_1 and I_2 are magnetically equivalent according to the standard definition.

The spin Hamiltonian may be divided up as in Equation A.34, with

$$\widehat{A} = \omega'(\hat{I}_{1z} + \hat{I}_{2z}) + \omega''\hat{I}_{3z} + 2\pi J''\left(\hat{\mathbf{I}}_1 + \hat{\mathbf{I}}_2\right)\cdot\hat{\mathbf{I}}_3$$

$$\widehat{B} = 2\pi J'\,\hat{\mathbf{I}}_1\cdot\hat{\mathbf{I}}_2$$

The commutation of $\widehat{A}$ and $\widehat{B}$ may be demonstrated by repeating the following reasoning for all the relevant terms:

$$\left[\left(\hat{I}_{1x} + \hat{I}_{2x}\right)\hat{I}_{3x}\,,\ \hat{I}_{1z}\hat{I}_{2z}\right] = \left[\hat{I}_{1x} + \hat{I}_{2x}, \hat{I}_{1z}\hat{I}_{2z}\right]\hat{I}_{3x} = 0 \tag{A.36}$$

Furthermore, all relevant observable operators also commute with $\widehat{B}$. This is because the observation process always involves a sum of contributions from all spins of the same isotopic type. For example, a typical observable operator corresponds to the sum of spin angular momentum along the x-axis:

$$\widehat{Q} = \hat{I}_{1x} + \hat{I}_{2x} + \hat{I}_{3x}$$

This operator also commutes with $\widehat{B}$. The theorem above indicates that the term $\widehat{B}$ may be dropped from the spin Hamiltonian without damage.

This reasoning may be extended to more complicated cases. Consider, for example, the case of four spins, in which the first three are magnetically equivalent:

$$\begin{aligned} \omega_1^0 &= \omega' & \omega_2^0 &= \omega' \\ \omega_3^0 &= \omega' & \omega_4^0 &= \omega'' \\ J_{12} &= J' & J_{13} &= J' \\ J_{14} &= J'' & J_{23} &= J' \\ J_{24} &= J'' & J_{34} &= J'' \end{aligned}$$

The Hamiltonian may be organized into two commuting terms as follows:

$$\begin{aligned} \widehat{A} &= \omega'(\hat{I}_{1z} + \hat{I}_{2z} + \hat{I}_{3z}) + \omega''\hat{I}_{4z} + 2\pi J''\left(\hat{\mathbf{I}}_1 + \hat{\mathbf{I}}_2 + \hat{\mathbf{I}}_3\right) \cdot \hat{\mathbf{I}}_4 \\ \widehat{B} &= 2\pi J'\left(\hat{\mathbf{I}}_1 \cdot \hat{\mathbf{I}}_2 + \hat{\mathbf{I}}_2 \cdot \hat{\mathbf{I}}_3 + \hat{\mathbf{I}}_3 \cdot \hat{\mathbf{I}}_4\right) \end{aligned} \tag{A.37}$$

If the observable operator has the form

$$\widehat{Q} = \hat{I}_{1x} + \hat{I}_{2x} + \hat{I}_{3x} + \hat{I}_{4x}$$

then the commutation properties shown in Equations A.34 and A.35 may be proved by repeating Equation A.36 for all relevant terms. The couplings within the group of magnetically equivalent spins may, therefore, be omitted from the spin Hamiltonian.

A.10 Spin Echo Sandwiches

In this appendix, I examine the properties of the spin echo sequence

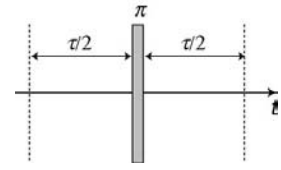

Figure A.10
Spin echo sandwich.

in coupled spin systems.

In the case of a general spin system in an isotropic liquid, the propagator for this pulse sequence element is given by

$$\widehat{U}_{\mathrm{SES}} = \widehat{U}(\tau/2)\widehat{R}_x(\pi)\widehat{U}(\tau/2) \tag{A.38}$$

where

$$\widehat{U}(\tau/2) = \exp\{-\mathrm{i}\widehat{\mathcal{H}}^0\tau/2\}$$

and the secular rotating-frame Hamiltonian has the form

$$\widehat{\mathcal{H}}^0 = \sum_j \Omega_j^0 \hat{I}_{jz} + \sum_{j<k}{}' 2\pi J_{jk}\hat{\mathbf{I}}_j \cdot \hat{\mathbf{I}}_k$$

This expression may be simplified, depending on the duration of the spin echo sequence and whether the spin system satisfies the weak-coupling conditions or not:

1. *The short-duration limit*. If the duration τ of the spin echo sequence satisfies

$$|(\Omega_j^0 - \Omega_k^0)\tau| << 1 \tag{A.39}$$

for all pairs of coupled spins j and k, then the propagator for the spin echo sandwich may be written as

$$\widehat{U}_{\text{SES}} \cong \widehat{U}_J^{\text{strong}}(\tau)\widehat{R}_x(\pi) \qquad \text{(short-duration limit)} \tag{A.40}$$

where $\widehat{U}_J^{\text{strong}}$ is given by

$$\widehat{U}_J^{\text{strong}}(\tau) = \exp\{-\text{i}\widehat{\mathcal{H}}_J^{\text{strong}}\tau\} \tag{A.41}$$

and

$$\widehat{\mathcal{H}}_J^{\text{strong}} = \sum_{j<k}{}' 2\pi J_{jk}\hat{\mathbf{I}}_j \cdot \hat{\mathbf{I}}_k \tag{A.42}$$

In the short-duration limit, the system is rotated by the π pulse, followed by evolution under the strongly coupled form of the J-couplings. Note that Equation A.40 always applies at short durations, even for systems that satisfy the usual weak-coupling condition.

2. *The long-duration limit*. If the spin system satisfies the weak-coupling condition

$$|(\Omega_j^0 - \Omega_k^0)| >> |\pi J_{jk}| \tag{A.43}$$

and the duration τ of the spin echo sequence is sufficiently long, i.e.

$$|(\Omega_j^0 - \Omega_k^0)\tau| >> 1 \tag{A.44}$$

for all pairs of magnetically equivalent coupled spins j and k, then the propagator for the spin echo sandwich is given by

$$\widehat{U}_{\text{SES}} \cong \widehat{U}_J^{\text{weak}}(\tau)\widehat{R}_x(\pi) \qquad \text{(long-duration limit)} \tag{A.45}$$

where $\widehat{U}_J^{\text{weak}}$ is given by

$$\widehat{U}_J^{\text{weak}}(\tau) = \exp\{-\text{i}\widehat{\mathcal{H}}_J^{\text{weak}}\tau\}$$

and

$$\widehat{\mathcal{H}}_J^{\text{weak}} = \sum_{j<k}{}' 2\pi J_{jk}\hat{I}_{jz}\hat{I}_{kz}$$

The expression for the propagator (Equation A.45) corresponds to Equation 15.25 in the case of an AX system. In the long-duration limit, the system is rotated by the π pulse, followed by evolution under the weakly coupled form of the J-couplings.

These properties are now proved.

A.10.1 Short-duration limit

In general, the propagator for the spin echo sandwich (Equation A.38) may be rewritten as follows:

$$\begin{aligned}\widehat{U}_{\text{SES}} &= \widehat{U}(\tau/2)\widehat{R}_x(\pi)\widehat{U}(\tau/2) \\ &= \widehat{U}(\tau/2)\cdot\widehat{R}_x(\pi)\widehat{U}(\tau/2)\widehat{R}_x(-\pi)\cdot\widehat{R}_x(\pi) \\ &= \widehat{U}(\tau/2)\widehat{U}'(\tau/2)\widehat{R}_x(\pi)\end{aligned}$$

where

$$\widehat{U}'(\tau/2) = \widehat{R}_x(\pi)\widehat{U}(\tau/2)\widehat{R}_x(-\pi)$$

By the arguments of Appendix A.3, this may be rearranged as

$$\begin{aligned}\widehat{U}'(\tau/2) &= \widehat{R}_x(\pi)\exp\{-\mathrm{i}\widehat{\mathcal{H}}^0\tau/2\}\widehat{R}_x(-\pi) \\ &= \exp\{-\mathrm{i}\,\widehat{R}_x(\pi)\widehat{\mathcal{H}}^0\widehat{R}_x(-\pi)\,\tau/2\} \\ &= \exp\{-\mathrm{i}\,\widehat{\mathcal{H}}^{0'}\,\tau/2\}\end{aligned}$$

where

$$\widehat{\mathcal{H}}^{0'} = \widehat{R}_x(\pi)\widehat{\mathcal{H}}^0\widehat{R}_x(-\pi)$$

The bracketing π_x rotations have the effect of inverting the chemical shift terms, leaving the sign of the J-coupling terms unchanged:

$$\widehat{\mathcal{H}}^{0'} = -\sum_j \Omega_j^0 \hat{I}_{jz} + {\sum_{j<k}}' 2\pi J_{jk}\hat{\mathbf{I}}_j\cdot\hat{\mathbf{I}}_k$$

The spin echo propagator is therefore given by

$$\widehat{U}_{\text{SES}} = \exp\{-\mathrm{i}\widehat{\mathcal{H}}^0\tau/2\}\exp\{-\mathrm{i}\widehat{\mathcal{H}}^{0'}\tau/2\}\widehat{R}_x(\pi)$$

So far, this expression is general.

In general, $\widehat{\mathcal{H}}^0$ and $\widehat{\mathcal{H}}^{0'}$ do not commute. However, if the duration τ is sufficiently small, then Equation 6.35 applies, which leads to the following approximate result:

$$\widehat{U}_{\text{SES}} \cong \exp\{-\mathrm{i}(\widehat{\mathcal{H}}^0 + \widehat{\mathcal{H}}^{0'})\tau/2\}\widehat{R}_x(\pi)$$

and hence

$$\widehat{U}_{\text{SES}} \cong \widehat{U}_J^{\text{strong}}(\tau)\widehat{R}_x(\pi) \tag{A.46}$$

as in Equation A.40.

A.10.2 Long-duration limit

The propagator for the spin echo sandwich

$$\widehat{U}_{\text{SES}} = \exp\{-\mathrm{i}\widehat{\mathcal{H}}^0\tau/2\}\exp\{-\mathrm{i}\widehat{\mathcal{H}}^{0'}\tau/2\}\widehat{R}_x(\pi) \tag{A.47}$$

cannot be simplified in general for large values of τ, since $\widehat{\mathcal{H}}^{0\prime}$ and $\widehat{\mathcal{H}}^{0}$ do not commute. However, if the system is weakly coupled, and the intervals $\tau/2$ are sufficiently long, then the secular approximation (Appendix A.6) may be applied locally within each precession interval. Under these conditions, the propagator may be approximated:

$$\widehat{U}_{\text{SES}} \cong \exp\{-\text{i}\widehat{\mathcal{H}}^{0}_{\text{weak}}\tau/2\}\exp\{-\text{i}\widehat{\mathcal{H}}^{0\prime}_{\text{weak}}\tau/2\}\widehat{R}_x(\pi)$$

where $\widehat{\mathcal{H}}^{0}_{\text{weak}}$ is the weakly coupled spin Hamiltonian in the rotating frame:

$$\widehat{\mathcal{H}}^{0}_{\text{weak}} \cong \sum_j \Omega^0_j \hat{I}_{jz} + {\sum_{j<k}}' 2\pi J_{jk}\hat{I}_{jz}\hat{I}_{kz} \tag{A.48}$$

and

$$\begin{aligned}\widehat{\mathcal{H}}^{0\prime}_{\text{weak}} &= \widehat{R}_x(-\pi)\widehat{\mathcal{H}}^{0}_{\text{weak}}\widehat{R}_x(\pi)\\ &= -\sum_j \Omega^0_j \hat{I}_{jz} + {\sum_{j<k}}' 2\pi J_{jk}\hat{I}_{jz}\hat{I}_{kz}\end{aligned}$$

Since the Hamiltonians $\widehat{\mathcal{H}}^{0}_{\text{weak}}$ and $\widehat{\mathcal{H}}^{0\prime}_{\text{weak}}$ commute, Equation 6.32 may be used to write the product of the propagators in Equation A.47 as

$$\widehat{U}_{\text{SES}} = \exp\{-\text{i}(\widehat{\mathcal{H}}^{0\prime}_{\text{weak}} + \widehat{\mathcal{H}}^{0}_{\text{weak}})\tau/2\}\widehat{R}_x(\pi) \tag{A.49}$$

which evaluates to

$$\widehat{U}_{\text{SES}} = \widehat{U}^{\text{weak}}_J(\tau)\widehat{R}_x(\pi) \tag{A.50}$$

as in Equation A.45.

The spin echo sandwich, therefore, has the same effect as a strong π pulse, followed by a period τ of evolution under the weak J-couplings. Since the operators commute, this sequence may also be applied the other way round.

The long-duration form of the spin echo sandwich is often used to manipulate spin systems under the weakly coupled J-couplings, without regard for the chemical shifts. This is the most common application of a spin echo sandwich, and is encountered in Sections 16.2, 16.3 and 18.12.

A.10.3 Two spin echo sequences

If two spin echo sequences follow each other immediately, as in the sequence

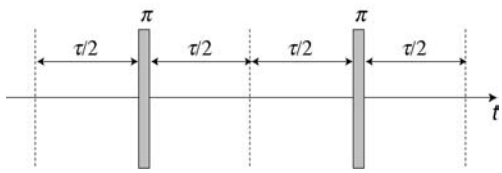

Figure A.11 Two spin-echo sandwiches.

then one may just multiply the propagators together, leading to

$$\widehat{U}_{\text{SES}}\widehat{U}_{\text{SES}} \cong \widehat{U}^{\text{strong}}_J(\tau)\widehat{R}_x(\pi)\widehat{U}^{\text{strong}}_J(\tau)\widehat{R}_x(\pi)$$

in the short-duration limit, and

$$\widehat{U}_{\mathrm{SES}}\widehat{U}_{\mathrm{SES}} \cong \widehat{U}_J^{\mathrm{weak}}(\tau)\widehat{R}_x(\pi)\widehat{U}_J^{\mathrm{weak}}(\tau)\widehat{R}_x(\pi)$$

in the long-duration limit.

In both cases, the π rotations commute with the spin coupling Hamiltonian, so the effective propagator under the double spin echo sequence is

$$\widehat{U}_{\mathrm{SES}}\widehat{U}_{\mathrm{SES}} \cong \widehat{U}_J^{\mathrm{weak}}(2\tau)\widehat{R}_x(2\pi)$$

in the long-duration limit, and

$$\widehat{U}_{\mathrm{SES}}\widehat{U}_{\mathrm{SES}} \cong \widehat{U}_J^{\mathrm{strong}}(2\tau)\widehat{R}_x(2\pi)$$

in the short-duration limit. The operator for a rotation by 2π may usually be omitted.[3]

In general, for n consecutive spin echo sequences, we get

$$\widehat{U}_{\mathrm{SES}}\widehat{U}_{\mathrm{SES}} \ldots \widehat{U}_{\mathrm{SES}} \cong \widehat{U}_J^{\mathrm{weak}}(n\tau)\widehat{R}_x(2n\pi) \tag{A.51}$$

in the long-duration limit, and

$$\widehat{U}_{\mathrm{SES}}\widehat{U}_{\mathrm{SES}} \ldots \widehat{U}_{\mathrm{SES}} \cong \widehat{U}_J^{\mathrm{strong}}(n\tau)\widehat{R}_x(2n\pi) \tag{A.52}$$

in the short-duration limit.

If n is even, then the operator $\widehat{R}_x(2n\pi)$ may be ignored,[3] so the application of a dense sequence of π pulses leads to evolution under the pure strongly coupled J-Hamiltonian. This property is used in the TOCSY pulse sequence (see Section 18.14).

A.10.4 Heteronuclear spin echo sequences

In heteronuclear systems, the Larmor frequency difference between spins of different type is very large. Both of the conditions in Equations A.43 and A.44 are always satisfied for the heteronuclear couplings. The heteronuclear part of the spin echo propagator always has the weakly coupled form.

In heteronuclear systems, the form of the spin echo propagator depends on whether the π pulse is applied to one or both of the spin species.

1. If a π pulse is applied to *both* spin species, then the following equivalence may be made:

   If the homonuclear couplings also satisfy the 'long limit' conditions, then the propagator for the heteronuclear spin echo sequence may be written as

   $$\widehat{U}_{\mathrm{SES}} = \widehat{U}_J^{\mathrm{weak}}(\tau)\widehat{R}_x^I(\pi)\widehat{R}_x^S(\pi)$$

   where $\widehat{R}_x^I(\pi)$ and $\widehat{R}_x^S(\pi)$ represent π rotations of the two spin species, and the weak coupling propagator is

   $$\widehat{U}_J^{\mathrm{weak}}(\tau) = \exp\{-\mathrm{i}\widehat{\mathcal{H}}_J^{\mathrm{weak}}\tau\}$$

   The weak-coupling Hamiltonian $\widehat{\mathcal{H}}_J^{\mathrm{weak}}$ contains all the couplings in the system (both homonuclear and heteronuclear). All chemical shift interactions are suppressed. A heteronuclear spin echo sandwich with a π pulse applied to both spin species behaves in the same way as a homonuclear spin echo sandwich:

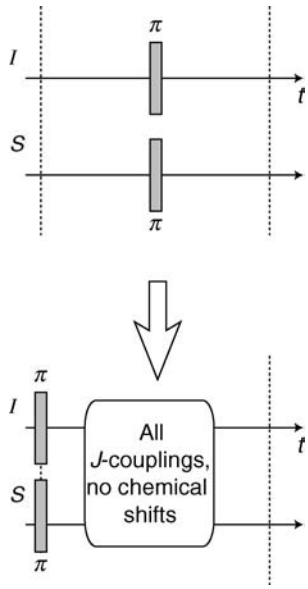

Figure A.12
Heteronuclear spin echo sequence, with π pulses on both channels.

2. If a π pulse is applied to *only one* spin species, on the other hand, the following equivalence applies:

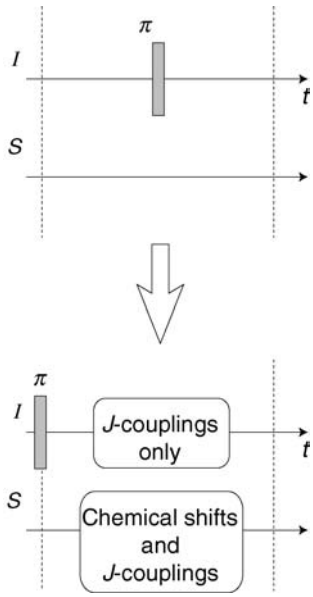

Figure A.13
Heteronuclear spin echo sequence, with a π pulse on the I-spin channel.

The spin echo sandwich suppresses chemical shifts for the irradiated species, but not for the non-irradiated species. Furthermore, the spin echo sandwich suppresses heteronuclear J-couplings, but retains homonuclear J-couplings. Formally, the propagator for this single-channel spin echo sandwich is

$$\widehat{U}_{\mathrm{SES}} = \widehat{U}_{II}^{\mathrm{weak}}(\tau)\widehat{U}_{S}^{\mathrm{weak}}(\tau)\widehat{R}_{x}^{I}(\pi)$$

where the propagators are

$$\widehat{U}_{II}^{\text{weak}}(\tau) = \exp\{-\mathrm{i}\widehat{\mathcal{H}}_{II}^{\text{weak}}\tau\}$$
$$\widehat{U}_{S}^{\text{weak}}(\tau) = \exp\{-\mathrm{i}\widehat{\mathcal{H}}_{S}\tau\}$$

and the Hamiltonians are

$$\widehat{\mathcal{H}}_{II}^{\text{weak}} = {\sum_{j<k}}' 2\pi J_{jk}\hat{I}_{jz}\hat{I}_{kz}$$
$$\widehat{\mathcal{H}}_{S} = \sum_{\ell}\Omega_{\ell}^{0}\hat{S}_{\ell z} + {\sum_{\ell<m}}' 2\pi J_{\ell m}\hat{S}_{\ell z}\hat{S}_{mz}$$

assuming that the weak-coupling conditions are satisfied for the S-spins.

A.11 Phase Cycling

In this appendix, I discuss the principles of *phase cycling*, which is a powerful and commonly used procedure for selecting certain types of NMR signals and suppressing others.

The basic practice of phase cycling is presented in Section 5.3. The phases of r.f. pulses and the the receiver phase are varied from transient to transient in a cyclic fashion, and the NMR signals from these different experiments are added together.

In this appendix, I discuss (i) how to predict which NMR signals are selected by a given phase-cycling procedure and (ii) how to design a phase cycle for a particular experiment, using a systematic algorithm. The discussion given here is necessarily superficial. A more thorough discussion may be found in *Further Reading*.

A.11.1 Coherence transfer pathways

The first step in phase cycling theory is to draw the *coherence transfer pathway diagram* for an experiment. This represents the history of coherence orders leading to the desired NMR signals in a particular experiment.[4] Consider, for example, the COSY pulse sequence discussed in Section 16.1. The basic pulse sequence for this experiment, and its associated coherence transfer pathway diagram, is as follows:

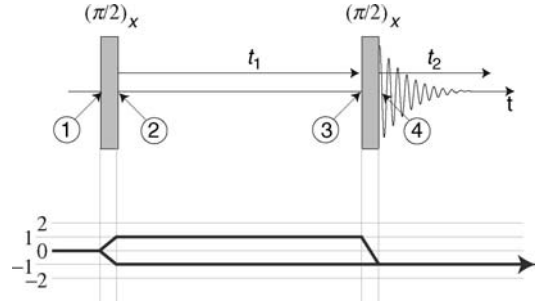

Figure A.14
COSY pulse sequence and its coherence transfer pathway.

This shows the 'cosine' pulse sequence in the States procedure. The 'sine' pulse sequence in the States procedure has the same coherence transfer pathway diagram.

In this book, thick black arrows indicate the desired histories of coherence orders leading to desirable NMR signals. In the case above, the desirable pathways are

$$0 \rightarrow +1 \rightarrow -1 \tag{A.53}$$

and

$$0 \rightarrow -1 \rightarrow -1 \tag{A.54}$$

All pathways start with order 0 (corresponding to spin populations) and terminate with order −1 (corresponding to observable (−1)-quantum coherences as detected in the quadrature receiver; see Appendix A.5).

The pathways given in Equations A.53 and A.54 indicate the conversion of spin populations into (±1)-quantum coherences by the first pulse, followed by conversion of these into observable (−1)-quantum coherences by the second pulse. The treatment given in Section 16.1 shows that *both* of these pathways are necessary to obtain pure absorption spectra using the States procedure. For example, the state $\hat{\rho}_{③}^{\cos}$ given in Equation 16.7 contains both (±1)-quantum coherences, and the States procedure would fail if any one of these pathways were suppressed. It is very important to maintain such essential dual pathways when designing phase-cycling procedures.

More complicated pulse sequences may have several coherence transfer steps, and a greater multiplicity of desirable signal pathways. For example, the INADEQUATE experiment (Section 16.2) has the following pulse sequence and coherence transfer pathway diagram:

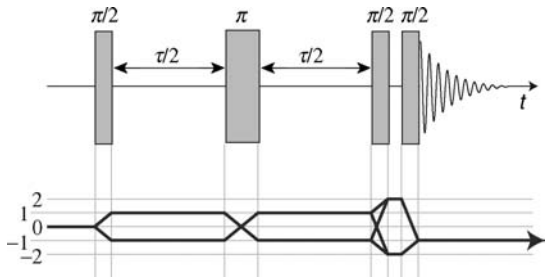

Figure A.15
INADEQUATE pulse sequence and its coherence transfer pathway.

There are four *desired coherence transfer pathways* in this case:

$$\begin{aligned} 0 &\rightarrow +1 \rightarrow -1 \rightarrow +2 \rightarrow -1 \\ 0 &\rightarrow +1 \rightarrow -1 \rightarrow -2 \rightarrow -1 \\ 0 &\rightarrow -1 \rightarrow +1 \rightarrow +2 \rightarrow -1 \\ 0 &\rightarrow -1 \rightarrow +1 \rightarrow -2 \rightarrow -1 \end{aligned} \tag{A.55}$$

In addition to these desirable signal pathways, it is also important to identify the *undesirable* signal pathways.

For example, in the COSY experiment, the signals passing through order 0 during the evolution interval t_1 may be relatively large, if the flip angle of the first pulse is not exactly $\pi/2$. These signals give rise to false two-dimensional peaks at the frequency coordinate $\Omega_1 = 0$ and must be suppressed to obtain a good result.

Similarly, in the INADEQUATE experiment, it is very important to suppress all signals that do not pass through (±2)-quantum coherences, in order to remove signals from isotopomers containing isolated ^{13}C spins.

A.11.2 Coherence transfer amplitudes

Phase cycling is based upon the transformation properties of the signals under phase shifts of the r.f. pulses.

Consider a general situation in which a pulse sequence element A, with phase ϕ, converts the coherence between two states $|r\rangle$ and $|s\rangle$ into a coherence between two different states $|u\rangle$ and $|v\rangle$:

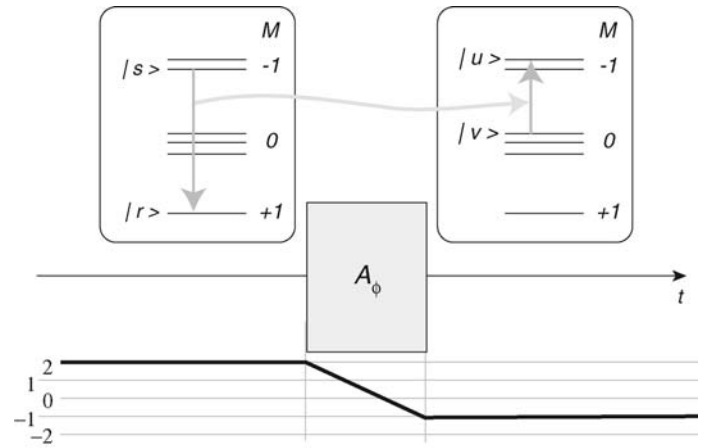

Figure A.16
A coherence transfer process.

In the example shown, the coherence between states $|r\rangle$ and $|s\rangle$ has order $p_{rs} = +2$, while the coherence between states $|u\rangle$ and $|v\rangle$ has order $p_{uv} = -1$. The change in coherence order is represented by the bold line on the coherence transfer pathway diagram.

This coherence transfer process may be represented mathematically as follows:

$$\widehat{A}_\phi |r\rangle\langle s| \widehat{A}_\phi{}^\dagger = \mathfrak{Z}(\phi)|u\rangle\langle v| + \ldots \tag{A.56}$$

where $\widehat{A}_\phi$ is the propagator for the pulse sequence element A, with phase ϕ, and $\mathfrak{Z}(\phi)$ is a complex number, called the *coherence transfer amplitude*.

The magnitude of $\mathfrak{Z}$ indicates how efficiently the coherence $|r\rangle\langle s|$ is converted into the coherence $|u\rangle\langle v|$ by the pulse sequence element A.

The coherence transfer amplitude $\mathfrak{Z}$ is easily evaluated by multiplying Equation A.56 on the left by $\langle u|$ and on the right by $|v\rangle$. By using the orthogonality of the spin eigenfunctions, we get

$$\mathfrak{Z}(\phi) = \langle u|\widehat{A}_\phi|r\rangle\langle s|\widehat{A}_\phi{}^\dagger|v\rangle$$

This equation relates the coherence transfer amplitude to the product of two operator matrix elements.

A.11.3 Coherence orders and phase shifts

We now examine how the coherence transfer amplitude $\mathfrak{Z}$ depends on the phase of the element A.

The propagator for the element A depends on the phase as follows:

$$\widehat{A}_\phi = \widehat{R}_z(\phi)\widehat{A}_0\widehat{R}_z(-\phi)$$

where $\widehat{R}_z(\phi)$ is the operator for a rotation by ϕ around the z-axis. It follows that the coherence transfer amplitude depends on the phase of A through

$$\mathfrak{Z}(\phi) = \langle u|\widehat{R}_z(\phi)\widehat{A}_0\widehat{R}_z(-\phi)|r\rangle\ \langle s|\widehat{R}_z(\phi)\widehat{A}_0{}^\dagger\widehat{R}_z(-\phi)|v\rangle \tag{A.57}$$

In high magnetic field, all four spin states $|r\rangle$, $|s\rangle$, $|u\rangle$ and $|v\rangle$ are eigenstates of the total angular momentum along the z-axis:

$$\hat{I}_z|r\rangle = M_r|r\rangle \qquad \hat{I}_z|s\rangle = M_s|s\rangle$$
$$\hat{I}_z|u\rangle = M_u|u\rangle \qquad \hat{I}_z|v\rangle = M_v|v\rangle$$

where M_r, M_s, M_u and M_v are the Zeeman quantum numbers of the states.

Since the rotation operator $\widehat{R}_z(-\phi)$ is equal to $\exp\{+\mathrm{i}\phi\hat{I}_z\}$, the results in Section 6.5 may be used to give

$$\widehat{R}_z(-\phi)|r\rangle = \exp\{+\mathrm{i}M_r\phi\}|r\rangle$$

$$\widehat{R}_z(-\phi)|v\rangle = \exp\{+\mathrm{i}M_u\phi\}|v\rangle$$

Similarly:

$$\langle s|\widehat{R}_z(\phi) = \langle s|\exp\{-\mathrm{i}M_s\phi\}$$

$$\langle u|\widehat{R}_z(\phi) = \langle u|\exp\{-\mathrm{i}M_u\phi\}$$

These equations may be substituted into Equation A.57 to get

$$\mathfrak{Z}(\phi) = \langle u|\widehat{A}_0|r\rangle\,\langle s|\widehat{A}_0{}^{\dagger}|v\rangle\,\exp\{\mathrm{i}(-M_u + M_r - M_s + M_v)\phi\}$$

which may be written as

$$\mathfrak{Z}(\phi) = \mathfrak{Z}(0)\exp\{-\mathrm{i}(p_{uv} - p_{rs})\phi\}$$

where $p_{uv} = M_u - M_v$ is the order of coherence $|u\rangle\langle v|$ and $p_{rs} = M_r - M_s$ is the order of coherence $|r\rangle\langle s|$.

The quantity $p_{uv} - p_{rs}$ corresponds to the *change in coherence order*. If the change in order is denoted Δp, we get the important equation

$$\mathfrak{Z}(\phi) = \mathfrak{Z}(0)\exp\{-\mathrm{i}\phi\,\Delta p\} \tag{A.58}$$

This indicates that changing the phase of a pulse sequence element multiplies each coherence transfer amplitude by a complex exponential factor. The phase of the exponential factor is proportional to the phase of the pulse multiplied by the change in coherence order Δp.

In the example above, $p_{rs} = +2$ and $p_{uv} = -1$, so the change in coherence order is $\Delta p = -3$. If the phase of the pulse is changed by ϕ, the phase of the amplitude for the process $|r\rangle\langle s| \Rightarrow |u\rangle\langle v|$ changes by 3ϕ.

A.11.4 The pathway phase

Consider a particular signal pathway, such as the following example:

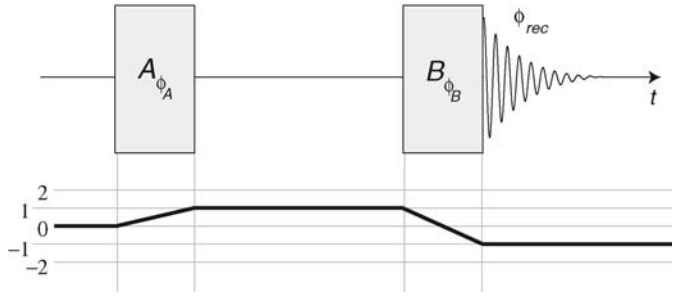

Figure A.17
An example of a coherence transfer pathway.

The first pulse sequence block A has phase ϕ_{A}, and the second block B has phase ϕ_{B}. The signal is detected and digitized using a receiver phase ϕ_{rec}.

The pathway is characterized by a shift in coherence order $\Delta p_{\mathrm{A}} = +1$ over the first block (the order increases from 0 to +1), and by a shift in coherence order $\Delta p_{\mathrm{B}} = -2$ over the second block (the order decreases from +1 to −1).

Suppose that an experiment is conducted with some value for the phases ϕ_A, ϕ_B and ϕ_{rec}. The NMR signal is the sum of contributions from many pathways, including the one shown. We may write this as

$$s(t;\phi_A,\phi_B,\phi_{rec}) = \sum_{path} s_{path}(t;\phi_A,\phi_B,\phi_{rec})$$

where the sum is taken over all possible signal pathways.

Now suppose that a 'reference' experiment is conducted, in which all phases ϕ_A, ϕ_B and ϕ_{rec} are equal to zero. The signal in the reference experiment is given by

$$s(t;0,0,0) = \sum_{path} s_{path}(t;0,0,0)$$

From Equation A.58, the signal contributions from each pathway have a simple relationship in the two experiments: They are related through

$$s_{path}(t;\phi_A,\phi_B,\phi_{rec}) = s_{path}(t;0,0,0)\exp\{-i\Phi_{path}\}$$

where Φ_{path} is the *total pathway phase*, given by

$$\Phi_{path} = \Delta p_A\phi_A + \Delta p_B\phi_B + \phi_{rec} \tag{A.59}$$

In the example above, the changes in coherence order are $\Delta p_A = +1$ and $\Delta p_B = -2$, so the total pathway phase is

$$\Phi_{path} = +\phi_A - 2\phi_B + \phi_{rec}$$

A.11.5 A sum theorem

Before proceeding, we require the following result.

Consider the following sum of n terms:

$$S = 1 + x + x^2 + x^3 + \ldots + x^{(\mathfrak{n}-2)} + x^{(\mathfrak{n}-1)} \tag{A.60}$$

where

$$x = \exp\{i\frac{2\pi\mathfrak{p}}{\mathfrak{n}}\} \tag{A.61}$$

and $\mathfrak{p}$ and $\mathfrak{n}$ are integers.

This sum has the following property:

$$S = \begin{cases} 0 \text{ if } \mathfrak{p} \neq \mathfrak{n} \times \text{integer} \\ \mathfrak{n} \text{ if } \mathfrak{p} = \mathfrak{n} \times \text{integer} \end{cases} \tag{A.62}$$

The theorem Equation A.62 may be proved in the following way. Multiply Equation A.60 by x on both sides:

$$Sx = x + x^2 + x^3 + \ldots + x^{(\mathfrak{n}-1)} + x^{\mathfrak{n}} \tag{A.63}$$

Now from the definition of x (Equation A.61), we have

$$x^{\mathfrak{n}} = \exp\{i2\pi\mathfrak{p}\} = 1$$

since $\mathfrak{p}$ is an integer. Hence Equation A.63 becomes

$$\begin{aligned} Sx &= x + x^2 + x^3 + \ldots + x^{(\mathfrak{n}-1)} + 1 \\ &= 1 + x + x^2 + x^3 + \ldots + x^{(\mathfrak{n}-1)} \end{aligned} \tag{A.64}$$

The right-hand sides of Equations A.64 and A.60 are equal. Hence, we have

$$Sx = S$$

which may be written as

$$S(x-1) = 0$$

Take the case that x is not equal to 1, so that $x - 1 \neq 0$. In this case, the sum S must vanish in order to satisfy the equality. If, on the other hand, x is equal to 1, then the sum S need not vanish, and the definition in Equation A.60 leads to the value $S = \mathfrak{n}$. We have, therefore, derived the following property of the sum S:

$$S = \begin{cases} 0 \text{ if } x \neq 1 \\ \mathfrak{n} \text{ if } x = 1 \end{cases}$$

Now from Equation A.61, x is only equal to 1 if $\mathfrak{p}$ is equal to an integer multiple of $\mathfrak{n}$. This proves the theorem Equation A.62.

A.11.6 Pathway selection I

The above theorem may be used to design a simple phase cycle. Suppose that NMR signals are added together with the phases being cycled according to the following four-step table ($\mathfrak{n} = 4$).

Cycle counter $\mathfrak{m}$	ϕ_A	ϕ_B	ϕ_{rec}
0	0	0	0
1	$\pi/2$	0	0
2	π	0	0
3	$3\pi/2$	0	0

(A.65)

The total number of transients $\mathfrak{N}$ is a multiple of 4. The phase cycle counter $\mathfrak{m}$ is given by $\mathfrak{m} = \text{mod}(\mathfrak{M}, 4)$, where the transient counter is $\mathfrak{M} = 0, 1, 2 \ldots \mathfrak{N} - 1$. The phase table is read from top to bottom again and again, adding together the NMR signals, until all $\mathfrak{N}$ transients have been acquired. This simple phase cycle is generated by the formulae

$$\begin{aligned} \phi_A &= \frac{2\pi}{4}\mathfrak{m} \\ \phi_B &= 0 \\ \phi_{rec} &= 0 \end{aligned}$$

In this and the following formulae, all phases are taken modulo 2π. For example, the following phases are all equivalent: $\{\ldots -3\pi/2, \pi/2, 5\pi/2, 9\pi/2 \ldots\}$. All of these equivalent phases are denoted as $\pi/2$ in the phase tables (sometimes, the computer software *requires* that phases are specified in the range 0 to 2π).

The signal component from a given coherence transfer pathway, at step $\mathfrak{m}$ in the phase cycle, is given by

$$s_{path}(t, \mathfrak{m}) = s_{path}(t, 0) \exp\{-i\Phi_{path}(\mathfrak{m})\}$$

where the pathway phase is equal to

$$\Phi_{\text{path}} = \Delta p_{\text{A}}\phi_{\text{A}} + \Delta p_{\text{B}}\phi_{\text{B}} + \phi_{\text{rec}}$$

In the present case, all phases are equal to zero except to ϕ_{A}. The pathway phase is therefore

$$\begin{aligned}\Phi_{\text{path}} &= \Delta p_{\text{A}}\phi_{\text{A}} \\ &= \frac{2\pi}{4}\Delta p_{\text{A}}\mathrm{m}\end{aligned}$$

The *total* signal from a certain pathway, summed over all four steps in the phase cycle, is therefore

$$s^{\text{tot}}_{\text{path}}(t) = \sum_{\mathrm{m}=0}^{3} s_{\text{path}}(t, \mathrm{m}) = s_{\text{path}}(t, 0)\sum_{\mathrm{m}=0}^{3} \exp\{-\mathrm{i}\frac{2\pi\Delta p_{\text{A}}\mathrm{m}}{4}\}$$

The sum on the right-hand side has the form of Equation A.62. The phase-cycled signal from a given pathway is therefore given by

$$s^{\text{tot}}_{\text{path}}(t) = \begin{cases} 0 & \text{if } \Delta p_{\text{A}} \neq 4 \times \text{integer} \\ 4s_{\text{path}}(t, 0) & \text{if } \Delta p_{\text{A}} = 4 \times \text{integer} \end{cases} \tag{A.66}$$

The phase-cycled pathway signal vanishes unless the change in order Δp_{A} is an integer multiple of four (including zero).

Since the coherence order before the first pulse is equal to zero, selection of the change in order Δp_{A} is the same as selecting the coherence order p after the first pulse sequence block A. The phase cycle in Equation A.65, therefore, allows signals passing through coherence orders $p = 0, \pm 4, \pm 8 \ldots$ between the pulse sequence blocks. If one disregards coherences with orders $|p| > 4$, then the allowed signal pathways are as follows:

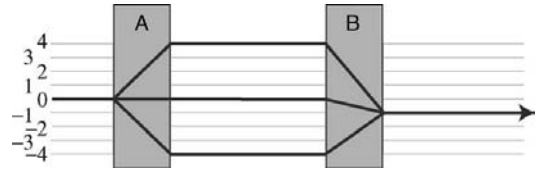

Figure A.18
Allowed signal pathways for Equation A.65.

Signals passing through all other pathways are suppressed:

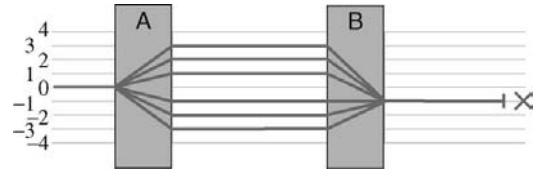

Figure A.19
Forbidden signal pathways for Equation A.65.

Note that the allowed pathways are separated in order by 4 units. This is a direct consequence of using four steps in the phase cycle.

A.11.7 Pathway selection II

Now suppose that one wants to detect signals passing through the following pathway:

$$0 \rightarrow +1 \rightarrow -1$$

while suppressing signals from neighbouring pathways.

Consider first the four-step phase cycle of Equation A.65. The table below shows the total phase Φ_{path} for the pathway $0 \to +1 \to -1$ at each step in the phase cycle, as specified from Equation A.59:

Cycle counter $\mathfrak{m}$	ϕ_{A}	ϕ_{B}	ϕ_{rec}	$\Phi_{\text{path}}(0 \to +1 \to -1)$
0	0	0	0	0
1	$\pi/2$	0	0	$\pi/2$
2	π	0	0	π
3	$3\pi/2$	0	0	$3\pi/2$

(A.67)

Since the total pathway phase varies from one step in the phase cycle to the next, the signals from the desired pathway $0 \to +1 \to -1$ cancel out exactly, under the phase cycle of Equation A.65, as predicted in Equation A.66.

Now suppose that the receiver phase ϕ_{rec} is changed in synchrony with the phase ϕ_{A}, in order to keep Φ_{path} constant for the desired pathway $0 \to +1 \to -1$. This may be done by setting the receiver phase equal to minus the last column in Equation A.67, providing

Cycle counter $\mathfrak{m}$	ϕ_{A}	ϕ_{B}	ϕ_{rec}	$\Phi_{\text{path}}(0 \to +1 \to -1)$
0	0	0	0	0
1	$\pi/2$	0	$-\pi/2$	0
2	π	0	$-\pi$	0
3	$3\pi/2$	0	$-3\pi/2$	0

The total pathway phase Φ_{path} is now equal to zero for all steps $\mathfrak{m}$, for the desired pathway $0 \to +1 \to -1$.

Phases may be converted into the interval 0 to 2π by the procedure $\phi \Rightarrow \text{mod}(\phi, 2\pi)$. We get the following table:

Cycle counter $\mathfrak{m}$	ϕ_{A}	ϕ_{B}	ϕ_{rec}
0	0	0	0
1	$\pi/2$	0	$3\pi/2$
2	π	0	π
3	$3\pi/2$	0	$\pi/2$

(A.68)

The phase cycle in Equation A.68 has $\Phi_{\text{path}} = 0$ for the pathway $0 \to +1 \to -1$, ensuring that signals passing through this pathway interfere constructively as the signals are accumulated.

Since ϕ_{A} is cycled in four steps, the phase cycle in Equation A.68 selects not only signals with Δp_{A}, but all signals obeying $\Delta p_{\text{A}} = +1 + 4 \times \text{integer}$, i.e. $\Delta p_{\text{A}} = \ldots -7, -3, +1, +5 \ldots$. If one disregards coherences with orders $|p| > 4$, then the allowed signal pathways are as follows:

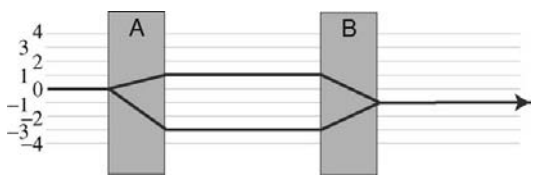

Figure A.20
Allowed signal pathways for Equation A.68.

Signals passing through all other pathways are suppressed:

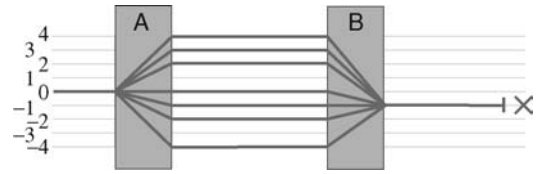

Figure A.21
Forbidden signal pathways for Equation A.68.

The four-step phase cycle in Equation A.68 again selects coherence orders in steps of four, but the motion of ϕ_{rec} in synchrony with ϕ_{A} shifts the centre position of the selection from order 0 to order +1.

It is often convenient to derive an explicit algorithm for calculating the phases. The total phase for the pathway $0 \rightarrow +1 \rightarrow -1$ is given by

$$\Phi_{\text{path}} = \Delta p_{\text{A}}\phi_{\text{A}} + \Delta p_{\text{B}}\phi_{\text{B}} + \phi_{\text{rec}} = +\phi_{\text{A}} - 2\phi_{\text{B}} + \phi_{\text{rec}} \tag{A.69}$$

since the pathway has $\Delta p_{\text{A}} = +1$ and $\Delta p_{\text{B}} = -2$. A constant pathway phase $\Phi_{\text{path}} = 0$ may, therefore, be imposed by using a receiver phase that satisfies the following equation:

$$\phi_{\text{rec}} = -\phi_{\text{A}} + 2\phi_{\text{B}} \tag{A.70}$$

The pulse phases in the phase cycle of Equation A.68 obey the following equations:

$$\begin{aligned} \phi_{\text{A}} &= \frac{2\pi}{4}\text{m} \\ \phi_{\text{B}} &= 0 \end{aligned} \tag{A.71}$$

This may be combined with Equation A.71 to give the following formula for the receiver phase:

$$\phi_{\text{rec}} = -\frac{2\pi}{4}\text{m} = -\frac{\pi}{2}\text{m}$$

This example illustrates a general principle for constructing phase cycles:

1. Identify the coherence transfer pathway of the *desirable* NMR signals.
2. Design the number of steps in the cycle according to the number of *neighbouring* signal pathways that must be suppressed.
3. Adjust the receiver phase on each step of the cycle to impose a constant total pathway phase Φ_{path} for the desired pathway.

A.11.8 Pathway selection III

A completely equivalent result may be obtained by cycling the phase ϕ_{B} of the second pulse sequence block B. If the phase cycle is constructed according to

$$\begin{aligned} \phi_{\text{A}}(\text{m}) &= 0 \\ \phi_{\text{B}}(\text{m}) &= \frac{2\pi\text{m}}{4} \end{aligned}$$

and the receiver phase is again adjusted to satisfy Equation A.70, then we get

$$\phi_{\text{rec}} = 2\frac{2\pi\text{m}}{4} = \pi\text{m}$$

This leads to the following $\mathfrak{n} = 4$ phase cycle:

Cycle counter $\mathfrak{m}$	ϕ_A	ϕ_B	ϕ_{rec}
0	0	0	0
1	0	$\pi/2$	π
2	0	π	0
3	0	$3\pi/2$	π

(A.72)

which has an identical effect to that in Equation A.68. Both cycles select the signal pathways in Figure A.20 and reject the signal pathways in Figure A.21.

A.11.9 Selection of a single pathway I

Suppose one is interested in selecting the *single* coherence transfer pathway $0 \rightarrow -3 \rightarrow -1$. The cycles given in Equations A.68 and A.72 do allow signals from this pathway, but they also allow signals from the pathway $0 \rightarrow +1 \rightarrow -1$.

In order to suppress signals from more coherence pathways, it is necessary to use more steps in the phase cycle. It is possible to select signals from the pathway $0 \rightarrow -3 \rightarrow -1$, at the same time as suppressing signals from all other pathways involving four-quantum coherences or lower, by using $\mathfrak{n} \geq 8$. A suitable phase cycle is

Cycle counter $\mathfrak{m}$	ϕ_A	ϕ_B	ϕ_{rec}
0	0	0	0
1	0	$\pi/4$	$3\pi/2$
2	0	$2\pi/4$	π
3	0	$3\pi/4$	$\pi/2$
4	0	$4\pi/4$	0
5	0	$5\pi/4$	$3\pi/2$
6	0	$6\pi/4$	π
7	0	$7\pi/4$	$\pi/2$

(A.73)

This eight-step cycle requires that the number of transients $\mathfrak{N}$ is a multiple of 8.

Since eight steps are used for ϕ_B, this cycle allows signal pathways with $\Delta p_A = -3 + 8 \times$ integer. If one disregards coherences with order larger than 4, only a single signal pathway is selected:

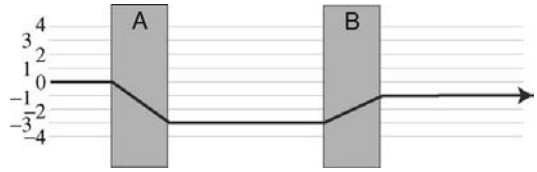

Figure A.22
Allowed signal pathway for Equation A.73.

All other signal pathways are suppressed:

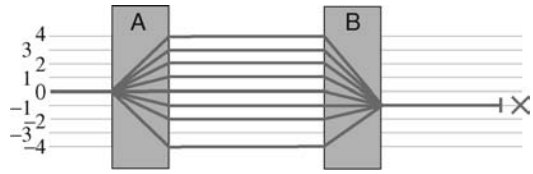

Figure A.23
Forbidden signal pathways for Equation A.73.

The phase cycle in Equation A.73 may be calculated in the systematic way developed above:

1. Identify $0 \rightarrow -3 \rightarrow -1$ as the desired signal pathway.

2. This pathway is characterized by $\Delta p_A = -3$ and $\Delta p_B = +2$. The pathway phase is therefore given by

$$\begin{aligned}\Phi_{path} &= \Delta p_A \phi_A + \Delta p_B \phi_B + \phi_{rec} \\ &= -3\phi_A + 2\phi_B + \phi_{rec}\end{aligned}$$

3. In order to suppress all other pathways with orders in the range $-5 < p < 5$, one requires at least eight phase cycle steps either for ϕ_A or ϕ_B (one can easily see this using Figure A.23: the seven orders $p = -2, -1 \ldots 3, 4$ must be suppressed between blocks A and B) . If one chooses to cycle ϕ_B, then the pulse phase definitions are

$$\begin{aligned}\phi_A &= 0 \\ \phi_B &= \frac{2\pi}{8}\mathrm{m} = \frac{\pi}{4}\mathrm{m}\end{aligned}$$

4. On each step of the phase cycle, adjust the receiver phase so as to hold the total pathway phase for $0 \rightarrow -3 \rightarrow -1$ equal to zero. This requires

$$\Phi_{path} = -3\phi_A + 2\phi_B + \phi_{rec} = 0$$

and hence

$$\phi_{rec} = 3\phi_A - 2\phi_B \tag{A.74}$$

leading to

$$\phi_{rec} = -2\frac{\pi}{4}\mathrm{m} = -\frac{\pi}{2}\mathrm{m}$$

This corresponds to the phase cycle given in Equation A.73 (after converting all phases into the range 0 to 2π).

A.11.10 Selection of a single pathway II

In the example above, suppose that we choose to cycle ϕ_A instead of ϕ_B. This time the definition of the pulse phases would be

$$\begin{aligned}\phi_A &= \frac{2\pi}{8}\mathrm{m} = \frac{\pi}{4}\mathrm{m} \\ \phi_B &= 0\end{aligned}$$

Equation A.74 then leads to

$$\phi_{\text{rec}} = \frac{3\pi}{4}\mathrm{m}$$

The phase cycle is therefore

Cycle counter m	ϕ_A	ϕ_B	ϕ_{rec}
0	0	0	0
1	$\pi/4$	0	$3\pi/4$
2	$2\pi/4$	0	$3\pi/2$
3	$3\pi/4$	0	$\pi/4$
4	$4\pi/4$	0	π
5	$5\pi/4$	0	$7\pi/4$
6	$6\pi/4$	0	$\pi/2$
7	$7\pi/4$	0	$5\pi/4$

(A.75)

This cycle has the same effect as that in Equation A.73.

On older NMR instruments, it may be easier to implement Equation A.73 (which employs receiver phase-shifts in multiples of $\pi/2$) than Equation A.75 (which employs smaller receiver phase shift values). This example shows that, although some phase cycles are fully equivalent mathematically, certain cycles may be more difficult to implement than others, because of hardware limitations.

A.11.11 Dual pathway selection

Suppose that it is desired to select signals arising from *two* different pathways, e.g. $0 \rightarrow +1 \rightarrow -1$ and $0 \rightarrow -1 \rightarrow -1$:

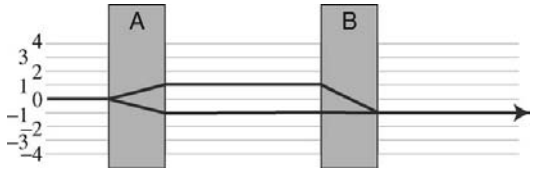

Figure A.24
Two coherence transfer pathways.

Such *dual pathway selection* is necessary for pure absorption two-dimensional spectroscopy using the States procedure (see Section 5.9.4). The two pathways given above are precisely those needed to obtain pure absorption COSY spectra (Section 16.1).

Selection of two pathways at the same time is accomplished by setting the number of steps in the cycle equal to the order separation between the two desired pathways. In the case above, this separation is equal to 2, so a two-step phase cycle is appropriate. The required phase cycle is a very simple one:

Cycle counter m	ϕ_A	ϕ_B	ϕ_{rec}
0	0	0	0
1	π	0	π

(A.76)

The phase cycle may be calculated formally by choosing one of the desired pathways (it doesn't matter which one), and following the systematic procedure given above. The pulse phase definitions are

$$\phi_{\mathrm{A}}(\mathrm{m}) = \frac{2\pi\mathrm{m}}{2} = \pi\mathrm{m}$$
$$\phi_{\mathrm{B}}(\mathrm{m}) = 0$$

The receiver phase may be worked out using the pathway $0 \rightarrow -1 \rightarrow -1$ (which has $\Delta p_{\mathrm{A}} = -1$ and $\Delta p_{\mathrm{B}} = 0$) as follows:

$$\begin{aligned}\Phi_{\mathrm{path}} &= \Delta p_{\mathrm{A}}\phi_{\mathrm{A}} + \Delta p_{\mathrm{B}}\phi_{\mathrm{B}} + \phi_{\mathrm{rec}} \\ &= -\phi_{\mathrm{A}} + \phi_{\mathrm{rec}}\end{aligned}$$

Setting $\Phi_{\mathrm{path}} = 0$ leads to the following relationship:

$$\phi_{\mathrm{rec}} = \phi_{\mathrm{A}}$$

and hence

$$\phi_{\mathrm{rec}} = \pi\mathrm{m}$$

as specified in Equation A.76.

As might be expected, this two-step phase cycle is not very selective. The following signal pathways are allowed:

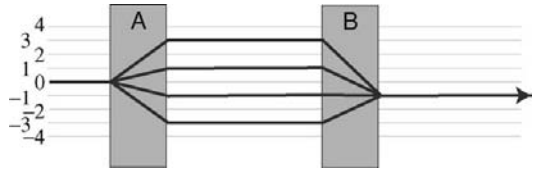

Figure A.25
Allowed signal pathways for Equation A.76.

while the following pathways are suppressed:

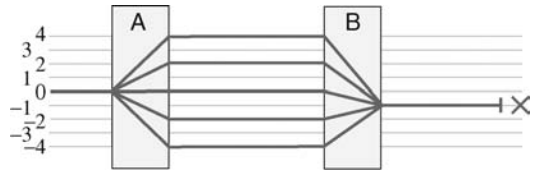

Figure A.26
Forbidden signal pathways for Equation A.76.

In particular, signals from the pathways $0 \rightarrow \pm 3 \rightarrow -1$ are allowed as well as the desired signals from $0 \rightarrow \pm 1 \rightarrow -1$.

It is not possible to select *only* the desired pair of pathways $0 \rightarrow \pm 1 \rightarrow -1$ while suppressing all others, using this particular approach to phase cycling. If necessary, this selection task may be accomplished by more sophisticated data-processing procedures[5] or by employing field gradient selection (see Appendix A.12).

A.11.12 Internal phases I

In general, each pulse sequence block may itself consist of many r.f. pulses, possibly with different phases. Phase cycling works properly only if the *relative* pulse phases *within* each block are rigorously conserved throughout the phase cycle.

For example, consider the four-step phase cycle in Equation A.68, and suppose that block A consists of a $(\pi/2)_x$ pulse and a $(\pi/2)_y$ pulse separated by a delay, while block B consists of a $(\pi/2)_{\bar{y}}$ pulse. This may be visualized as follows:

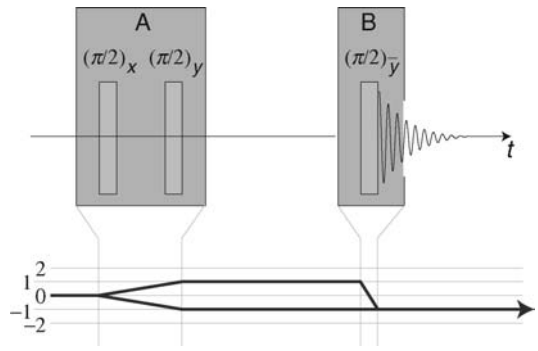

Figure A.27
Three pulses in two phase cycling blocks.

The phases of the pulses are related to those of the blocks as follows:

$$\begin{aligned}\phi_1 &= \phi_A \\ \phi_2 &= \phi_A + \pi/2 \\ \phi_3 &= \phi_A + 3\pi/2\end{aligned}$$

These relationships must be rigorously followed if the phase cycle is to work properly.

For example, the phase cycle given in Equation A.76 takes the following form for this three-pulse sequence:

Cycle counter m	ϕ_1	ϕ_2	ϕ_3	ϕ_{rec}
0	0	$\pi/2$	$3\pi/2$	0
1	π	$3\pi/2$	$3\pi/2$	π

(A.77)

The phase cycle determines which types of signal are allowed and which are suppressed. *The phase cycle does not determine the magnitude or phase of the allowed signals*. Those parameters depend on the internal phases of the pulses within each block, and must be determined using the detailed reasoning given in this book.

Note that a pulse sequence block may contain a single phase-shifted pulse, as for the third pulse in Figure A.27.

A.11.13 Internal phases II

Consider the INADEQUATE pulse sequence, as discussed in Section 16.2. The pulse sequence and coherence transfer pathway diagram may be interpreted in terms of two blocks as follows:

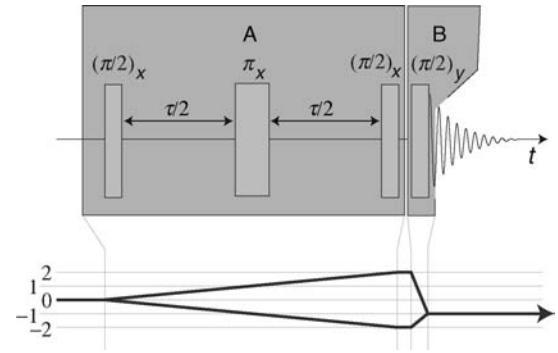

Figure A.28
INADEQUATE pulse sequence formulated as two blocks.

The first three pulses convert populations into (±2)-quantum coherences, and the last pulse converts the (±2)-quantum coherences into observable (−1)-quantum coherences.

The relationship between the four pulse phases and the two block phases is as follows:

$$\phi_1 = \phi_A \qquad \phi_2 = \phi_A$$
$$\phi_3 = \phi_A \qquad \phi_4 = \phi_B + \pi/2 \tag{A.78}$$

A four-step phase cycle for selecting the dual pathways $0 \rightarrow +2 \rightarrow -1$ and $0 \rightarrow -2 \rightarrow -1$ may be calculated using the arguments above:

Cycle counter m	ϕ_A	ϕ_B	ϕ_{rec}
0	0	0	0
1	0	$\pi/2$	$3\pi/2$
2	0	π	π
3	0	$3\pi/2$	$\pi/2$

(A.79)

An explicit phase cycle for this experiment is therefore

Cycle counter m	ϕ_1	ϕ_2	ϕ_3	ϕ_4	ϕ_{rec}
0	0	0	0	$\pi/2$	0
1	0	0	0	π	$3\pi/2$
2	0	0	0	$3\pi/2$	π
3	0	0	0	0	$\pi/2$

(A.80)

This phase cycle was used in Section 16.2.

Note that the phase of the last pulse starts at $\pi/2$. This has no bearing on the operation of the phase cycle, which only concerns *changes* in the relative phases of the pulse sequence blocks. The initial value of ϕ_4 is decided by external arguments. In the case of Equation A.80, the initial value $\phi_4 = \pi/2$ causes the spin-pair peaks to be in absorption mode, as discussed in Section 16.2.

A.11.14 Nested phase cycles I

Sometimes more than one stage of coherence transfer pathway selection is required in a pulse sequence. Consider, for example, the pulse sequence for double-quantum-filtered COSY, shown below:

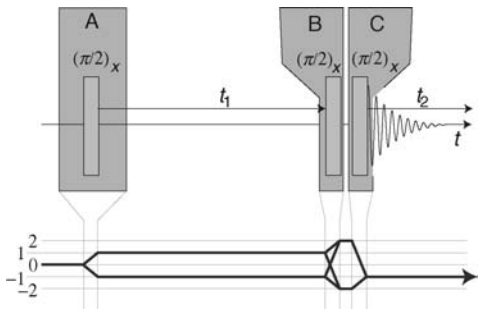

Figure A.29
Double-quantum-filtered COSY pulse sequence formulated as three blocks.

The indicated coherence transfer pathways may be selected by suppressing all signal paths that do not involve coherence order steps $\Delta p_A = \pm 1$ over the first block A, as well as those that do not involve coherence order steps $\Delta p_C = +1$ or -3 over the third block C.

The selection of coherence order steps $\Delta p_A = \pm 1$ implies that the block phase ϕ_A must be cycled in two steps. The selection of coherence order steps $\Delta p_C = +1$ or -3 implies that the block phase ϕ_C must be cycled in four steps. In order to select signal pathways with the desired values for both Δp_A and Δp_C, the phase cycles for blocks A and C are *nested*. This means that, for every step in the cycle of block A, a complete cycle of block C is performed. This leads to a full cycle consisting of $2 \times 4 = 8$ steps.

The mathematical function floor(x) proves to be useful for specifying nested phase cycles. The function floor(x) returns the largest integer that is not greater than x. It 'rounds down' the argument x to the next integer. Some examples are: floor(0.9) = 0; floor(1) = 1; floor(1.9) = 1; floor(-1.9) = -2.

A two-step phase cycle for ϕ_A, nested inside a four-step cycle for ϕ_C, may be specified as follows:

$$\phi_A = \frac{2\pi \mathrm{m}}{2} = \pi \mathrm{m}$$
$$\phi_B = 0$$
$$\phi_C = \frac{2\pi}{4}\mathrm{floor}(\mathrm{m}/2) = \frac{\pi}{2}\mathrm{floor}(\mathrm{m}/2)$$

The following table shows how the floor function generates the nested cycles:

Cycle counter m	floor(m/2)	ϕ_A	ϕ_B	ϕ_C
0	0	0	0	0
1	0	π	0	0
2	1	0	0	$\pi/2$
3	1	π	0	$\pi/2$
4	2	0	0	π
5	2	π	0	π
6	3	0	0	$3\pi/2$
7	3	π	0	$3\pi/2$

The value of ϕ_{rec} may be calculated for each step of the phase cycle by keeping the total phase for one of the desired pathways constant (once again, it doesn't matter which of the desired pathways one selects). For example, the pathway $0 \rightarrow +1 \rightarrow +2 \rightarrow -1$ has the following changes in coherence order: $\Delta p_{\text{A}} + 1$; $\Delta p_{\text{B}} = +1$; $\Delta p_{\text{C}} = -3$, which leads to the following condition:

$$\begin{aligned}\Phi_{\text{path}} &= \Delta p_{\text{A}}\phi_{\text{A}} + \Delta p_{\text{B}}\phi_{\text{B}} + \Delta p_{\text{C}}\phi_{\text{C}} + \phi_{\text{rec}} \\ &= +\pi\mathfrak{m} - \frac{3\pi}{2}\text{floor}(\mathfrak{m}/2) + \phi_{\text{rec}} \\ &= 0\end{aligned}$$

The receiver phase is therefore given by

$$\phi_{\text{rec}} = -\pi\mathfrak{m} + \frac{3\pi}{2}\text{floor}(\mathfrak{m}/2)$$

which leads to the following eight-step phase cycle:

Cycle counter $\mathfrak{m}$	ϕ_1	ϕ_2	ϕ_3	ϕ_{rec}
0	0	0	0	0
1	π	0	0	π
2	0	0	$\pi/2$	$3\pi/2$
3	π	0	$\pi/2$	$\pi/2$
4	0	0	π	π
5	π	0	π	0
6	0	0	$3\pi/2$	$\pi/2$
7	π	0	$3\pi/2$	$3\pi/2$

A.11.15 Nested phase cycles II

The nesting algorithm may be extended to any number of phase cycling steps. Suppose, for example, that a pulse sequence consists of four blocks, A, B, C and D, and that one wishes to select the steps in coherence order at blocks A, B and D. A nested phase cycle is constructed in which block A is cycled in $\mathfrak{n}_{\text{A}}$ steps, block B is cycled in $\mathfrak{n}_{\text{B}}$ steps, and block D is cycled in $\mathfrak{n}_D$ steps. The following algorithm does the trick:

$$\begin{aligned}\phi_{\text{A}} &= \frac{2\pi}{\mathfrak{n}_{\text{A}}}\mathfrak{m} \\ \phi_{\text{B}} &= \frac{2\pi}{\mathfrak{n}_{\text{B}}}\text{floor}(\frac{\mathfrak{m}}{\mathfrak{n}_{\text{A}}}) \\ \phi_{\text{C}} &= 0 \\ \phi_{\text{D}} &= \frac{2\pi}{\mathfrak{n}_{\text{D}}}\text{floor}(\frac{\mathfrak{m}}{\mathfrak{n}_{\text{A}}\mathfrak{n}_{\text{B}}})\end{aligned}$$

Note how the floor functions always act on the cycle counter $\mathfrak{m}$ divided by the total number of steps for all *previous* levels. For example, the specification for ϕ_{B} contains $\text{floor}(\mathfrak{m}/\mathfrak{n}_{\text{A}})$, while the specification for ϕ_{D} contains $\text{floor}(\mathfrak{m}/\mathfrak{n}_{\text{A}}\mathfrak{n}_{\text{B}})$.

The total number of steps in such a nested phase cycle is $\mathfrak{n} = \mathfrak{n}_{\text{A}}\mathfrak{n}_{\text{B}}\mathfrak{n}_{\text{D}}$.

The following table shows how the nesting works for the case $n_A = 2$, $n_B = 2$ and $n_D = 4$:

Cycle counter m	floor($m/2$)	floor($m/4$)	ϕ_A	ϕ_B	ϕ_C	ϕ_D
0	0	0	0	0	0	0
1	0	0	π	0	0	0
2	1	0	0	π	0	0
3	1	0	π	π	0	0
4	0	1	0	0	0	$\pi/2$
5	0	1	π	0	0	$\pi/2$
6	1	1	0	π	0	$\pi/2$
7	1	1	π	π	0	$\pi/2$
8	0	2	0	0	0	π
9	0	2	π	0	0	π
10	1	2	0	π	0	π
11	1	2	π	π	0	π
12	0	3	0	0	0	$3\pi/2$
13	0	3	π	0	0	$3\pi/2$
14	1	3	0	π	0	$3\pi/2$
15	1	3	π	π	0	$3\pi/2$

At each step, the receiver phase ϕ_{rec} may be calculated so as to give a total phase of zero for any one of the desired signal pathways.

As an example, consider a more sophisticated version of the INADEQUATE phase cycle, in which the first two pulses are cycled independently, as well as the last pulse:

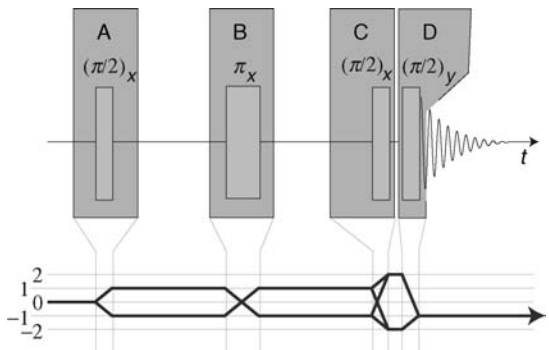

Figure A.30
INADEQUATE pulse sequence formulated as four blocks.

The pulse phases are related to the phases of the blocks through

$$\begin{aligned}\phi_1 &= \phi_A \\ \phi_2 &= \phi_B \\ \phi_3 &= \phi_C \\ \phi_4 &= \phi_D + \pi/2\end{aligned} \tag{A.81}$$

The phase of the first block ϕ_A is cycled in $n_A = 2$ steps (in order to select $\Delta p_A = \pm 1$); the phase of the second block ϕ_B is cycled in $n_B = 4$ steps (in order to select $\Delta p_B = \pm 2$); the phase of the fourth block ϕ_D is cycled in $n_D = 4$ steps (in order to select $\Delta p_D = +1$ and -3). The algorithm for the pulse phases is therefore

$$\begin{aligned}\phi_A(m) &= \frac{2\pi}{n_A} m = \pi m \\ \phi_B(m) &= \frac{2\pi}{n_B} \mathrm{floor}(\frac{m}{n_A}) = \frac{\pi}{2} \mathrm{floor}(\frac{m}{2}) \\ \phi_C(m) &= 0 \\ \phi_D(m) &= \frac{2\pi}{n_D} \mathrm{floor}(\frac{m}{n_A n_B}) = \frac{\pi}{2} \mathrm{floor}(\frac{m}{8})\end{aligned} \tag{A.82}$$

The total number of steps in this phase cycle is $n = n_A n_B n_D = 32$.

For each step in the phase cycle, the receiver phase may be calculated using the total phase equation for any one of desired pathways, e.g. $0 \rightarrow +1 \rightarrow -1 \rightarrow -2 \rightarrow -1$, which has $\Delta p_A = +1$, $\Delta p_B = -2$, $\Delta p_C = -1$, $\Delta p_D = +1$:

$$\begin{aligned}\Phi_{path} &= \Delta p_A \phi_A + \Delta p_B \phi_B + \Delta p_C \phi_C + \Delta p_D \phi_D + \phi_{rec} \\ &= +\pi m - \pi \mathrm{floor}(\frac{m}{2}) + \frac{\pi}{2} \mathrm{floor}(\frac{m}{8}) + \phi_{rec} \\ &= 0\end{aligned}$$

The algorithm for the receiver phase is therefore

$$\phi_{rec} = -\pi m + \pi \mathrm{floor}(\frac{m}{2}) - \frac{\pi}{2} \mathrm{floor}(\frac{m}{8}) \tag{A.83}$$

The explicit 32-step phase cycle is shown in Table A.1.

Whenever possible, it is best to allow the computer software to calculate the phases using an algorithm of the form given above, rather than by using laborious and error-prone phase tables. Unfortunately, pulse-programming software on commercial NMR instruments does not yet facilitate a rational approach.

Table A.1 A 32-step phase cycle for INADEQUATE.

Cycle counter $\mathfrak{m}$	ϕ_A	ϕ_B	ϕ_C	ϕ_D	ϕ_{rec}
0	0	0	0	$\pi/2$	0
1	π	0	0	$\pi/2$	π
2	0	$\pi/2$	0	$\pi/2$	π
3	π	$\pi/2$	0	$\pi/2$	0
4	0	π	0	$\pi/2$	0
5	π	π	0	$\pi/2$	π
6	0	$3\pi/2$	0	$\pi/2$	π
7	π	$3\pi/2$	0	$\pi/2$	0
8	0	0	0	π	$3\pi/2$
9	π	0	0	π	$\pi/2$
10	0	$\pi/2$	0	π	$\pi/2$
11	π	$\pi/2$	0	π	$3\pi/2$
12	0	π	0	π	$3\pi/2$
13	π	π	0	π	$\pi/2$
14	0	$3\pi/2$	0	π	$\pi/2$
15	π	$3\pi/2$	0	π	$3\pi/2$
16	0	0	0	$3\pi/2$	π
17	π	0	0	$3\pi/2$	0
18	0	$\pi/2$	0	$3\pi/2$	0
19	π	$\pi/2$	0	$3\pi/2$	π
20	0	π	0	$3\pi/2$	π
21	π	π	0	$3\pi/2$	0
22	0	$3\pi/2$	0	$3\pi/2$	0
23	π	$3\pi/2$	0	$3\pi/2$	π
24	0	0	0	0	$\pi/2$
25	π	0	0	0	$3\pi/2$
26	0	$\pi/2$	0	0	$3\pi/2$
27	π	$\pi/2$	0	0	$\pi/2$
28	0	π	0	0	$\pi/2$
29	π	π	0	0	$3\pi/2$
30	0	$3\pi/2$	0	0	$3\pi/2$
31	π	$3\pi/2$	0	0	$\pi/2$

A.11.16 Different ways of constructing phase cycles

Nested phase cycling may readily be extended to any number of coherence order selection steps. However, the number of required phase-cycle increments increases very rapidly with the number of selection steps. The nested approach usually becomes impractical for more than four or five selection steps. In certain cases, alternative strategies, such as *cogwheel phase cycling*, are far more economical with instrument time. The basic principle in cogwheel phase cycling is to advance all available phases at the same time in a concerted manner, like a set of interlocking cogs. In some cases, cogwheel phase

cycling is orders of magnitude more efficient than nested phase cycling. More details are given in *Further Reading*.

The required number of phase-cycle steps may also be greatly reduced by combining phase cycling with field gradient selection (see below).

A.12 Coherence Selection by Pulsed Field Gradients

Phase cycling requires numerous repetitions of an entire pulse sequence, with a different set of r.f. phases. This is associated with several problems:

1. The repetition of near-identical experiments is very inefficient with respect to experimental time.
2. Phase cycling makes high demands on instrumental performance, since the degree of destructive interference between consecutive signal acquisitions depends on the instrumental stability.
3. Irreproducibility in the initial condition of the spin system, due to imperfect thermal equilibration between transients, or temperature fluctuations, also degrades the performance of phase cycling.

Pulsed field gradients may be used to accomplish many of the same pathway selection tasks as phase cycling, while avoiding many of these problems. In essence, the use of field gradient pulses allows the different phase cycle steps to be performed in parallel in different parts of the sample volume, with a great advantage of speed. In addition, undesired signals from unwanted coherence transfer pathways destructively interfere over the entire sample volume, i.e. during the signal induction process itself, and not in the post-processing stage in the computer. The demands of instrumental reproducibility are therefore greatly reduced.

Nevertheless, field gradient selection does have some restrictions and technical difficulties of its own.

A.12.1 Field gradient dephasing

Consider a time-dependent field gradient $G_z(t)$ along the z-axis, applied to a homonuclear spin system between time points t_a and t_b:

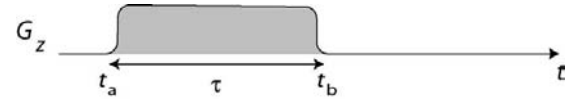

Figure A.31
A pulsed field gradient pulse.

During the pulse, the magnetic field is supplemented by a spatially dependent field $zG_z(t)$, where z is the spatial coordinate along the z-axis. The rotating-frame spin Hamiltonian during the field gradient pulse is given by

$$\widehat{\mathcal{H}}^0(\mathbf{r}, t) = \widehat{\mathcal{H}}_{\text{int}} + \widehat{\mathcal{H}}_G(\mathbf{r}, t) \tag{A.84}$$

where

$$\widehat{\mathcal{H}}_G(\mathbf{r}, t) = \omega_G(\mathbf{r}, t)\hat{I}_z$$

and the field-gradient-induced Larmor frequency shift is

$$\omega_{\text{G}}(\mathbf{r}, t) = -\gamma G_z(t)z$$

Crucially, the two terms in Equation A.84 commute, assuming the secular approximation for the internal spin Hamiltonian. This allows the spin system propagator to be factored into two commuting terms:

$$\widehat{U}(t_b, t_a) = \widehat{U}_{\text{int}}(t_b, t_a)\widehat{U}_G(t_b, t_a) \tag{A.85}$$

where the propagator under the field gradient pulse is

$$\widehat{U}_G(t_b, t_a) = \widehat{R}_z(\Phi_{\text{G}}(\mathbf{r})) \tag{A.86}$$

and the spatially dependent rotation angle is

$$\Phi_{\text{G}}(\mathbf{r}) = \int_{t_a}^{t_b} \omega_G(\mathbf{r}, t)\mathrm{d}t \tag{A.87}$$

Since the two terms in Equation A.85 commute, they may be considered independently. The propagator $\widehat{U}_{\text{int}}$ under the internal Hamiltonian may, therefore, be ignored for the moment, since it acts in just the same way as it does in the absence of the field gradient. One should simply remember that the internal spin interactions continue to act during the entire interval τ.

As shown in Equation A.86, the field gradient pulse induces a spatially dependent rotation around the z-axis, through the angle Φ_{G}. The effect on a Hamiltonian eigenstate is as follows:

$$\widehat{R}_z(\Phi_{\text{G}}(\mathbf{r}))|r\rangle = \exp\{\mathrm{i}M_r\Phi_{\text{G}}(\mathbf{r})\}|r\rangle$$

where M_r is the total Zeeman quantum number of the state

$$\hat{I}_z|r\rangle = M_r|r\rangle$$

The effect of the field gradient pulse on a spin coherence ρ_{rs} is therefore

$$\rho_{rs}(t_b) = \rho_{rs}(t_a)\exp\{\mathrm{i}p_{rs}\Phi_{\text{G}}(\mathbf{r})\}$$

where p_{rs} is the coherence order. This shows that the phase of a coherence p_{rs} is rotated by the field-gradient pulse, through the angle $p_{rs}\Phi_{\text{G}}(\mathbf{r})$. The phase rotation angle of the coherence is therefore proportional to

1. the coherence order p_{rs};
2. the amplitude of the gradient G_z, integrated over time (see Equation A.87);
3. the spatial coordinate z;
4. the gyromagnetic ratio γ.

After the field gradient pulse the phase of the coherence is given by

$$\phi_{rs}(\mathbf{r}) = \frac{2\pi z}{\Lambda_{rs}}$$

where Λ_{rs} is given by

$$\Lambda_{rs} = -2\pi \Big/ \left(p_{rs}\int_{t_a}^{t_b} \gamma B_z(t)\mathrm{d}t \right)$$

The phase of the coherence after the pulse, therefore, forms a helix with respect to the spatial coordinate z. The wavelength of the helix is given by Λ_{rs}:

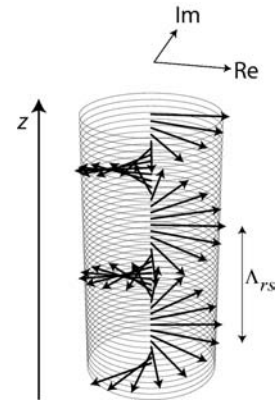

Figure A.32
Helix of phases for a coherence ρ_{rs} after a field gradient pulse.

The higher the coherence order p_{rs}, and the more powerful the gradient pulse, the shorter the wavelength Λ_{rs}.

If the wavelength Λ_{rs} is small compared with the length of the sample along the z-axis, the coherence ρ_{rs} dephases completely under the field gradient pulse. Any NMR signal that derives from this coherence vanishes, when integrated over the sample volume.

A.12.2 Pathway phase

Consider, now, a pulse sequence segment in which two field gradient pulses of different lengths and strengths bracket a pulse sequence block A. We follow a coherence transfer pathway involving order p_1 before the pulse and p_2 after the pulse:

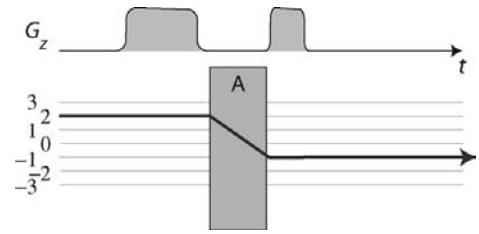

Figure A.33
Two pulsed field gradient pulses and a pulse sequence block.

The phase for the pathway $p_1 \rightarrow p_2$ is the equal to the accumulated phase for the two coherence orders:

$$\Phi_{p_1 \rightarrow p_2}(\mathbf{r}) = \frac{2\pi z}{\Lambda_{p_1 \rightarrow p_2}}$$

where the helix wavelength is given by

$$\Lambda_{p_1 \rightarrow p_2} = -2\pi \Big/ \left(p_1 \int_{t_{a1}}^{t_{b1}} \gamma B_z(t) \mathrm{d}t \; + \; p_2 \int_{t_{a2}}^{t_{b2}} \gamma B_z(t) \mathrm{d}t \right)$$

Here $\{t_{a1}, t_{b1}\}$ and $\{t_{a2}, t_{b2}\}$ are the start and end time points of the two field gradient pulses.

As before, if the helix wavelength $\Lambda_{p_1 \rightarrow p_2}$ is small compared with the sample length, all signals deriving from the pathway $p_1 \rightarrow p_2$ vanish when integrated over the sample volume.

A.12.3 Coherence transfer echoes

The wavelength of the phase helix for any coherence transfer pathway may be adjusted by varying the field gradient strengths or time profiles. If the wavelength $\Lambda_{p_1 \to p_2}$ becomes larger than the sample dimensions, then the defocusing effect is reversed and a *coherence transfer echo* is formed.

For example, suppose that the two field gradient pulses have an equal integral over time:

$$\int_{t_{a1}}^{t_{b1}} B_z(t)\mathrm{d}t = \int_{t_{a2}}^{t_{b2}} B_z(t)\,\mathrm{d}t$$

In this case, a coherence transfer echo is formed for pathways with the relationship

$$p_1 = -p_2$$

This condition includes the ordinary Hahn echo ($(+1) \to (-1)$).

Consider the case where the field gradient pulses are instead adjusted so that the first one has twice the integral of the second one:

$$\int_{t_{a1}}^{t_{b1}} B_z(t)\mathrm{d}t = 2\int_{t_{a2}}^{t_{b2}} B_z(t)\,\mathrm{d}t$$

The coherence transfer echo is formed under the following condition:

$$p_2 = -2p_1$$

The echo pathways now involve double-quantum coherences, e.g. $(+1) \to (-2)$ and $(-1) \to (+2)$.

A.12.4 Pathway selection

Signals from individual coherence transfer pathways may therefore be selected by adjusting the strengths and time profiles of the field gradient pulses so as to form a coherence transfer echo for the desired pathway, while winding tight phase helices for the undesired pathways. If the helix winding is sufficiently tight, then the signals from all unwanted pathways average to zero over the sample volume, leaving only the echo signal from the desired pathway. All of this may be achieved in a single transient.

It is often difficult to engineer the selection of more than one coherence transfer pathway at the same time using pulsed field gradients. Since at least two pathways are often required in, for example, pure-absorption two-dimensional experiments, it is common to combine field gradient selection with a short phase cycle.

If two or more pathways are required to generate the NMR signal, then the experiment must often be repeated with a different field gradient scheme in order to acquire the signals from complementary pathways independently. In such cases, field gradients lead to a loss in signal-to-noise, since some desirable signal is inevitably destroyed in each experiment.

A.12.5 Heteronuclear coherence transfer echoes

When pulsed field gradients are used for coherence transfer pathway selection in *heteronuclear* systems, one must take into account the different gyromagnetic ratios for the two species. Consider, for example, the case where an echo is formed by transferring coherences of order p_I of a spin species I to coherences of order p_S of a different spin species S. The condition for the formation of the echo in this case is as follows:

$$\gamma_I p_I \int_{t_{a1}}^{t_{b1}} B_z(t)\,\mathrm{d}t + \gamma_S p_S \int_{t_{a2}}^{t_{b2}} B_z(t)\,\mathrm{d}t = 0$$

For example, a (−1)-quantum coherence ^{1}H coherence forms an echo with a (+1)-quantum coherence ^{13}C coherence if the gradient pulse under which the ^{13}C coherence evolves has roughly four times the integral of the ^{1}H gradient pulse.

A.13 Bloch Equations

The isolated spins-1/2 ensemble may be treated using the magnetization vector, as described in Section 11.5. The motion of the magnetization vector during short strong r.f. pulses is described in Section 11.6, and the motion of the magnetization vector during intervals between pulses is described in Section 11.9. Relaxation and the resonance offset are taken into account between pulses, but not during the pulses.

If a pulse is weak or long then these results are not applicable, since off-resonance effects and relaxation are significant in this case. The *Bloch equations* provide a general framework for treating the simultaneous effects of relaxation, r.f. fields, and resonance offset for the isolated spin-1/2 ensemble.

The Bloch equations are a set of three coupled differential equations for the components of the magnetization vector. They may be written as follows:

$$\frac{\mathrm{d}}{\mathrm{d}t}\begin{pmatrix} M_x \\ M_y \\ M_z \end{pmatrix} = \begin{pmatrix} 0 & -\Omega^0 & \omega_{\mathrm{nut}} \sin\phi \\ \Omega^0 & 0 & -\omega_{\mathrm{nut}} \cos\phi \\ -\omega_{\mathrm{nut}} \sin\phi & \omega_{\mathrm{nut}} \cos\phi & 0 \end{pmatrix} \begin{pmatrix} M_x \\ M_y \\ M_z \end{pmatrix} - \begin{pmatrix} {T_2}^{-1} M_x \\ {T_2}^{-1} M_y \\ {T_1}^{-1}(M_z - 1) \end{pmatrix} \tag{A.88}$$

where Ω^0 is the resonance offset, ω_{nut} is the nutation frequency of the pulse, and ϕ is the phase of the r.f. field. Equation A.88 employs the definition of the magnetization vector given in Section 11.5, so that the thermal equilibrium value of the z-magnetization is $M_z = 1$.

It is readily shown that Equation A.88 leads to the behaviour described in Section 11.6, if the resonance offset Ω^0 and the relaxation rate constants ${T_1}^{-1}$ and ${T_2}^{-1}$ are all set to zero. Equation A.88 also leads to the behaviour described in Section 11.9, if the nutation frequency ω_{nut} is set to zero.

The Bloch equations are also capable of treating the complicated dynamics of spins that experience r.f. fields and relaxation at the same time. For example, suppose that an on-resonance r.f. field is applied for a very long time. What is the final value of the transverse magnetization?

The problem is complicated, because there are conflicting forces that create and destroy transverse magnetization. Transverse relaxation continually destroys transverse magnetization; so, at long times, one may expect that the transverse magnetization should be zero. However, at the same time, spin–lattice relaxation continously generates longitudinal magnetization, which is rotated into the transverse plane by the r.f. field. At a sufficiently long time, the system settles down into a *steady state*, under which these two tendencies are balanced.

The Bloch equations allow the steady-state value of the transverse magnetization to be predicted easily. If the phase ϕ and resonance offset Ω^0 are both equal to zero, then the equations for the time derivatives of the magnetization components M_y and M_z are

$$\frac{\mathrm{d}}{\mathrm{d}t} M_y = -{T_2}^{-1} M_y - \omega_{\mathrm{nut}} M_z$$

$$\frac{\mathrm{d}}{\mathrm{d}t} M_z = \omega_{\mathrm{nut}} M_y - {T_1}^{-1}(M_z - 1)$$

In the steady state, both time derivatives vanish, which allows one to solve for the two magnetization components:

$$M_y(\text{steady state}) = -\frac{T_2\omega_{\text{nut}}}{1 + T_1T_2\omega_{\text{nut}}^2}$$

$$M_z(\text{steady state}) = \frac{1}{1 + T_1T_2\omega_{\text{nut}}^2} \tag{A.89}$$

This shows that steady-state magnetization can exist, as long as T_2 is not too short and the nutation frequency ω_{nut} is not too large. However, if the nutation frequency ω_{nut} is strong compared with the relaxation rate constants, then the spin magnetization is destroyed in the steady state. This is called *saturation*.

Before 1966, most chemical applications of NMR were performed using *continuous-wave* spectrometers, which relied on the detection of the steady-state transverse magnetization, as a function of the static magnetic field. The Bloch equations lost their central place in NMR theory when the continuous-wave method was displaced by the Fourier transform technique, which is much more versatile and sensitive.

A.14 Chemical Exchange

In this appendix, I discuss the theory of spin dynamics in the presence of symmetrical two-site exchange, as used for the calculation of lineshapes in Section 19.5 and for the calculation of the two-dimensional exchange spectrum in Section 19.7.

Consider a symmetrical two-site exchange of the form:

$$A \underset{k}{\overset{k}{\rightleftharpoons}} B$$

where the species A and B have equal probability. The rate constants k are equal to the transition probability per unit time between the two species, and are the same for the forward and backward reaction.

The definition of the spin density operator, as given in Section 11.1, is

$$\hat{\rho} = \overline{|\psi\rangle\langle\psi|}$$

where the overbar indicates the average over all spin systems in the sample. If the sample contains $\mathbb{N}_{\text{A}}$ molecules of type A and $\mathbb{N}_{\text{B}}$ molecules of type B, then the density operator may be written as

$$\hat{\rho} = \frac{\mathbb{N}_{\text{A}}}{\mathbb{N}}\hat{\rho}^A + \frac{\mathbb{N}_{\text{B}}}{\mathbb{N}}\hat{\rho}^B$$

where the total number of molecules is $\mathbb{N} = \mathbb{N}_{\text{A}} + \mathbb{N}_{\text{B}}$. The density operator of spins in molecules A is given by

$$\hat{\rho}^A = \overline{|\psi\rangle\langle\psi|}^A$$

where the overbar indicates averaging over all molecules of type A. Similarly, the density operator of spins in molecules B is given by

$$\hat{\rho}^B = \overline{|\psi\rangle\langle\psi|}^B$$

where the overbar indicates averaging over all molecules of type B.

In the case of isolated spins-1/2, each density operator term may be written in terms of two populations and two coherences, which are defined in the usual way:

$$\rho^{\text{A}}_{\boxed{\alpha}} = \overline{\langle\alpha|\psi\rangle\langle\psi|\alpha\rangle}^A$$

$$\rho^{\text{A}}_{\boxed{+}} = \overline{\langle\alpha|\psi\rangle\langle\psi|\beta\rangle}^A$$

$$\rho^{\mathrm{B}}_{\boxed{-}} = \overline{\langle\beta|\psi\rangle\langle\psi|\alpha\rangle}^{B}$$

and so on.

We need to develop a dynamic equation for the four populations and four coherences, under the influence of the spin Hamiltonian, as well as the chemical exchange process. The behaviour of the spins under the spin Hamiltonian is called *coherent dynamics*, since the spin Hamiltonian is the same for all molecules of a certain type. The exchange behaviour is termed *incoherent dynamics*, since the precise instant at which each molecule changes state is unpredictable.

A.14.1 The incoherent dynamics

Consider first *only* the exchange process, omitting the magnetic fields and other interactions. Consider the term $\rho^{\mathrm{A}}_{\boxed{\alpha}}$, which represents the population of state $|\alpha\rangle$, averaging over the $\mathbb{N}_{\mathrm{A}}$ molecules that are in state A. Imagine the fate of this population during a small interval of time $\mathrm{d}t$.

On average, $k\mathbb{N}_{\mathrm{A}}\mathrm{d}t$ molecules change state from A to B in an interval $\mathrm{d}t$, carrying their spins with them. The contribution to $\rho^{\mathrm{A}}_{\boxed{\alpha}}$ from these spins will therefore be lost. However, at the same time, the population $\rho^{\mathrm{A}}_{\boxed{\alpha}}$ receives an influx from the $k\mathbb{N}_{\mathrm{B}}\mathrm{d}t$ spins that change their state in the opposite direction, from B to A. These spins carry their population $\rho^{\mathrm{B}}_{\boxed{\alpha}}$ with them.

If one assumes that the spin states do not change under the exchange process (which is a good approximation if the jumps are very fast), then the equation of motion for the population $\rho^{\mathrm{A}}_{\boxed{\alpha}}$, taking into account only the exchange process, is

$$\frac{\mathrm{d}}{\mathrm{d}t}\rho^{\mathrm{A}}_{\boxed{\alpha}} = -k\rho^{\mathrm{A}}_{\boxed{\alpha}} + k\rho^{\mathrm{B}}_{\boxed{\alpha}} \qquad \text{(exchange only)}$$

Similarly, the equation of motion for $\rho^{\mathrm{B}}_{\boxed{\alpha}}$, taking into account only the exchange process, is

$$\frac{\mathrm{d}}{\mathrm{d}t}\rho^{\mathrm{B}}_{\boxed{\alpha}} = -k\rho^{\mathrm{B}}_{\boxed{\alpha}} + k\rho^{\mathrm{A}}_{\boxed{\alpha}} \qquad \text{(exchange only)}$$

These equations may be combined to obtain

$$\frac{\mathrm{d}}{\mathrm{d}t}\begin{pmatrix}\rho^{\mathrm{A}}_{\boxed{\alpha}}\\ \rho^{\mathrm{B}}_{\boxed{\alpha}}\end{pmatrix} = \begin{pmatrix}-k & +k\\ +k & -k\end{pmatrix}\begin{pmatrix}\rho^{\mathrm{A}}_{\boxed{\alpha}}\\ \rho^{\mathrm{B}}_{\boxed{\alpha}}\end{pmatrix} \qquad \text{(exchange only)}$$

An equivalent equation is obtained for each component of the density operator. For example, for the (-1)-quantum coherences we get

$$\frac{\mathrm{d}}{\mathrm{d}t}\begin{pmatrix}\rho^{\mathrm{A}}_{\boxed{-}}\\ \rho^{\mathrm{B}}_{\boxed{-}}\end{pmatrix} = \begin{pmatrix}-k & +k\\ +k & -k\end{pmatrix}\begin{pmatrix}\rho^{\mathrm{A}}_{\boxed{-}}\\ \rho^{\mathrm{B}}_{\boxed{-}}\end{pmatrix} \qquad \text{(exchange only)} \tag{A.90}$$

These equations assume that the chemical exchange is a *Markow process*, implying that the probability of a jump during a small interval $\mathrm{d}t$ is independent of the previous history of the molecule. In practice, this is a good approximation for chemical reactions.

A.14.2 The coherent dynamics

The spins also evolve under their spin interactions. For example, if exchange were absent, then the rotating-frame (-1)-quantum coherences of spins in molecules of type A evolve according to

$$\rho^{\mathrm{A}}_{\boxed{-}}(t_b) = \rho^{\mathrm{A}}_{\boxed{-}}(t_a)\exp\{(\mathrm{i}\Omega^0_A - \lambda)\tau\} \qquad \text{(no exchange)}$$

where τ is the interval between time points t_a and t_b, and λ is the natural decay rate constant. This equation may be differentiated to obtain

$$\frac{\mathrm{d}}{\mathrm{d}t}\rho^{\mathrm{A}}_{[-]} = (\mathrm{i}\Omega^0_A - \lambda)\rho^{\mathrm{A}}_{[-]} \qquad \text{(no exchange)}$$

The analogous equation for the (−1)-quantum coherences of spins in molecules of type B is

$$\frac{\mathrm{d}}{\mathrm{d}t}\rho^{\mathrm{B}}_{[-]} = (\mathrm{i}\Omega^0_B - \lambda)\rho^{\mathrm{B}}_{[-]} \qquad \text{(no exchange)}$$

These equations may be combined to give

$$\frac{\mathrm{d}}{\mathrm{d}t}\begin{pmatrix}\rho^{\mathrm{A}}_{[-]}\\ \rho^{\mathrm{B}}_{[-]}\end{pmatrix} = \begin{pmatrix}\mathrm{i}\Omega^0_A - \lambda & 0\\ 0 & \mathrm{i}\Omega^0_B - \lambda\end{pmatrix}\begin{pmatrix}\rho^{\mathrm{A}}_{[-]}\\ \rho^{\mathrm{B}}_{[-]}\end{pmatrix} \qquad \text{(no exchange)} \tag{A.91}$$

A.14.3 The spectrum

In practice, exchange and coherent evolution takes place at the same time. This may be taken into account by simply adding Equations A.90 and A.91 together. We get

$$\frac{\mathrm{d}}{\mathrm{d}t}\begin{pmatrix}\rho^{\mathrm{A}}_{[-]}\\ \rho^{\mathrm{B}}_{[-]}\end{pmatrix} = \mathbf{L}_{[-]}\begin{pmatrix}\rho^{\mathrm{A}}_{[-]}\\ \rho^{\mathrm{B}}_{[-]}\end{pmatrix} \tag{A.92}$$

where the matrix $\mathbf{L}_{[-]}$ is equal to

$$\mathbf{L}_{[-]} = \begin{pmatrix}\mathrm{i}\Omega^0_A - \lambda - k & +k\\ +k & \mathrm{i}\Omega^0_B - \lambda - k\end{pmatrix}$$

In order to calculate the NMR spectrum, we need to figure out how the (−1)-quantum coherences evolve in time. This is easily done by integrating Equation A.92:

$$\begin{pmatrix}\rho^{\mathrm{A}}_{[-]}(t)\\ \rho^{\mathrm{B}}_{[-]}(t)\end{pmatrix} = \mathbf{V}_{[-]}(t)\begin{pmatrix}\rho^{\mathrm{A}}_{[-]}(0)\\ \rho^{\mathrm{B}}_{[-]}(0)\end{pmatrix}$$

where the propagator $\mathbf{V}_{[-]}$ is given by

$$\mathbf{V}_{[-]}(t) = \exp\{\mathbf{L}_{[-]}t\}$$

As shown in Section 6.5.8[2] the exponential may be written as follows:

$$\exp\{\mathbf{L}_{[-]}t\} = \mathbf{X}_{[-]}\exp\{\mathbf{D}_{[-]}t\}\mathbf{X}_{[-]}{}^{-1}$$

where $\mathbf{X}_{[-]}$ is a matrix whose columns are given by the eigenvectors of $\mathbf{L}_{[-]}$, $\mathbf{X}_{[-]}{}^{-1}$ is the inverse of $\mathbf{X}_{[-]}$, and $\mathbf{D}_{[-]}$ is a diagonal matrix with diagonal elements equal to the eigenvalues of $\mathbf{L}_{[-]}$. Evaluation of the eigenvalues and eigenvectors gives the following formulae:

$$\mathbf{D}_{[-]} = \begin{pmatrix}d_1 & 0\\ 0 & d_2\end{pmatrix}$$

$$\mathbf{X}_{\boxed{-}} = \begin{pmatrix} -\mathrm{i}(2\mathbb{R} + \Omega_\Delta) & \mathrm{i}(2\mathbb{R} - \Omega_\Delta) \\ 2k & 2k \end{pmatrix}$$

$$\mathbf{X}_{\boxed{-}}^{-1} = \frac{1}{8Rk} \begin{pmatrix} 2\mathrm{i}k & 2\mathbb{R} - \Omega_\Delta \\ -2\mathrm{i}k & 2\mathbb{R} + \Omega_\Delta \end{pmatrix}$$

where

$$\Omega_\Delta = \Omega_A^0 - \Omega_B^0$$

$$\mathbb{R} = \sqrt{(\Omega_\Delta/2)^2 - k^2}$$

and the two eigenvalues are

$$d_1 = \overline{\Omega} - \mathrm{i}\mathbb{R} - k - \lambda$$

$$d_2 = \overline{\Omega} + \mathrm{i}\mathbb{R} - k - \lambda$$

Here, $\overline{\Omega}$ is defined in Equation 19.5 as

$$\overline{\Omega} = \frac{1}{2}(\Omega_A^0 + \Omega_B^0)$$

The complex quantity $\mathbb{R}$ is related to the real quantity R defined in Equation 19.5 as follows:

$$\mathbb{R} = R \qquad \text{if } k < \Omega_\Delta/2$$

$$\mathbb{R} = \mathrm{i}R \qquad \text{if } k \geq \Omega_\Delta/2$$

Since $\mathbf{D}_{\boxed{-}}$ is diagonal, the exponential is given by (see Section 6.5)

$$\exp\{\mathbf{D}_{\boxed{-}}t\} = \begin{pmatrix} \exp\{d_1 t\} & 0 \\ 0 & \exp\{d_2 t\} \end{pmatrix}$$

If the (-1)-quantum coherences are excited by a $(\pi/2)_x$ pulse, then the initial coherences are

$$\begin{pmatrix} \rho^{\mathrm{A}}_{\boxed{-}}(0) \\ \rho^{\mathrm{B}}_{\boxed{-}}(0) \end{pmatrix} = \frac{1}{4\mathrm{i}} \begin{pmatrix} 1 \\ 1 \end{pmatrix}$$

The (-1)-quantum part of the spin density operator at time t is therefore

$$\begin{pmatrix} \rho^{\mathrm{A}}_{\boxed{-}}(t) \\ \rho^{\mathrm{B}}_{\boxed{-}}(t) \end{pmatrix} = \frac{1}{4\mathrm{i}} \mathbf{X}_{\boxed{-}} \exp\{\mathbf{D}_{\boxed{-}}t\} \mathbf{X}_{\boxed{-}}^{-1} \cdot \begin{pmatrix} 1 \\ 1 \end{pmatrix}$$

The quadrature NMR signal is proportional to the amplitude of the (-1)-quantum coherences, multiplied by 2i (ignoring the receiver and digitizer phase). The time-domain signal may therefore be written as

$$s(t) = (\,2\mathrm{i}\,, \quad 2\mathrm{i}\,) \cdot \begin{pmatrix} \rho^{\mathrm{A}}_{\boxed{-}}(t) \\ \rho^{\mathrm{B}}_{\boxed{-}}(t) \end{pmatrix}$$

$$= \frac{1}{2}(\,1\,, \quad 1\,) \cdot \mathbf{X}_{\boxed{-}} \exp\{\mathbf{D}_{\boxed{-}}t\} \mathbf{X}_{\boxed{-}}^{-1} \cdot \begin{pmatrix} 1 \\ 1 \end{pmatrix}$$

Since $\mathbf{D}_{\boxed{-}}$ has two eigenvalues, the signal is given by the sum of two exponential decays, and has the form

$$s(t) = \frac{1}{2}(1 + \frac{\mathrm{i}k}{\mathbb{R}}) \exp\{d_1 t\} + \frac{1}{2}(1 - \frac{\mathrm{i}k}{\mathbb{R}}) \exp\{d_2 t\}$$

FT of the signal gives two Lorentzians, as in Equations 19.4 and 19.6.

A.14.4 Longitudinal magnetization exchange

The calculation of longitudinal magnetization exchange must take into account the transitions between state $|\alpha\rangle$ and state $|\beta\rangle$ through spin–lattice relaxation processes, as well as the chemical exchange of molecules.

For example, the population $\rho^{\mathrm{A}}_{\boxed{\alpha}}$ is converted into $\rho^{\mathrm{A}}_{\boxed{\beta}}$ according to the spin–lattice transition probability W (see Section 20.3.6), and is also converted into $\rho^{\mathrm{B}}_{\boxed{\alpha}}$ by the chemical exchange. A suitable dynamic equation for the two pairs of populations is therefore

$$\frac{\mathrm{d}}{\mathrm{d}t} \begin{pmatrix} \rho^{\mathrm{A}}_{\boxed{\alpha}} \\ \rho^{\mathrm{A}}_{\boxed{\beta}} \\ \rho^{\mathrm{B}}_{\boxed{\alpha}} \\ \rho^{\mathrm{B}}_{\boxed{\beta}} \end{pmatrix} = \mathbf{L}_{\mathrm{pop}} \begin{pmatrix} \rho^{\mathrm{A}}_{\boxed{\alpha}} \\ \rho^{\mathrm{A}}_{\boxed{\beta}} \\ \rho^{\mathrm{B}}_{\boxed{\alpha}} \\ \rho^{\mathrm{B}}_{\boxed{\beta}} \end{pmatrix}$$

where

$$\mathbf{L}_{\mathrm{pop}} = \begin{pmatrix} -W-k & W & k & 0 \\ W & -W-k & 0 & k \\ k & 0 & -W-k & W \\ 0 & k & W & -W-k \end{pmatrix}$$

This equation neglects the asymmetry in the upwards and downwards transition probabilities (see Section 20.3.6), and assumes that the spin–lattice relaxation rate constants are the same in the two types of molecule. Since this equation neglects the difference in the upwards and downwards transition probabilities, it does not lead to the correct thermal equilibrium magnetization, but this defect is of no account when applied to the mixing interval of a two-dimensional exchange experiment. The phase cycling anyway removes the signal contribution from the magnetization that has been thermally equilibrated during τ_m.

The z-magnetization components are proportional to the difference in the populations of the $|\alpha\rangle$ and $|\beta\rangle$ states:

$$\begin{aligned} \langle \hat{I}_z \rangle^{\mathrm{A}} &\sim \rho^{\mathrm{A}}_{\boxed{\alpha}} - \rho^{\mathrm{A}}_{\boxed{\beta}} \\ \langle \hat{I}_z \rangle^{\mathrm{B}} &\sim \rho^{\mathrm{B}}_{\boxed{\alpha}} - \rho^{\mathrm{B}}_{\boxed{\beta}} \end{aligned}$$

The differential equation for the Zeeman components is therefore

$$\frac{\mathrm{d}}{\mathrm{d}t} \begin{pmatrix} \langle \hat{I}_z \rangle^{\mathrm{A}} \\ \langle \hat{I}_z \rangle^{\mathrm{B}} \end{pmatrix} = \mathbf{L}_z \begin{pmatrix} \langle \hat{I}_z \rangle^{\mathrm{A}} \\ \langle \hat{I}_z \rangle^{\mathrm{B}} \end{pmatrix} \tag{A.93}$$

where

$$\mathbf{L}_z = \begin{pmatrix} -2W - k & k \\ k & -2W - k \end{pmatrix}$$

The relevant eigenvalue and eigenvector matrices in this case are

$$\mathbf{D}_z = \begin{pmatrix} d_1 & 0 \\ 0 & d_2 \end{pmatrix}$$

$$\mathbf{X}_z = \begin{pmatrix} -1 & 1 \\ 1 & 1 \end{pmatrix}$$

$$\mathbf{X}_z{}^{-1} = \frac{1}{2}\begin{pmatrix} -1 & 1 \\ 1 & 1 \end{pmatrix}$$

where the two eigenvalues are

$$d_1 = -2k - 2W = -2k - T_1{}^{-1}$$
$$d_2 = -2W = -T_1{}^{-1}$$

The amplitude for Zeeman magnetization transfer from molecules A to molecules B is therefore given by

$$a_{\mathrm{A}\to\mathrm{B}}(\tau_m) = (0\,, \quad 1) \cdot \mathbf{X}_z \exp\{\mathbf{D}_z\tau_m\}\mathbf{X}_z{}^{-1} \cdot \begin{pmatrix} 1 \\ 0 \end{pmatrix}$$

which evaluates to

$$a_{\mathrm{A}\to\mathrm{B}}(\tau_m) = \sinh(k\tau_m)\exp\{-(k + T_1{}^{-1})\tau_m\}$$

Similarly, the amplitude for Zeeman magnetization to remain on the molecules A is

$$a_{\mathrm{A}\to\mathrm{A}}(\tau_m) = (1\,, \quad 0) \cdot \mathbf{X}_z \exp\{\mathbf{D}_z\tau_m\}\mathbf{X}_z{}^{-1} \cdot \begin{pmatrix} 1 \\ 0 \end{pmatrix}$$

which evaluates to

$$a_{\mathrm{A}\to\mathrm{A}}(\tau_m) = \cosh(k\tau_m)\exp\{-(k + T_1{}^{-1})\tau_m\}$$

The amplitudes of the diagonal peaks in a two-site two-dimensional exchange spectrum are therefore

$$a_{\mathrm{diag}} = a_{\mathrm{A}\to\mathrm{A}} = a_{\mathrm{B}\to\mathrm{B}} = \cosh(k\tau_m)\exp\{-(k + T_1{}^{-1})\tau_m\} \tag{A.94}$$

The amplitudes of the cross-peaks are

$$a_{\mathrm{cross}} = a_{\mathrm{A}\to\mathrm{B}} = a_{\mathrm{B}\to\mathrm{A}} = \sinh(k\tau_m)\exp\{-(k + T_1{}^{-1})\tau_m\} \tag{A.95}$$

as in Equation 19.7.

A.15 Solomon Equations

The relaxation equations for the populations in an ensemble of homonuclear two-spin systems may be cast in the following form:

$$\frac{\mathrm{d}}{\mathrm{d}t}\mathbb{P} = \mathbb{W}_{\mathrm{P}}\mathbb{P}$$

where the population vector is

$$\mathbb{P} = \begin{pmatrix} \rho_{\boxed{\alpha\alpha}} \\ \rho_{\boxed{\alpha\beta}} \\ \rho_{\boxed{\beta\alpha}} \\ \rho_{\boxed{\beta\beta}} \end{pmatrix}$$

and the kinetic matrix for the populations is

$$\mathbb{W}_{\mathrm{P}} = \begin{pmatrix} (-W_{\boxed{\alpha-}} - W_{\boxed{-\alpha}} - W_{\boxed{--}}) & W_{\boxed{\alpha+}} & W_{\boxed{+\alpha}} & W_{\boxed{++}} \\ W_{\boxed{\alpha-}} & (-W_{\boxed{\alpha+}} - W_{\boxed{-+}} - W_{\boxed{-\beta}}) & W_{\boxed{+-}} & W_{\boxed{+\beta}} \\ W_{\boxed{-\alpha}} & W_{\boxed{-+}} & (-W_{\boxed{+\alpha}} - W_{\boxed{+-}} - W_{\boxed{\beta-}}) & W_{\boxed{\beta+}} \\ W_{\boxed{--}} & W_{\boxed{-\beta}} & W_{\boxed{\beta-}} & (-W_{\boxed{++}} - W_{\boxed{+\beta}} - W_{\boxed{\beta+}}) \end{pmatrix}$$

The diagonal elements ensure that the sum of all populations remains constant. The transition probabilities $W_{\boxed{\alpha-}}$, $W_{\boxed{-\alpha}}$ ... are given in Equation 20.10.

In order to define the state of the ensemble in terms of product operators, introduce the *Zeeman order vector*:

$$\mathbb{Z} = \begin{pmatrix} \widehat{\langle 1 \rangle} \\ \langle \hat{I}_{1z} \rangle \\ \langle \hat{I}_{2z} \rangle \\ \langle 2\hat{I}_{1z}\hat{I}_{2z} \rangle \end{pmatrix}$$

The vector of populations may be transformed into the Zeeman order vector as follows:

$$\mathbb{Z} = \mathbb{T}_{\mathrm{ZP}}\mathbb{P}$$

where the transformation matrix is

$$\mathbb{T}_{\mathrm{ZP}} = \frac{1}{2}\begin{pmatrix} 1 & 1 & 1 & 1 \\ 1 & 1 & -1 & -1 \\ 1 & -1 & 1 & -1 \\ 1 & -1 & -1 & 1 \end{pmatrix}$$

The kinetic matrix may be transformed between the two bases using

$$\mathbb{W}_Z = \mathbb{T}_{ZP}\mathbb{W}_P\mathbb{T}_{PZ}$$

where

$$\mathbb{T}_{PZ} = \mathbb{T}_{ZP}{}^{-1} = \mathbb{T}_{ZP}$$

The result is

$$\mathbb{W}_Z = \begin{pmatrix} 0 & 0 & 0 & 0 \\ \mathbb{B}(W_1+W_2) & -(W_0+2W_1+W_2) & W_0-W_2 & \mathbb{B}W_2 \\ \mathbb{B}(W_1+W_2) & W_0-W_2 & -(W_0+2W_1+W_2) & \mathbb{B}W_2 \\ 0 & \mathbb{B}W_1 & \mathbb{B}W_1 & -4W_1 \end{pmatrix} \tag{A.96}$$

The equation of motion of the Zeeman order vector $\mathbb{Z}$ is therefore

$$\frac{\mathrm{d}}{\mathrm{d}t}\mathbb{Z} = \mathbb{W}_Z\mathbb{Z} \tag{A.97}$$

The thermal equilibrium value of the Zeeman order vector is defined by

$$\frac{\mathrm{d}}{\mathrm{d}t}\mathbb{Z}_{eq} = \mathbb{W}_Z\mathbb{Z}_{eq} = 0$$

and is given by

$$\mathbb{Z}_{eq} \cong \begin{pmatrix} 1 \\ \frac{1}{2}\mathbb{B} \\ \frac{1}{2}\mathbb{B} \\ 0 \end{pmatrix} \tag{A.98}$$

to first order in the Boltzmann factor $\mathbb{B}$, which is very small. Hence, Equation A.97 may be written as:

$$\frac{\mathrm{d}}{\mathrm{d}t}(\mathbb{Z}-\mathbb{Z}_{eq}) = \mathbb{W}_Z(\mathbb{Z}-\mathbb{Z}_{eq}) \tag{A.99}$$

Since the difference vector $\mathbb{Z}-\mathbb{Z}_{eq}$ has elements that are only of the order of the Boltzmann factor $\mathbb{B}$, it is possible to drop elements of the order $\mathbb{B}$ in the kinetic matrix $\mathbb{W}_Z$, in order to obtain results that are accurate to first order in the Boltzmann factor. The expression Equation A.96, therefore, may be replaced by

$$\mathbb{W}_Z \cong \begin{pmatrix} 0 & 0 & 0 & 0 \\ 0 & -(W_0+2W_1+W_2) & W_0-W_2 & 0 \\ 0 & W_0-W_2 & -(W_0+2W_1+W_2) & 0 \\ 0 & 0 & 0 & -4W_1 \end{pmatrix}$$

providing the matrix $\mathbb{W}_Z$ is used in the context of Equation A.99. The block-diagonal form of this matrix allows the central two rows and columns to be extracted, giving

$$\frac{\mathrm{d}}{\mathrm{d}t}\begin{pmatrix}\langle\hat{I}_{1z}\rangle\\ \langle\hat{I}_{2z}\rangle\end{pmatrix} = \begin{pmatrix}-R_{\text{auto}} & R_{\text{cross}}\\ R_{\text{cross}} & -R_{\text{auto}}\end{pmatrix}\begin{pmatrix}\langle\hat{I}_{1z}\rangle - \langle\hat{I}_{1z}\rangle^{\text{eq}}\\ \langle\hat{I}_{2z}\rangle - \langle\hat{I}_{2z}\rangle^{\text{eq}}\end{pmatrix}$$

which are the Solomon equations, with

$$\begin{aligned} R_{\text{auto}} &= W_0 + 2W_1 + W_2\\ R_{\text{cross}} &= W_0 - W_2 \end{aligned}$$

as used in the text.

The treatment given here is readily generalized by allowing pairs of transition probabilities such as $W_{\boxed{-\alpha}}$ and $W_{\boxed{-\beta}}$ to be different, in order to take into account cross-correlation effects (see Section 20.8). This leads to the *generalized Solomon equations*, in which the two-spin order $\langle 2\hat{I}_{1z}\hat{I}_{2z}\rangle$ participates in the dynamic equations together with the one-spin orders $\langle\hat{I}_{1z}\rangle$ and $\langle\hat{I}_{2z}\rangle$ (see *Further Reading*).

A.16 Cross-Relaxation Dynamics

The equation of motion for the magnetization exchange between spins I_1 and I_2 under the mixing interval of a NOESY experiment is given by the simplified Solomon equations (Equation 20.30), in which the thermal equilibrium terms are dropped:

$$\frac{\mathrm{d}}{\mathrm{d}t}\begin{pmatrix}\langle\hat{I}_{1z}\rangle\\ \langle\hat{I}_{2z}\rangle\end{pmatrix} = \mathbf{L}_{\text{Solomon}}\begin{pmatrix}\langle\hat{I}_{1z}\rangle\\ \langle\hat{I}_{2z}\rangle\end{pmatrix}$$

where

$$\mathbf{L}_{\text{Solomon}} = \begin{pmatrix}-R_{\text{auto}} & R_{\text{cross}}\\ R_{\text{cross}} & -R_{\text{auto}}\end{pmatrix}$$

and the auto- and cross-relaxation rate constants are given in Equations 20.16 and 20.17. The situation is precisely analogous to that holding under two-site chemical exchange (Equation A.93), if one makes the following substitutions:

$$\begin{aligned} \langle\hat{I}_z\rangle^{\text{A}} &\Rightarrow \langle\hat{I}_{1z}\rangle & \langle\hat{I}_z\rangle^{\text{B}} &\Rightarrow \langle\hat{I}_{2z}\rangle\\ 2W = {T_1}^{-1} &\Rightarrow R_{\text{auto}} - R_{\text{cross}} & k &\Rightarrow R_{\text{cross}} \end{aligned}$$

The amplitudes for the magnetization transfer processes may therefore be obtained by making the appropriate substitutions in Equations A.94 and A.95:

$$\begin{aligned} a_{1\to1}(\tau_{\text{m}}) = a_{2\to2}(\tau_{\text{m}}) &= \cosh(R_{\text{cross}}\tau_{\text{m}})\exp\{-R_{\text{auto}}\tau_{\text{m}}\}\\ a_{1\to2}(\tau_{\text{m}}) = a_{2\to1}(\tau_{\text{m}}) &= \sinh(R_{\text{cross}}\tau_{\text{m}})\exp\{-R_{\text{auto}}\tau_{\text{m}}\} \end{aligned} \qquad \text{(A.100)}$$

This result is used in Equations 20.34 and 20.42.

Notes

1. For a different proof of Equation A.9, see C. P. Slichter *Principles of Magnetic Resonance*, 3rd edition, Springer, Berlin, 1989.

2. See, for example, G. Strang, *Linear Algebra and its Applications*, 3rd edition, Harcourt Brace Jovanovich, San Diego, 1988.

3. For a system of N spins-1/2, the operator for a rotation through the angle 2π is given by

$$\widehat{R}_x(2\pi) = (-1)^N \widehat{1}$$

   The factor of $(-1)^N$ is usually irrelevant, since propagators always act on the spin density operator in pairs (e.g. see Equation 11.27). The product of two $\widehat{R}_x(2\pi)$ propagators is always equal to unity.

4. The coherence transfer pathway technique was described almost simultaneously by A. D. Bain, *J. Magn. Reson.* **56**, 418–427 (1984) and G. Bodenhausen, H. Kogler and R. R. Ernst, *J. Magn. Reson.* **58**, 370–388 (1984).

5. See N. Ivchenko, C. E. Hughes and M. H. Levitt, *J. Magn. Reson.* **160**, 52–58 (2003).

Further Reading

- For a full discussion of the quadrupolar Hamiltonian, see A. Jerschow, *Prog. NMR Spectrosc.* **46**, 63–78 (2005).
- For more on the selection of coherence transfer pathways by phase cycling and pulsed field gradients, see J. Keeler, *Understanding NMR Spectroscopy*, Wiley, Chichester, 2005.
- For cogwheel phase cycling, see: M. H. Levitt, P. K. Madhu and C. E. Hughes, *J. Magn. Reson.* **155**, 300–306 (2002); A. Jerschow and R. Kumar, *J. Magn. Reson.* **160**, 59–64 (2003) and N. Ivchenko, C. E. Hughes and M. H. Levitt, *J. Magn. Reson.* **164**, 286–293 (2003); G. Zuckerstätter and N. Müller, *Concepts in Magn. Reson.*, **30A**, 81–99 (2007).
- For the selection of coherence transfer pathways by pulsed field gradients, see R. E. Hurd, in *Encyclopedia of Nuclear Magnetic Resonance*, D. M. Grant and R. K. Harris (eds) Wiley, 1996, vol. 3, p. 1990, and A. Jerschow and N. Müller, *J. Magn. Reson.*, **134**, 17–29 (1998).
- For the generalized Solomon equations, including cross-correlated relaxation, see C. Dalvit and G. Bodenhausen, *Adv. Magn. Reson.*, **14**, 1 (1990).
- For more theory of NMR in chemically exchanging systems, see A. D. Bain, *Prog. NMR Spectrosc.* **43**, 63–103 (2003).

Appendix B: Symbols and Abbreviations

$\widehat{0}$	null operator
$\widehat{1}$	unity operator
$\widehat{1}_j, \widehat{1}_k$	unity operators for spins I_j and I_k
$\widehat{1}_1, \widehat{1}_2 \ldots$	unity operators for spins I_1, $I_2 \ldots$
①, ②, ③ ...	time points in a pulse sequence
$\|1\rangle, \|2\rangle \ldots$	energy eigenstates in a coupled spin system
a	complex amplitude
a_ℓ	complex amplitude of signal component s_ℓ
a_j	peak amplitudes for spins j
a_{cross}	amplitude of a cross-peak
a_{diag}	amplitude of a diagonal peak
$a_{1\rightarrow 1}, a_{1\rightarrow 2} \ldots$	amplitudes for auto-relaxation and cross-relaxation processes in NOESY
$a_{\mathrm{A}\rightarrow\mathrm{A}}, a_{\mathrm{A}\rightarrow\mathrm{B}} \ldots$	amplitudes for magnetization transfer processes in two-site exchange
$a_{\boxed{-\alpha}}, a_{\boxed{-\beta}} \ldots$	amplitudes of (-1)-quantum coherence signals, in an ensemble of spin-1/2 pairs
$\alpha_{\boxed{-\alpha\alpha}}, \alpha_{\boxed{-\alpha\beta}} \ldots$	amplitudes of signals from coherences $\rho_{\boxed{-\alpha\alpha}}, \rho_{\boxed{-\alpha\beta}} \ldots$ in an ensemble of three-spin-1/2 systems
$a_{\boxed{p_q}}$	amplitudes of signal from a coherence of quantum order p and satellite order q in an ensemble of quadrupolar nuclei
a_{rs}	amplitudes of signal from coherence ρ_{rs}
$a^{[\mathfrak{m}]}$	signal amplitude for the pulse sequence corresponding to phase cycle index $\mathfrak{m}$
$a^{[\mathfrak{m}]}_{\boxed{-\beta}}$	signal amplitude from coherence $\rho_{\boxed{-\beta}}$, for phase cycle index $\mathfrak{m}$
$a^{\mathrm{av}}_{\boxed{-\beta}}$	phase-cycled signal amplitude from coherence $\rho_{\boxed{-\beta}}$
a_n	eigenvalues of the operator $\widehat{A}$
α	an Euler angle
α^{BA}	last Euler angle used when transforming the reference axes of frame A into those of frame B
α_{AB}	passive notation for α^{BA}
$\|\alpha\rangle$	state of spin-1/2 with angular momentum of $+1/2$ along the z-axis
$\|\alpha\alpha\rangle, \|\alpha\beta\rangle \ldots$	states of a spin-1/2 pair
$\|\alpha\alpha\alpha\rangle, \|\alpha\alpha\beta\rangle \ldots$	spin states in an ensemble of three-spin-1/2 systems

Spin Dynamics: Basics of Nuclear Magnetic Resonance, Second Edition Malcolm H. Levitt

A	pre-exponential factor in Arrhenius equation
AB	strongly coupled two-spin-1/2 system
AX	weakly coupled two-spin-1/2 system
$\widehat{A}$	arbitrary operator
$\widehat{A}^{\dagger}$	adjoint of operator $\widehat{A}$
$\widehat{A}^{-1}$	inverse of operator $\widehat{A}$
$\widehat{A}^{N}$	Nth power of operator $\widehat{A}$
$\widehat{A}_{\phi}$	propagator for a pulse sequence element A with phase ϕ
$\mathbf{A}$	an arbitrary matrix
$\mathcal{A}$	absorption Lorentzian function
b_{jk}	dipole–dipole coupling constant between spins I_j and I_k
b_{IS}	dipole–dipole coupling constant between spins I and S
B	rotational constant
B^0	magnitude of static (main) magnetic field
B_x, B_y, B_z	Cartesian components of the magnetic field
B^{RF}	magnitude of r.f. magnetic field
B_{RF}	peak value of the r.f. magnetic field
$B_{j,x}^{\mathrm{induced}}$, $B_{j,y}^{\mathrm{induced}}$, $B_{j,z}^{\mathrm{induced}}$	Cartesian components of the induced magnetic field at the site of spin I_j
$\mathbf{B}$	magnetic field
$\mathbf{B}^0$	static field vector
$\mathbf{B}^{\mathrm{tot}}$	total magnetic field
$\mathbf{B}_j^{\mathrm{induced}}$	induced magnetic field at the site of spin I_j
$\mathbf{B}_j^{\mathrm{loc}}$	local magnetic field at the site of spin I_j
$\mathbf{B}_{\mathrm{RF}}$	r.f. field vector
$\mathbf{B}_{\mathrm{non\,res}}^{\mathrm{RF}}$	non-resonant component of the r.f. field vector
$\mathbf{B}_{\mathrm{res}}^{\mathrm{RF}}$	resonant component of the r.f. field vector
$\mathbf{B}_x^{\mathrm{grad}}$	gradient field, corresponding to a variation of field along the z-axis with respect to the x-coordinate
$\mathbf{B}_y^{\mathrm{grad}}$	gradient field, corresponding to a variation of field along the z-axis with respect to the y-coordinate
$\mathbf{B}_z^{\mathrm{grad}}$	gradient field, corresponding to a variation of field along the z-axis with respect to the z-coordinate
$\widehat{B}$	arbitrary operator
$\widehat{B}^0$	secular part of the operator $\widehat{B}$
$\mathbb{B}$	Boltzmann factor
$\mathbb{B}_I$, $\mathbb{B}_S$	Boltzmann factors for spin species I and S
β	an Euler angle
β^{BA}	second Euler angle used when transforming the reference axes of frame A into those of frame B
β_{AB}	passive notation for β^{BA}
β_{p}	flip angle of r.f. pulse
$\beta_{\mathrm{p}}^{\mathrm{C}}$	central transition flip angle
$\left(\beta_{\mathrm{p}}\right)_{\phi_p}$	r.f. pulse with flip angle β_{p} and phase ϕ_{p}
$\left(\beta_{\mathrm{p}}\right)_{x}$	r.f. pulse with flip angle β_{p} and phase $\phi_{\mathrm{p}} = 0$
$\left(\beta_{\mathrm{p}}\right)_{\bar{x}}$	r.f. pulse with flip angle β_{p} and phase $\phi_{\mathrm{p}} = \pi$
$\left(\beta_{\mathrm{p}}\right)_{y}$	r.f. pulse with flip angle β_{p} and phase $\phi_{\mathrm{p}} = \pi/2$
$\left(\beta_{\mathrm{p}}\right)_{\bar{y}}$	r.f. pulse with flip angle β_{p} and phase $\phi_{\mathrm{p}} = 3\pi/2$

$\|\beta\rangle$	state of spin-1/2 with angular momentum of $-1/2$ along the z-axis
cosh	hyperbolic cosine $\cosh x = \frac{1}{2}(\mathrm{e}^{x} + \mathrm{e}^{-x})$
COSY	COrrelation SpectroscopY, a simple form of two-dimensional spectroscopy useful for mapping coherence transfer processes and assigning peaks
c_r	superposition coefficient of state $\|r\rangle$
c_α, c_β	superposition coefficients for one spin-1/2
$c_{\alpha\alpha}$, $c_{\alpha\beta}\ldots$	superposition coefficients for a spin-1/2 pair
C_M	value of matching capacitor
C_T	value of tuning capacitor
C_Q	quadrupolar coupling
$\widehat{C}$	arbitrary operator
$\mathbb{C}$	electric charge density
$\mathbb{C}^{(0)}$, $\mathbb{C}^{(1)}\ldots$	multipole components of the nuclear electric charge density
Da	Dalton, a unit of molecular mass; the mass of one ^{12}C atom is 12 Da
d_{IS}	secular dipole–dipole coupling between spins I and S
d_{jk}	secular dipole–dipole coupling between spins I_j and I_k
D_x	diffusion coefficient in the x-direction
$\widehat{D}_x$	operator for the first derivative with respect to x
$\widehat{D}_x^2$	operator for the second derivative with respect to x
$\mathfrak{D}$	dispersion Lorentzian function
$\mathbf{D}$	a diagonal matrix
$\mathbf{D}_{\boxed{-}}$	diagonal matrix with elements given by the eigenvalues of $\mathbf{L}_{\boxed{-}}$
$\mathbf{D}_z$	diagonal matrix with elements given by the eigenvalues of $\mathbf{L}_z$
δ_{mn}	Kronecker delta: $\delta_{mn} = 0$ for $m \neq n$; $\delta_{mn} = 1$ for $m = n$
δ	chemical shift (dimensionless)
δ_1, $\delta_2\ldots$	isotropic chemical shifts of spins I_1, $I_2\ldots$
δ_j^iso	isotropic chemical shift of spin I_j
δ_j^aniso	chemical shift anisotropy of spin I_j
δ_ref	equivalent chemical shift of the spectrometer reference frequency
δ_{xx}^j, $\delta_{xy}^j\ldots$	components of the chemical shift tensor of spin I_j
δ_{XX}^j, δ_{YY}^j, δ_{ZZ}^j	principal values of the chemical shift tensor of spin I_j
δ^j	chemical shift tensor of spin I_j
e	electric charge of the proton; $e = 1.602 \times 10^{-19}$ C
eq	largest principal value of the electric field gradient tensor
e	Euler's number, $\mathrm{e} = 2.71828\ldots$
$\exp\{\widehat{A}\}$	exponential of operator $\widehat{A}$
E_J	energy of a rotational state with quantum number J
E_n	energy level (=Hamiltonian eigenvalue)
E_act	activation energy in Arrhenius equation
E_elec	electric interaction energy
$E_\mathrm{elec}^{(0)}$, $E_\mathrm{elec}^{(1)}\ldots$	multipole components of the electric interaction energy
$\mathbf{e}_x$, $\mathbf{e}_y$, $\mathbf{e}_z$	unit vectors along three orthogonal axes
$\mathbf{e}'_x$, $\mathbf{e}'_y$, $\mathbf{e}'_z$	rotating frame axes
$\mathbf{e}_x^\mathrm{A}$, $\mathbf{e}_y^\mathrm{A}$, $\mathbf{e}_z^\mathrm{A}$	orthogonal axis system of reference frame A
$\mathbf{e}_x^\mathrm{B}$, $\mathbf{e}_y^\mathrm{B}$, $\mathbf{e}_z^\mathrm{B}$	orthogonal axis system of reference frame B
$\mathbf{e}_{jk}$	unit vector parallel to the vector between spins I_j and I_k
$\mathbf{E}$	electric field

ϵ_{NOE}	nuclear Overhauser enhancement factor, defined as the ratio between the enhanced and the non-enhanced magnetization
FID	free induction decay = NMR signal
floor	floor function; floor(x) returns the largest integer that is not greater than x
$\mathbf{f}$	vector representation of function $f(x)$
$f_1, f_2 \ldots$	coefficients of the expansion of $f(x)$ in the basis of functions $\psi_n(x)$
$\|f\rangle$	Dirac notation for the function $f(x)$
ϕ	r.f. phase
ϕ_{p}	phase of an r.f. pulse
$\phi_1, \phi_2 \ldots$	phases of r.f. pulses
$\phi_{\mathrm{A}}, \phi_{\mathrm{B}} \ldots$	phases of pulse sequence blocks A,B...
ϕ_{rec}	combined phase shift of NMR signal, including receiver phase shift and post-digitization phase shift
ϕ_{dig}	phase shift of digitized NMR signal
ϕ_ℓ	phase of signal component s_ℓ
ϕ_{ref}	angle of the rotating frame at time $t = 0$
$\phi_{\boxed{-}}$	phase of the coherence $\rho_{\boxed{-}}$
$\phi^{(1)}$	first-order part of the frequency dependence of the peak phase
$\phi^{(0)}$	zero-order part of the frequency dependence of the peak phase
$\phi^{(1)}_{\mathrm{corr}}$	first-order phase correction parameter
$\phi^{(0)}_{\mathrm{corr}}$	zero-order phase correction parameter
Φ	rotation angle of rotating frame
Φ_{G}	rotation angle induced by gradient pulse
Φ_{path}	total pathway phase
G	gauss, an old unit of magnetic field (non-SI); $1\,\mathrm{G} = 10^{-4}\,\mathrm{T}$
G_x	magnitude of the gradient in the z-component of the field with respect to the x-axis
G_y	magnitude of the gradient in the z-component of the field with respect to the y-axis
G_z	magnitude of the gradient in the z-component of the field with respect to the z-axis
G_{max}	maximum gradient strength
$\mathbb{G}(\tau)$	autocorrelation function of a random process
$\mathbb{G}_m(\tau)$	autocorrelation function of a second-rank spherical harmonic
γ	gyromagnetic ratio; also, an Euler angle
$\gamma_j, \gamma_k \ldots$	gyromagnetic ratios of nuclei I_j, $I_k \ldots$
γ_I, γ_S	gyromagnetic ratios of two different isotopes
γ^{BA}	first Euler angle used when transforming the reference axes of frame A into those of frame B
γ_{AB}	passive notation for γ^{BA}
h	Planck's constant; $h = 6.626 \times 10^{-34}\,\mathrm{J\,s}$
$\hbar$	Planck's constant divided by 2π; $\hbar = 1.055 \times 10^{-34}\,\mathrm{J\,s}$
Hz	hertz, cycles per second (unit of frequency)
$\widehat{\mathrm{H}}$	Hamiltonian operator, in SI units
$\mathbf{H}$	matrix representation of a Hamiltonian
$\widehat{\mathcal{H}}$	Hamiltonian operator (in natural units)
$\widehat{\mathcal{H}}^0$	secular spin Hamiltonian
$\widehat{\mathcal{H}}^{\mathrm{DD}}$	secular dipole–dipole interaction (for all spin pairs)

$\widehat{\mathcal{H}}^{\mathrm{DD,full}}$	full form of the dipole–dipole interaction (for all spin pairs)
$\widehat{\mathcal{H}}_{\mathrm{ext}}$	external spin Hamiltonian
$\widehat{\mathcal{H}}_{\mathrm{full}}$	complete Hamiltonian operator of the sample
$\widehat{\mathcal{H}}_{\mathrm{grad}}$	Hamiltonian for the interaction with the gradient field
$\widehat{\mathcal{H}}_{\mathrm{int}}$	internal spin Hamiltonian
$\widehat{\mathcal{H}}_{\mathrm{int}}^{\mathrm{iso}}$	isotropic part of a secular spin interaction $\widehat{\mathcal{H}}_{\mathrm{int}}^{0}$
$\widehat{\mathcal{H}}_{\mathrm{int}}^{0}$	secular part of internal spin Hamiltonian $\widehat{\mathcal{H}}_{\mathrm{int}}$
$\bar{\widehat{\mathcal{H}}}_{\mathrm{int}}^{0}$	motionally averaged secular Hamiltonian
$\widehat{\mathcal{H}}_{j}^{\mathrm{CS}}$	chemical shift interaction of spin I_j
$\widehat{\mathcal{H}}_{j}^{\mathrm{CS,iso}}$	isotropic chemical shift interaction of spin I_j
$\widehat{\mathcal{H}}_{j}^{\mathrm{elec}}$	electric part of the Hamiltonian for spin I_j
$\widehat{\mathcal{H}}_{jk}^{\mathrm{DD}}$	secular dipole–dipole interaction between spins I_j and I_k
$\widehat{\mathcal{H}}_{jk}^{\mathrm{DD,full}}$	full form of the dipole–dipole interaction between spins I_j and I_k
$\widehat{\mathcal{H}}_{jk}^{\mathrm{iso}}$	isotropic J-coupling interaction between spins I_j and I_k
$\widehat{\mathcal{H}}_{jk}^{\mathrm{J}}$	secular J-coupling interaction between spins I_j and I_k
$\widehat{\mathcal{H}}_{jk}^{\mathrm{J,full}}$	full form of the J-coupling interaction between spins I_j and I_k
$\widehat{\mathcal{H}}_{j}^{\mathrm{mag}}$	magnetic part of the Hamiltonian for spin I_j
$\widehat{\mathcal{H}}_{\mathrm{j}}^{\mathrm{Q}}$	electric quadrupole interaction of nucleus I_j
$\widehat{\mathcal{H}}_{j}^{\mathrm{RF}}$	r.f. spin Hamiltonian for nucleus I_j
$\widehat{\mathcal{H}}_{J}^{\mathrm{strong}}$	J-coupling Hamiltonian in the strongly coupled limit
$\widehat{\mathcal{H}}_{J}^{\mathrm{weak}}$	J-coupling Hamiltonian in the weakly coupled limit
$\widehat{\mathcal{H}}_{\mathrm{RF}}$	r.f. part of external spin Hamiltonian
$\widehat{\mathcal{H}}_{\mathrm{Q}}^{(1)}$	first-order quadrupolar Hamiltonian
$\widehat{\mathcal{H}}_{\mathrm{Q}}^{(2)}$	second-order quadrupolar Hamiltonian
$\widehat{\mathcal{H}}_{\mathrm{static}}$	static part of external spin Hamiltonian
$\widehat{\mathcal{H}}_{12}^{0}$	secular Hamiltonian for the coupling between spins I_1 and I_2
$\widehat{\mathcal{H}}^{0\prime}$	secular spin Hamiltonian with the opposite sign of the chemical shift terms
$\hat{\widehat{\mathcal{H}}}^{0}$	secular spin Hamiltonian, in the rotating frame
$\widehat{\mathcal{H}}_{\mathrm{weak}}^{0}$	weakly coupled form of the secular spin Hamiltonian
$\widehat{\mathcal{H}}_{\mathrm{weak}}^{0\prime}$	weakly coupled form of the secular spin Hamiltonian, with the opposite sign of the chemical shift terms
$\widehat{\mathcal{H}}_{1}^{0}, \widehat{\mathcal{H}}_{2}^{0} \ldots$	secular Hamiltonians for spins $I_1, I_2 \ldots$
η	old definition of the NOE enhancement factor. $\eta = 1$ indicates a doubling of the signal (see ϵ_{NOE})
η_j	biaxiality (asymmetry parameter) of chemical shift tensor of spin I_j
η_{Q}	biaxiality (asymmetry parameter) of electric field gradient tensor
i	square root of -1
Im	imaginary part of a complex number

INADEQUATE	Incredible Natural Abundance DoublE QUAnTum Experiment, a pulse sequence that selects peaks passing through double-quantum coherences, suppressing isolated spin signals
INEPT	Insensitive Nuclei Enhanced by Polarization Transfer, a pulse sequence that implements magnetization transfer from one spin species to another, using the J-couplings
I	nuclear spin quantum number; in addition, a nuclear spin species
$\hat{I}_x, \hat{I}_y, \hat{I}_z$	operators for the three components of nuclear spin angular momentum
$\hat{I}^+, \hat{I}^-$	nuclear spin shift operators
$\hat{I}^\alpha$	projection operator onto state $\|\alpha\rangle$ for a single spin-1/2
$\hat{I}^\beta$	projection operator onto state $\|\beta\rangle$ for a single spin-1/2
$\hat{I}_{1x}, \hat{I}_{1y}, \hat{I}_{1z}$	angular momentum operators for spin I_1
$\hat{I}_{2x}, \hat{I}_{2y}, \hat{I}_{2z}$	angular momentum operators for spin I_2
$\hat{I}_{jx}, \hat{I}_{jy}, \hat{I}_{jz}$	spin angular momentum operators of nucleus I_j
$\hat{I}_1^\alpha, \hat{I}_2^\alpha \ldots$	projection operators onto state $\|\alpha\rangle$ for spins $I_1, I_2 \ldots$
$\hat{I}_1^\beta, \hat{I}_2^\beta \ldots$	projection operators onto state $\|\beta\rangle$ for spins $I_1, I_2 \ldots$
$\hat{\mathbf{I}}_j$	vector operator for the spin angular momentum of nucleus I_j, $\hat{\mathbf{I}}_j = \hat{I}_{jx}\mathbf{e}_x + \hat{I}_{jy}\mathbf{e}_y + \hat{I}_{jz}\mathbf{e}_z$
$\hat{\mathbf{I}}_j \cdot \hat{\mathbf{I}}_k$	scalar product of angular momentum operators, equal to $\hat{I}_{jx}\hat{I}_{kx} + \hat{I}_{jy}\hat{I}_{ky} + \hat{I}_{jz}\hat{I}_{kz}$
$\|I, M\rangle$	state of spin-I nucleus with azimuthal quantum number M
$\mathbf{I}^+$	matrix representation of the operator $\hat{I}^+$
j	a spin index
J	J-coupling (in hertz); in addition, angular momentum quantum number
J', J''	J-couplings
J_1, J_2, J_3	total angular momentum quantum numbers
J_{CH}	J-coupling between ^{13}C and ^{1}H (units of hertz)
J_{jk}	isotropic J-coupling between spins I_j and I_k
$J_{12}, J_{13} \ldots$	J-couplings between spins I_1 and I_2, etc.
J_{IS}	heteronuclear J-coupling constant (in hertz)
^1J	one-bond J-coupling
^2J	two-bond J-coupling
^3J	three-bond J-coupling
$\mathbf{J}_{jk}$	J-coupling tensor between spins I_j and I_k
$J_{xx}^{jk}, J_{xy}^{jk} \ldots$	components of the J-coupling tensor between spins I_j and I_k
$\mathbb{J}(\omega)$	spectral density
$\mathcal{J}(\omega)$	normalized spectral density
k	a spin index; in addition, a kinetic rate constant
k'	a kinetic rate constant
k_{B}	Boltzmann constant = $1.381 \times 10^{-23}\,\mathrm{J\,K^{-1}}$
K	equilibrium constant of an exchange process
$\widehat{\mathrm{K}}$	kinetic energy operator
$\mathbb{K}_{\mathrm{AB}}$	cross-correlation function of two random processes
$\mathbb{K}_{\mathrm{CH,CH}}$	cross-correlation of the dipole–dipole interactions within two ^{13}C–^{1}H pairs
κ	strength of a gradient pulse
ℓ	an index for signal components and for spectral peaks;in addition, orbital angular momentum quantum number
$\hat{l}_x, \hat{l}_y, \hat{l}_z$	angular momentum operators (in natural units)
$\hat{l}^2$	operator for the total square angular momentum (in natural units)

$\hat{l}^+, \hat{l}^-$	angular momentum shift operators
$\|\ell, m\rangle$	angular momentum eigenstate with total square angular momentum $l(l+1)\hbar$ and z-angular momentum $m\hbar$
L	inductance of coil
L_{tot}	total angular momentum
$\mathfrak{L}$	complex Lorentzian function
$\mathbf{L}_{\boxed{-}}$	dynamic matrix for the evolution of (-1)-quantum coherences in a two-site exchange problem
$\mathbf{L}_{\text{pop}}$	dynamic matrix for the evolution of populations in a two-site exchange problem
$\mathbf{L}_{\text{Solomon}}$	Solomon matrix for relaxation in a two-spin-1/2 system
$\mathbf{L}_z$	dynamic matrix for the evolution of Zeeman magnetizations in a two-site exchange problem
λ	decay rate constant of a coherence (or transverse magnetization); $\lambda = {T_2}^{-1}$; peakwidth at half-height = 2λ in units of radians per second
λ'	coherence decay rate constant in slow two-site exchange; sum of the natural decay rate constant λ and the exchange rate constant k
λ_j	linewidth parameter for spins j
λ_ℓ	decay rate constant of signal component s_ℓ
$\lambda_\ell^{(1)}$	width parameter of a two-dimensional peak in the Ω_1 dimension
$\lambda_\ell^{(2)}$	width parameter of a two-dimensional peak in the Ω_2 dimension
λ_{rs}	decay rate constant of coherence ρ_{rs}
Λ_{rs}	spatial wavelength of phase helix induced by gradient pulse, for coherence ρ_{rs}
mod	modulo function; mod(a, b) takes the remainder when a is divided by b
ms	millisecond, 10^{-3} s
m	an integer; in addition, mass of a particle
$m_j^{(r)}$	azimuthal quantum number of spin I_j in the state $\|r\rangle$
M_J	azimuthal quantum number for a rotating object; $M_J = -J, -J+1 \ldots +J$
M_r	angular momentum of state $\|r\rangle$ along z-axis
M_s	angular momentum of state $\|s\rangle$ along z-axis
M_S	azimuthal quantum number for a spin; $M_S = -S, -S+1 \ldots +S$
M_x, M_y, M_z	components of the magnetization vector
$M_x^{\text{nuc}}, M_y^{\text{nuc}}, M_z^{\text{nuc}}$	components of nuclear magnetization
$M_{\text{eq}}^{\text{nuc}}$	equilibrium value of nuclear magnetization along z-axis
$\mathbf{M}$	magnetization vector
$\mathbf{M}^{\text{eq}}$	equilibrium nuclear magnetization vector
$\mathfrak{m}$	phase cycle counter, $\mathfrak{m} = 0, 1 \ldots \mathfrak{n} - 1$
$\mathfrak{M}$	transient counter, $\mathfrak{M} = 0, 1 \ldots \mathfrak{N} - 1$
μ_0	magnetic constant; $\mu_0 = 4\pi \times 10^{-7}\,\text{H}\,\text{m}^{-1}$. Often required for electromagnetic equations in SI units
$\boldsymbol{\mu}$	magnetic moment
μ_{induced}	induced magnetic moment
$\hat{\boldsymbol{\mu}}$	operator for the magnetic moment vector
NOE	nuclear Overhauser effect, the change in the magnetization of one nuclear spin species when a second spin species is saturated. The original Overhauser effect involved nuclei and electrons in metals
NOESY	Nuclear Overhauser SpectroscopY, a form of two-dimensional spectroscopy in which the cross-peaks are generated by dipole–dipole cross-relaxation.

nm	nanometre, 10^{-9} m
ns	nanosecond, 10^{-9} s
n	an integer
n_{sample}	number of signal sampling points
N	number of spins in a spin system; in addition, number of pulses; in addition, an integer
N	normalization constant
$\mathfrak{n}$	total number of steps in a phase cycle
$\mathfrak{n}_{\mathrm{A}}, \mathfrak{n}_{\mathrm{B}} \ldots$	number of steps in the phase cycles for individual pulse sequence blocks A, B...
$\mathfrak{N}$	number of acquired transients
$\mathbb{N}$	number of members of the spin ensemble
$\mathbb{N}_{\mathrm{A}}, \mathbb{N}_{\mathrm{B}}$	number of molecules of types A and B
$\mathbb{N}_{\mathrm{A}}$	Avogadro's number, i.e. number of molecules in a mole of substance = 6.022×10^{23}
ppm	parts per million, 10^{-6}
p	coherence order
p_{rs}	order of the coherence ρ_{rs}
Δp	change in coherence order
$\Delta p_{\mathrm{A}}, \Delta p_{\mathrm{B}} \ldots$	changes in coherence order over pulse sequence blocks A, B...
P	probability
$\mathrm{P}_{\mathrm{I}}, \mathrm{P}_{\mathrm{II}} \ldots$	probabilities of isotopomers
$\mathrm{P}(q_n)$	probability of observing the result q_n
$\mathrm{P}_{\alpha\rightarrow\beta}$	probability of a spin-1/2 making a transition $\lvert\alpha\rangle \rightarrow \lvert\beta\rangle$
p	probability density function
$\mathrm{p}(\Theta) \quad \mathrm{d}\Theta$	probability of a molecule having an orientation in the range Θ to $\Theta + \mathrm{d}\Theta$
$\mathfrak{p}$	an integer
$\mathbb{P}$	vector of populations in a two-spin-1/2 system
π	mathematical constant, $\pi = 3.1415\ldots$
$(\pi/2)_x$	pulse of flip angle $\pi/2$ and phase $\phi_{\mathrm{p}} = 0$
$(\pi/2)_y$	pulse of flip angle $\pi/2$ and phase $\phi_{\mathrm{p}} = \pi/2$
$(\pi/2)_{\overline{x}}$	pulse of flip angle $\pi/2$ and phase $\phi_{\mathrm{p}} = \pi$
$(\pi/2)_{\overline{y}}$	pulse of flip angle $\pi/2$ and phase $\phi_{\mathrm{p}} = 3\pi/2$
π_x	pulse of flip angle π and phase $\phi_{\mathrm{p}} = 0$
π_y	pulse of flip angle π and phase $\phi_{\mathrm{p}} = \pi/2$
$\pi_{\overline{x}}$	pulse of flip angle π and phase $\phi_{\mathrm{p}} = \pi$
$\pi_{\overline{y}}$	pulse of flip angle π and phase $\phi_{\mathrm{p}} = 3\pi/2$
$(\pi/2)_x^I$	$\pi/2$ pulse applied to spin species I
$(\pi/2)_x^S$	$\pi/2$ pulse applied to spin species S
q	largest principal value of the electric field gradient tensor, divided by e; also satellite order
q_n	an eigenvalue of the operator $\widehat{Q}$
q_{rs}	satellite order of the coherence ρ_{rs}
Q	electric quadrupole moment
Q_{macro}	result of a macroscopic observation of the operator $\widehat{Q}$
$Q_{\alpha\alpha}, Q_{\alpha\beta} \ldots$	matrix elements of a spin-1/2 operator $\widehat{Q}$
$\widehat{Q}$	arbitrary operator
$\langle\widehat{Q}\rangle$	expectation value of the operator $\widehat{Q}$
$\langle\widehat{Q}\rangle^{\mathrm{eq}}$	expectation value of the operator $\widehat{Q}$ in thermal equilibrium

θ_1, θ_2	tilt angles of rotation axes for spins I_1 and I_2
$\theta_{\mathrm{CH,CH}}$	angle between two ^{13}C–^{1}H internuclear vectors
θ_{IS}	angle subtended by the molecular long axis and the vector between spins I and S
θ_{Q}	angle between the unique axis of an uniaxial electric field gradient tensor and the static magnetic field
θ_{RF}	angle between the r.f. and static magnetic fields
Θ	molecular orientation
Θ_{magic}	the magic angle, $\Theta_{\mathrm{magic}} = \arctan\sqrt{2} = 54.7356^\circ$
Θ_{IS}	angle subtended by the external field and the vector between spins I and S
Θ_{jk}	angle between the vector $\mathbf{e}_{jk}$ and the magnetic field
r.f.	radio-frequency
Re	real part of a complex number
ROESY	Rotating-frame nuclear Overhauser SpectroscopY, a form of two-dimensional spectroscopy in which the cross-peaks are generated by transverse cross-relaxation in the presence of an r.f. field
$\mathbf{r}$	spatial position, written as a three-dimensional vector
r_{jk}	distance between spins I_j and I_k
$R, \mathbb{R}$	expressions appearing in the theory of two-site exchange
$\mathcal{R}(\alpha, \beta, \gamma)$	three-dimensional rotation matrix, written using Euler angles
$\mathcal{R}^j$	rotation matrix describing the orientation of the principal axis system of the chemical shift tensor for spin I_j with respect to the static field
$\mathcal{R}_{\mathrm{Q}}$	rotation matrix describing the orientation of the principal axis system of the electric field gradient tensor with respect to the static field
$R^j_{xX}, R^j_{xY} \ldots$	elements of the matrix $\mathcal{R}^j$
R_{auto}	auto-relaxation rate constant in Solomon equations
$R^{\mathrm{T}}_{\mathrm{auto}}$	transverse auto-relaxation rate constant
R_{cross}	cross-relaxation rate constant in Solomon equations (with sign corrected)
$R^{\mathrm{T}}_{\mathrm{cross}}$	transverse cross-relaxation rate constant (with sign corrected)
R_{sum}	relaxation rate constant for the sum magnetization
$\widehat{R}_x(\beta)$	operator for the rotation through the angle β about the rotating-frame x-axis
$\widehat{R}_y(\beta)$	operator for the rotation through the angle β about the rotating-frame y-axis
$\widehat{R}_z(\beta)$	operator for the rotation through the angle β about the z-axis
$\widehat{R}_{\phi_{\mathrm{p}}}(\beta_{\mathrm{p}})$	operator for a rotation of one or more spins through the angle β_{p} about the axis $\mathbf{e}'_x \cos\phi_{\mathrm{p}} + \mathbf{e}'_y \sin\phi_{\mathrm{p}}$
$\widehat{R}_{1x}(\beta)$	operator for the rotation of spin I_1 through the angle β about the rotating-frame x-axis
$\widehat{R}_{2z}(\beta)$	operator for the rotation of spin I_2 through the angle β about the z-axis
$\widehat{R}_{1,\phi_{\mathrm{p}}}(\beta_{\mathrm{p}}), \widehat{R}_{2,\phi_{\mathrm{p}}}(\beta_{\mathrm{p}}) \ldots$	operators for rotations of individual spins $I_1, I_2 \ldots$ through the angle β_{p} about the axis $\mathbf{e}'_x \cos\phi_{\mathrm{p}} + \mathbf{e}'_y \sin\phi_{\mathrm{p}}$
ρ_{rr}	population of state $\lvert r\rangle$
ρ_{rs}	coherence between states $\lvert r\rangle$ and $\lvert s\rangle$
ρ^{eq}_{rr}	thermal equilibrium value of the population ρ_{rr}
ρ^{eq}_{rs}	thermal equilibrium value of the coherence ρ_{rs}
$\rho_{\boxed{\alpha}}, \rho_{\boxed{\beta}}$	populations of states $\lvert\alpha\rangle$ and $\lvert\beta\rangle$, in a spin-1/2 ensemble
$\rho_{\boxed{+}}, \rho_{\boxed{-}}$	coherences in a spin-1/2 ensemble

$\rho^{\mathrm{eq}}_{\boxed{\alpha}}$, $\rho^{\mathrm{eq}}_{\boxed{\beta}}$	thermal equilibrium populations of states $\|\alpha\rangle$ and $\|\beta\rangle$, in a spin-1/2 ensemble
$\rho_{\|+1\rangle}$	population of state $\|1, +1\rangle$ in a spin-1 ensemble
$\rho_{\|0\rangle}$	population of state $\|1, 0\rangle$ in a spin-1 ensemble
$\rho_{\|-1\rangle}$	population of state $\|1, -1\rangle$ in a spin-1 ensemble
$\rho_{\|+3/2\rangle}$	population of state $\|I, +3/2\rangle$ in an ensemble of half-integer spins $I \geq 3/2$
$\rho_{\|+1/2\rangle}$	population of state $\|I, +1/2\rangle$ in an ensemble of half-integer spins $I \geq 3/2$
$\rho_{\|-1/2\rangle}$	population of state $\|I, -1/2\rangle$ in an ensemble of half-integer spins $I \geq 3/2$
$\rho_{\|-3/2\rangle}$	population of state $\|I, -3/2\rangle$ in an ensemble of half-integer spins $I \geq 3/2$
$\rho_{\boxed{p_q}}$	coherence in an ensemble of quadrupolar nuclei, with coherence order p and satellite order q
$\rho_{\boxed{-1_0}}$	central transition (-1)-quantum coherence in an ensemble of half-integer spins $I \geq 3/2$
$\rho_{\boxed{\alpha\alpha}}$, $\rho_{\boxed{\alpha+}}\ldots$	populations and coherences for an ensemble of spin-1/2 pairs
$\rho^{\mathrm{eq}}_{\boxed{\alpha\alpha}}$, $\rho^{\mathrm{eq}}_{\boxed{\alpha\beta}}\ldots$	thermal equilibrium populations in an ensemble of spin-1/2 pairs
$\rho_{\boxed{\alpha\alpha\alpha}}$, $\rho_{\boxed{\alpha\alpha+}}\ldots$	populations and coherences in an ensemble of three-spin-1/2 systems
$\rho_{\boxed{\alpha--\alpha}}$, $\rho_{\boxed{\alpha--\beta}}\ldots$	(-2)-quantum coherences in an ensemble of four-spin systems
$\rho_{\boxed{-\alpha+\alpha\beta}}\ldots$	coherences in an ensemble of five-spin-1/2 systems
$\rho^{\mathrm{A}}_{\boxed{\alpha}}$, $\rho^{\mathrm{A}}_{\boxed{+}}\ldots$	populations and coherences for molecules of type A
$\rho^{\mathrm{B}}_{\boxed{\alpha}}$, $\rho^{\mathrm{B}}_{\boxed{+}}\ldots$	populations and coherences for molecules of type B
$\rho^{[\mathfrak{m}]}_{\boxed{-\beta}}$⑤	coherence $\rho_{\boxed{-\beta}}$ at time point ⑤, for the pulse sequence corresponding to phase cycle index $\mathfrak{m}$
$\hat{\rho}$	spin density operator
$\hat{\rho}^{\mathrm{eq}}$	thermal equilibrium spin density operator
$\hat{\rho}^{\mathrm{A}}$, $\hat{\rho}^{\mathrm{B}}$	components of the spin density operator in a two-site exchange problem
$\hat{\rho}_{①}$, $\hat{\rho}_{②}\ldots$	spin density operator at time points ①, ②…
$\hat{\rho}^{\cos}_{①}$, $\hat{\rho}^{\cos}_{②}\ldots$	spin density operator at time points ①, ②… during the 'cosine' pulse sequence of a States data-acquisition scheme
$\hat{\rho}^{\sin}_{①}$, $\hat{\rho}^{\sin}_{②}\ldots$	spin density operator at time points ①, ②… during the 'sine' pulse sequence of a States data-acquisition scheme
$\hat{\rho}^{[\mathfrak{m}]}_{⑤}$	density operator at time point ⑤, for the pulse sequence corresponding to phase cycle index $\mathfrak{m}$
$\hat{\tilde{\rho}}$	rotating-frame spin density operator
$\tilde{\rho}_{\boxed{\alpha}}$, $\tilde{\rho}_{\boxed{\beta}}$	spin-1/2 populations in the rotating frame
$\tilde{\rho}_{\boxed{-}}$, $\tilde{\rho}_{\boxed{+}}$	spin-1/2 coherences in the rotating frame
s	second (unit of time)
sinh	hyperbolic sine, $\sinh x = \frac{1}{2}(\mathrm{e}^{x} - \mathrm{e}^{-x})$
$s(t)$	complex NMR signal emerging from the digitizer
$s(\tau, t)$	signal matrix of an arrayed experiment with variation of the interval τ
$s(t_1, t_2)$	two-dimensional signal surface
$s(t_1, t_2, t_3)$	three-dimensional signal surface
$s^{\cos}(t_1, t_2)$	cosine signal surface in the two-dimensional States procedure
$s^{\sin}(t_1, t_2)$	sine signal surface in the two-dimensional States procedure
$s_\ell(t)$	signal component corresponding to one spectral peak in a one-dimensional spectrum
$s_\ell(t_1, t_2)$	signal component corresponding to one spectral peak in a two-dimensional spectrum

s_{FID}	r.f. NMR signal emerging from the probe
$s_{\mathrm{A}}, s_{\mathrm{B}}$	output signals of quadrature receiver
s_{NMR}	component of the digitized signal $s(t)$ due to the nuclear spins
s_{noise}	component of the digitized signal $s(t)$ due to noise
s_{guess}	guessed form of NMR signal
s_{synth}	r.f. output signal of the synthesizer
s_{path}	signal component with a certain history of coherence orders
$s^{\mathrm{tot}}_{\mathrm{path}}$	signal component with a certain history of coherence orders, summed over all steps in a phase cycle
$s^{\mathrm{A}}_{\mathrm{rec}}, s^{\mathrm{B}}_{\mathrm{rec}}$	r.f. reference signals for the quadrature receiver
$s^{\mathrm{cos}}_{\mathrm{A}\to\mathrm{A}}, s^{\mathrm{cos}}_{\mathrm{A}\to\mathrm{B}} \ldots$	components of the cosine signal surface in a two-dimensional exchange experiment
$s^{\mathrm{sin}}_{\mathrm{A}\to\mathrm{A}}, s^{\mathrm{sin}}_{\mathrm{A}\to\mathrm{B}} \ldots$	components of the sine signal surface in a two-dimensional exchange experiment
$s_{\boxed{-\alpha}\to\boxed{\alpha-}}$	two-dimensional signal component for one coherence transfer process in a COSY experiment
S	a nuclear spin species
$S(\Omega)$	one-dimensional NMR spectrum
$S(\tau, \Omega)$	NMR spectrum as a function of the variable interval τ
$S(\Omega_1, \Omega_2)$	two-dimensional NMR spectrum
$S_{\mathrm{States}}(\Omega_1, \Omega_2)$	States two-dimensional spectrum
$S(\Omega_1, \Omega_2, \Omega_3)$	three-dimensional NMR spectrum
$S_\ell(\Omega)$	one peak in a one-dimensional NMR spectrum
$S_\ell(\Omega_1, \Omega_2)$	one peak in a two-dimensional NMR spectrum
$S_{\mathrm{A}\to\mathrm{A}}, S_{\mathrm{A}\to\mathrm{B}} \ldots$	components of a two-dimensional exchange spectrum
$\hat{S}_x, \hat{S}_y \ldots$	operators for the spin angular momentum components of spin S
$\hat{S}_{1x}, \hat{S}_{1y} \ldots$	operators for the spin angular momentum components of spin S_1
$\hat{\mathbf{S}}$	vector operator for the spin angular momentum, $\hat{\mathbf{S}} = \hat{S}_x\mathbf{e}_x + \hat{S}_y\mathbf{e}_y + \hat{S}_z\mathbf{e}_z$
$\lvert S_0\rangle$	singlet state
σ	old definition of the cross-relaxation rate constant in the Solomon equations (see R_{cross}); in addition, chemical shielding factor (opposite in sign to the chemical shift δ). Both meanings of σ are avoided in this book
$\hat{\sigma}$	alternative notation for spin density operator $\hat{\rho}$ (not used in this book)
σ_{G}	shape factor for gradient pulse
σ_{noise}	mean-square noise
$\sum'_{j<k}$	sum over spin pairs, excluding those that are magnetically equivalent
tanh	hyperbolic tangent, where $\tanh x = \sinh x / \cosh x$
t	a time point, and a time coordinate
$t_{\mathrm{a}}, t_{\mathrm{b}}$	two time points
t_1	incremented time interval in a two-dimensional experiment
t_2	signal acquisition interval in a two-dimensional experiment
$t_{\mathrm{on}}, t_{\mathrm{off}}$	time points at which a field is turned on and off
T	tesla, unit of magnetic field
Tr	trace of a matrix representation (sum of diagonal elements)
TOCSY	TOtal Correlation SpectroscopY, a form of two-dimensional spectroscopy generating cross-peaks for all spins belonging to the same spin system
TMS	tetramethylsilane, $\mathrm{Si(CH_3)_4}$
T	absolute temperature in units of Kelvin

T_1	longitudinal relaxation time constant = spin–lattice relaxation time constant
T_1^j	spin–lattice relaxation time of spins I_j
T_1^k	spin–lattice relaxation time constant of spins I_k
T_1^{A}, T_1^{B}	spin–lattice relaxation time constants of spins in chemical species A and B
$T_{1\rho}$	spin–lattice relaxation time constant in the rotating frame = transverse relaxation time constant in the presence of a spin-locking field
T_2	transverse relaxation time constant = spin–spin relaxation time constant
T_2^*	fictitious transverse relaxation time constant corresponding to the inhomogeneously broadened linewidth
$\|T_{+1}\rangle$, $\|T_0\rangle$, $\|T_{-1}\rangle$	triplet states
$\mathbb{T}_{\mathrm{PZ}}$	matrix for the transformation of Zeeman orders into populations
$\mathbb{T}_{\mathrm{ZP}}$	matrix for the transformation of populations into Zeeman orders
$\mathbf{T}$	a spin interaction tensor
$[\mathbf{T}]^{\mathrm{A}}$	matrix representation of a spin interaction tensor, in reference frame A
τ	an interval between two time points
τ_{m}	mixing interval in TOCSY, NOESY and ROESY pulse sequences
τ_{p}	r.f. pulse duration
τ_{G}	gradient pulse duration
τ^0	Larmor time-scale
τ_{c}	correlation time of a random process
$\tau_{\mathrm{c}}^{\mathrm{crit}}$	critical rotational correlation time (at which cross-relaxation disappears)
τ_{acq}	signal detection interval
τ_{spec}	spectral time-scale
τ_{sample}	interval between signal sampling points
$\widehat{U}(\tau)$	free precession propagator over an interval τ
$\widehat{U}_1$, $\widehat{U}_2 \ldots$	free precession propagators under the Hamiltonians $\widehat{\mathcal{H}}_1^0$, $\widehat{\mathcal{H}}_2^0 \ldots$
$\widehat{U}_{12}$	free precession propagator under the Hamiltonian $\widehat{\mathcal{H}}_{12}^0$
$\widehat{U}_{\mathrm{G}}$	propagator under a field gradient pulse
$\widehat{U}_J^{\mathrm{strong}}$	propagator under the strongly coupled J-coupling Hamiltonian $\widehat{\mathcal{H}}_J^{\mathrm{strong}}$
$\widehat{U}_J^{\mathrm{weak}}$	propagator under the weakly coupled J-coupling Hamiltonian $\widehat{\mathcal{H}}_J^{\mathrm{weak}}$
$\widehat{U}_{\mathrm{mix}}$	propagator for the mixing interval of a pulse sequence
$\widehat{U}_{\mathrm{SES}}$	propagator for a spin echo sandwich
V	volume; in addition, electric potential
$\widehat{\mathrm{V}}$	potential energy operator
$\mathbf{V}$	electric field gradient tensor
$V^{(0)}$, $V^{(1)} \ldots$	multipole components of the electric potential
V_{xx}, $V_{xy} \ldots$	Cartesian components of the electric field gradient at spin I_j
V_{XX}, V_{YY}, V_{ZZ}	principal values of the electric field gradient tensor at spin I_j
$\mathbf{V}_{\boxed{-}}$	propagator for (−1)-quantum coherences in a two-site exchange problem
W	mean transition probability per unit time in a spin-1/2 ensemble
W_0	mean zero-quantum transition probability per unit time in a homonuclear spin pair ensemble
W_2	mean double-quantum transition probability per unit time in a homonuclear spin pair ensemble
W_1	mean single-quantum transition probability per unit time in a homonuclear spin pair ensemble

W_{1I}, W_{1S}	mean single-quantum transition probabilities per unit time for species I and S
$W_{\boxed{+}}$, $W_{\boxed{-}}$	transition probabilities per unit time in a spin-1/2 ensemble
$W_{\boxed{-\alpha}}$, $W_{\boxed{-\beta}}\ldots$	transition probabilities per unit time in a 2-spin-1/2 ensemble
$\mathbb{W}_{\mathrm{P}}$	kinetic matrix for the evolution of populations in a 2-spin-1/2 system
ω	frequency in units of radians per second
$\omega/2\pi$	frequency in units of hertz
ω^0	signed) precession frequency (=Larmor frequency) in units of radians per second
$\omega^0/2\pi$	signed) precession frequency (=Larmor frequency) in units of hertz
ω_j^0, $\omega_k^0\ldots$	chemically shifted Larmor frequencies of spins I_j, $I_k\ldots$
ω_1^0, $\omega_2^0\ldots$	chemically shifted Larmor frequencies of spins I_1, $I_2\ldots$
ω_{12}^{A}, ω_{12}^{B}	components of the spin–spin coupling between spins I_1 and I_2
ω_{IS}	heteronuclear spin–spin coupling in anisotropic phase
ω_{G}	field-gradient-induced Larmor frequency shift
$\omega_{\mathrm{Q}}^{(1)}$	first-order quadrupole coupling
$\omega_Q^{(2)}$	second-order quadrupole coupling
ω_n	eigenvalue of the Hamiltonian $\widehat{\mathcal{H}}$ = energy level (in units of $\hbar$)
ω_{nut}^j	nutation frequency of spin I_j
$\omega_{\mathrm{nut}}^{\mathrm{C}}$	central transition nutation frequency
ω_{osc}	oscillation frequency of tuned circuit in probe
ω_{ref}	signed) spectrometer reference frequency in units of radians per second
ω_I^0	resonance offset frequency of spins I
ω_S^0	resonance offset frequency of spins S
ω_{TMS}^0	Larmor frequency of spins in $Si(CH_3)_4$ in units of radians per second
ω', ω''	chemical shift frequencies
$\omega_{\alpha\alpha}$, $\omega_{\alpha\beta}\ldots$	energy eigenvalues for a weakly coupled spin-1/2 pair
ω_x, ω_y, ω_z	Cartesian components of the magnetic field, expressed as frequencies (e.g. $\omega_x = -\gamma B_x$)
Ω	signed) frequency relative to spectrometer reference (=resonance offset frequency) in units of radians per second
$\Omega/2\pi$	signed) frequency relative to spectrometer reference (=frequency coordinate in spectrum) in units of hertz
Ω^0	Larmor frequency relative to spectrometer reference (=resonance offset frequency) in units of radians per second
$\Omega^0/2\pi$	Larmor frequency relative to spectrometer reference (=resonance offset frequency = frequency coordinate of spectral peak) in units of hertz
Ω_1	frequency coordinate of a two-dimensional spectrum (in the indirectly detected dimension)
Ω_2	frequency coordinate of a two-dimensional spectrum (in the directly detected dimension)
Ω_Δ	difference in chemical shift frequencies
Ω_Σ	sum of chemical shift frequencies
Ω_ℓ	rotating-frame frequency of a spectral peak
$\Omega_\ell^{(1)}$	frequency coordinate of a two-dimensional peak in the Ω_1 dimension
$\Omega_\ell^{(2)}$	frequency coordinate of a two-dimensional peak in the Ω_2 dimension
Ω_{guess}	guessed frequency of NMR signal
Ω_1^0, $\Omega_2^0\ldots$	resonance offset frequencies of spins I_1, $I_2\ldots$

$\Omega_j^0, \Omega_k^0 \ldots$	resonance offset frequencies of spins $I_j, I_k \ldots$
$\Omega^0(1)$	resonance offset frequency in the t_1 interval
$\Omega^0(2)$	resonance offset frequency in the t_2 interval
Ω_A^0, Ω_B^0	resonance offset frequency of a spin in two different chemical species, A and B
$\overline{\Omega}$	mean resonance offset frequency of a spin in a chemically exchanging molecule
$\Omega_{\alpha\alpha}, \Omega_{\alpha\beta} \ldots$	eigenvalues of the rotating-frame Hamiltonian, for a weakly coupled spin-1/2 pair
Ω_{rs}	rotating-frame frequency of coherence ρ_{rs}
$\Omega_{\boxed{-\alpha}}, \Omega_{\boxed{-\beta}} \ldots$	rotating-frame precession frequencies of coherences in an ensemble of spin-1/2 pairs
$\Omega_{\boxed{+-\alpha}}$	frequency of a coherence $\rho_{\boxed{+-\alpha}}$ in an ensemble of three-spin-1/2 systems
$\Omega_{\boxed{-\alpha+\beta-}}$	frequency of a coherence $\rho_{\boxed{-\alpha+\beta-}}$ in an ensemble of five-spin-1/2 systems
$\Omega_{\boxed{\alpha--\alpha}}, \Omega_{\boxed{\alpha--\beta}} \ldots$	frequencies of (−2)-quantum coherences in an ensemble of four-spin systems
Ω^{BA}	set of Euler angles $\{\alpha^{BA}, \beta^{BA}, \gamma^{BA}\}$ that may be used to transform the reference axes of frame A into those of frame B
Ω_{AB}	passive notation for the Euler angle set Ω^{BA}
x	spatial coordinate; in addition, used to indicate an r.f. phase $\phi = 0$
$\overline{x}$	indicates an r.f. phase $\phi = \pi$
x_Ω	position in space corresponding to a resonance offset Ω, in the presence of a field gradient G_x
x_{Ω_1}	position in space corresponding to a resonance offset Ω_1, in the presence of a field gradient G_x
$\hat{x}$	operator for multiplication by the coordinate x
$\lvert + x\rangle$	spin-1/2 state with angular momentum $+1/2$ along the x-axis
$\lvert - x\rangle$	spin-1/2 state with angular momentum $-1/2$ along the x-axis
$\mathbf{X}$	matrix with columns given by the eigenvectors of $\mathbf{A}$
$\mathbf{X}_z$	matrix with columns given by the eigenvectors of $\mathbf{L}_z$
$\mathbf{X}_{\boxed{-}}$	matrix with columns given by the eigenvectors of $\mathbf{L}_{\boxed{-}}$
χ	magnetic susceptibility
χ_{nuc}	nuclear contribution to the magnetic susceptibility
ξ	angle appearing in the theory of the AB system
y	spatial coordinate; in addition, used to indicate an r.f. phase $\phi = \pi/2$
$\overline{y}$	indicates an r.f. phase $\phi = 3\pi/2$
$\lvert + y\rangle$	spin-1/2 state with angular momentum $+1/2$ along the y-axis
$\lvert - y\rangle$	spin-1/2 state with angular momentum $-1/2$ along the y-axis
$Y_{2m}(\theta, \phi)$	second-rank spherical harmonic
$\psi(x, t)$	one-dimensional particle wavefunction
$\psi_n(x)$	one of a set of continuous orthonormal functions of x
$\lvert\psi\rangle$	Dirac notation ('ket-psi') for an arbitrary spin state, or the spatial wavefunction $\psi(x, t)$
$\langle\psi\rvert$	Dirac notation ('bra-psi') for the adjoint of $\lvert\psi\rangle$
$\lvert\psi\rangle_{①}, \lvert\psi\rangle_{②} \ldots$	spin states at time points ①, ② …
$\lvert\psi_{full}\rangle$	complete wavefunction of the sample
$\lvert\psi_{spin}\rangle$	quantum state of the nuclear spins
Ψ	additional r.f. phase shift in States procedure
z	spatial coordinate, usually in the direction of the main magnetic field

z_{Ω_2}	position in space corresponding to a resonance offset Ω_2, in the presence of a field gradient G_z
Z	atomic number = nuclear charge/e
$\mathfrak{Z}$	coherence transfer amplitude
$\mathbb{Z}$	vector of Zeeman orders in a two-spin-1/2 system
$\mathbb{Z}_{\text{eq}}$	vector of thermal equilibrium Zeeman orders in a two-spin-1/2 system
$\otimes$	direct product
$\langle m\|n\rangle$	Dirac bracket of $\langle m\|$ and $\|n\rangle$
$\left[\widehat{A}, \widehat{B}\right]$	commutator $\widehat{A}\widehat{B} - \widehat{B}\widehat{A}$
$\xrightarrow{(\pi/2)_x}$	propagation under a $(\pi/2)_x$ pulse
$\xrightarrow{\pi J_{12}\tau}$	propagation under the J-coupling between spins I_1 and I_2 over an interval τ
$\xrightarrow{\pi_x}$	propagation under a π_x pulse
$\xrightarrow{\Omega_1^0\tau}$	propagation under the chemical shift of spin I_1 over an interval τ
$\xrightarrow{\Omega_2^0\tau}$	propagation under the chemical shift of spin I_2 over an interval τ
$\xrightarrow{\text{SES}}$	propagation under a spin echo sandwich
$[\text{A}]_{\text{eq}}$	equilibrium concentration of chemical species A
$\langle\widehat{Q}\rangle$	expectation value of the operator $\widehat{Q}$
$\circlearrowleft$	cyclic commutation

Answers to the Exercises

Chapter 1

1.1 (i) Might possibly be correct. The total number of nucleons is odd, so the ground-state spin is a half-integer. More cannot be said using the simple rules for spin. In fact, the ground-state spin is $I = 1/2$, so the statement is correct.

(ii) Cannot be correct. The numbers of protons and neutrons are both even, so the ground-state spin must be $I = 0$.

(iii) Might possibly be correct. The total number of nucleons is odd, so the ground-state spin must be a half-integer. In fact, the ground-state spin is $I = 5/2$.

(iv) Must be correct. The numbers of protons and neutrons are both even, so the ground-state spin is $I = 0$.

(v) Cannot be correct. The numbers of protons and neutrons are both odd, so the ground-state spin must be an integer larger than zero. In fact, $I = 5$.

1.2 1, 2, 3 or 4.

Chapter 2

2.1 The field and magnetization trajectories are as follows:

Spin Dynamics: Basics of Nuclear Magnetic Resonance, Second Edition Malcolm H. Levitt

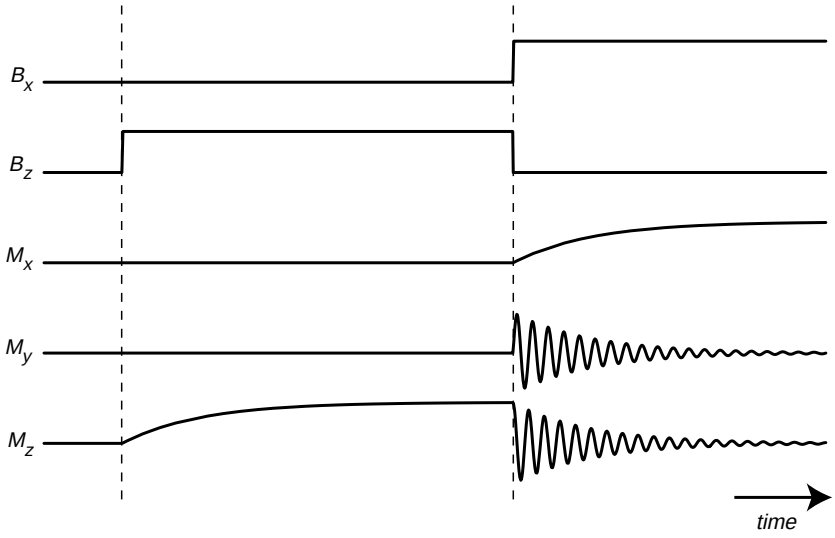

Chapter 3

3.1 (i) The ^{1}H spectrum contains a doublet with a splitting of around 7 Hz on the right-hand side of the spectrum (low δ) and a quartet with a splitting of around 7 Hz on the left-hand side of the spectrum (high δ). The integrated intensity of the doublet is three times more than that of the quartet.

(ii) The ^{13}C spectrum contains a doublet with a splitting of around 135 Hz on the left-hand side of the spectrum (high δ) and a quartet with a splitting of around 135 Hz on the right-hand side of the spectrum (low δ). The quartet and the doublet have approximately the same integrated intensity. When viewed with high resolution, each component of the doublet displays a quartet fine structure, and each peak of the quartet displays a doublet fine structure.

(iii) In the presence of proton decoupling, the ^{13}C spectrum takes the form of two narrow peaks. A close inspection should reveal two very small 'satellites' on each side of both peaks, due to the rare isotopomers with two ^{13}C nuclei in each molecule.

3.2 The isotopomers, their relative proportions, and their ^{1}H-decoupled ^{13}C spectra are as follows:

(i) Isotopomer I: $(^{12}CH_3)_2{}^{12}CO$. Abundance = 21.6%. No ^{13}C spectrum.

(ii) Isotopomer II: $^{13}CH_3{}^{12}CH_3{}^{12}CO$. Abundance = 28.8%. A single peak at low δ (right-hand side of the spectrum).

(iii) Isotopomer III: $(^{12}CH_3)_2{}^{13}CO$. Abundance = 14.4%. A single peak at high δ (left-hand side of the spectrum).

(iv) Isotopomer IV: $^{13}CH_3{}^{12}CH_3{}^{13}CO$. Abundance = 19.2%. A doublet at high δ, and another doublet at low δ.

(v) Isotopomer V: $(^{13}CH_3)_2{}^{12}CO$. Abundance = 9.6%. A single peak at low δ.

(vi) Isotopomer VI: $(^{13}CH_3)_2{}^{13}CO$. Abundance = 6.4%. A triplet at high δ, and a doublet with twice the integrated intensity at low δ.

The ^{1}H-decoupled ^{13}C spectrum, and the assignments of the peaks to the isotopomers, are as follows:

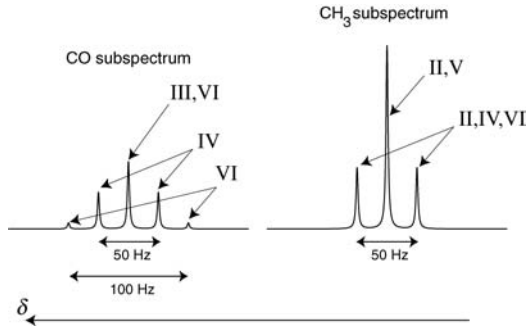

3.3 (i) $B^0 = 13.341\,\mathrm{T}$.

(ii) $\delta_{\mathrm{ref}} = 72.0\,\mathrm{ppm}$.

Chapter 5

5.1 The horizontal axes show frequency $\Omega/2\pi$ in units of hertz:

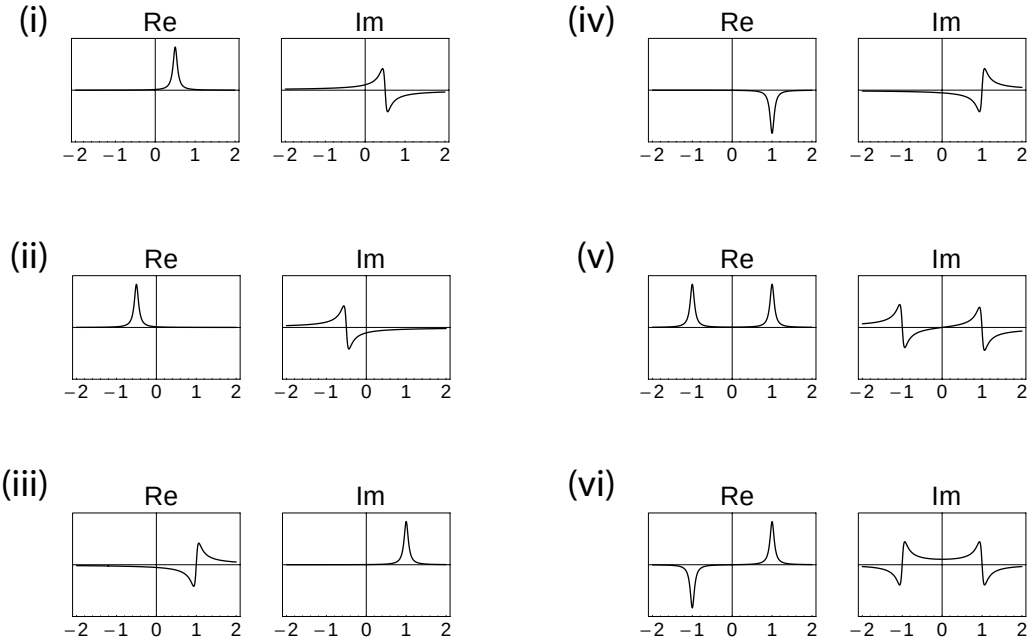

5.2 Running for 2 h at 40 °C with a delay of 5 s between transients gives a signal-to-noise ratio that is a factor of $\sqrt{4/3}$ better than running for 3 h at 20 °C with a delay of 10 s between transients.

Chapter 6

6.1 (iii) $N = 4 \times 5^{-1/2}$.

6.3 $\left[\hat{x}, \widehat{D}_x^2\right] = -2\widehat{D}_x$

6.6 (i) Suppose that the operator $\widehat{A}$ is hermitian, and that $|a\rangle$ is an eigenvector of $\widehat{A}$ with eigenvalue a, i.e.

$$\widehat{A}|a\rangle = a|a\rangle \tag{1}$$

The adjoint of both sides gives

$$\langle a|\widehat{A}^\dagger = a^*\langle a|$$

Since $\widehat{A}$ is hermitian, we can write $\widehat{A}^\dagger = \widehat{A}$, and multiplying with $|a\rangle$ from the right gives

$$\langle a|\widehat{A}|a\rangle = a^*\langle a|a\rangle$$

Similarly, multiplying Equation (1) from the left with $\langle a|$ gives

$$\langle a|\widehat{A}|a\rangle = a\langle a|a\rangle$$

The two last equations may be subtracted from each other to give

$$(a - a^*)\langle a|a\rangle = 0$$

It follows that the eigenvalue a is real, except in the pathological (and trivial) case where $|a\rangle$ is a vector of zeros, so that $\langle a|a\rangle = 0$.

(ii) Suppose that $|1\rangle$ and $|2\rangle$ are eigenvectors of the hermitian operator $\widehat{A}$ with eigenvalues a_1 and a_2 respectively, i.e.

$$\begin{aligned}\widehat{A}|1\rangle &= a_1|1\rangle \\ \widehat{A}|2\rangle &= a_2|2\rangle\end{aligned} \tag{2}$$

The adjoint of the second equation in Equation (2) gives

$$\langle 2|\widehat{A}^\dagger = {a_2}^*\langle 2|$$

and hence

$$\langle 2|\widehat{A} = a_2\langle 2|$$

using the hermiticity of $\widehat{A}$ and the fact that α_2 is real. Multiplying with $|1\rangle$ from the right gives

$$\langle 2|\widehat{A}|1\rangle = a_2\langle 2|1\rangle$$

Similarly, multiplying the first equation in Equation (2) with $\langle 2|$ from the left gives

$$\langle 2|\widehat{A}|1\rangle = a_1\langle 2|1\rangle$$

Subtracting the last two equations from each other gives

$$(a_2 - a_1)\langle 2|1\rangle = 0 \tag{3}$$

If the eigenvalues a_1 and a_2 are different (non-degenerate case), then the bracketed term is non-zero. In this case, Equation (3) may only be satisfied if $\langle 2|1\rangle = 0$, which proves the orthogonality of $|1\rangle$ and $|2\rangle$. If, on the other hand, the eigenvalues a_1 and a_2 are the same (degenerate case), then (Equation (3)) is satisfied even if $\langle 2|1\rangle$ is non-zero. The eigenvectors may be non-orthogonal in this case.

Chapter 7

7.1 (i)

$$\begin{aligned}\left[2\hat{I}_{1x}\hat{I}_{2y}, 2\hat{I}_{1x}\hat{I}_{2z}\right] &= \mathrm{i}\hat{I}_{2x}\\ \left[\hat{I}_{2x}, 2\hat{I}_{1x}\hat{I}_{2y}\right] &= \mathrm{i}2\hat{I}_{1x}\hat{I}_{2z}\\ \left[2\hat{I}_{1x}\hat{I}_{2z}, \hat{I}_{2x}\right] &= \mathrm{i}2\hat{I}_{1x}\hat{I}_{2y}\end{aligned}$$

(ii)

$$\exp\{-\mathrm{i}\theta 2\hat{I}_{1x}\hat{I}_{2y}\}2\hat{I}_{1x}\hat{I}_{2z}\exp\{+\mathrm{i}\theta 2\hat{I}_{1x}\hat{I}_{2y}\} = 2\hat{I}_{1x}\hat{I}_{2z}\cos\theta + \hat{I}_{2x}\sin\theta$$

(iii)

$$\exp\{-\mathrm{i}\theta 2\hat{I}_{1x}\hat{I}_{2y}\}\hat{I}_{2x}\exp\{+\mathrm{i}\theta 2\hat{I}_{1x}\hat{I}_{2y}\} = \hat{I}_{2x}\cos\theta - 2\hat{I}_{1x}\hat{I}_{2z}\sin\theta$$

7.2 (i) The state $\psi_1(x)$ in Equation 6.1 is an eigenstate of $\widehat{D}_x^2$ with eigenvalue $-\pi^2$ (see Equation 6.24). The probability of obtaining the value $-\pi^2$, therefore, is given by

$$\mathrm{P}(-\pi^2) = |\langle 1|f\rangle|^2$$

This evaluates to

$$|\langle 1|f\rangle|^2 = \left(\frac{5}{3}\sqrt{\frac{2}{7}}\right)^2 = \frac{50}{63} = 0.794$$

using the expansion coefficient given in Equation 6.8.

(ii) The state $\psi_3(x)$ in Equation 6.1 is an eigenstate of $\widehat{D}_x^2$ with eigenvalue $-9\pi^2$ (see Equation 6.24). The probability of obtaining the value $-9\pi^2$, therefore, is given by

$$\mathrm{P}(-9\pi^2) = |\langle 3|f\rangle|^2 = \frac{25}{126} = 0.198$$

(iii) The probability of obtaining the value 2 is exactly zero, since 2.0 is not an eigenvalue of $\widehat{D}_x^2$.

(iv) The average of many observations tends to the expectation value of $\widehat{D}_x^2$ for particles in state $|f\rangle$, which is given by

$$\langle f|\widehat{D}_x^2|f\rangle = \int_0^1 \mathrm{d}x f(x)^* \widehat{D}_x^2 f(x) = -\frac{25}{9}\pi^2$$

7.3 One way to prove this is as follows (the dots are only intended to clarify the working, and have no meaning):

$$\begin{aligned}\widehat{R}_x(\pi/2)\widehat{R}_y(\pi)\widehat{R}_x(\pi/2) &= \widehat{R}_x(\pi/2)\widehat{R}_y(\pi)\widehat{R}_x(\pi/2)\cdot\widehat{1}\\ &= \widehat{R}_x(\pi/2)\widehat{R}_y(\pi)\widehat{R}_x(\pi/2)\cdot\widehat{R}_y(-\pi)\widehat{R}_y(\pi)\\ &= \widehat{R}_x(\pi/2)\cdot\widehat{R}_y(\pi)\widehat{R}_x(\pi/2)\widehat{R}_y(-\pi)\cdot\widehat{R}_y(\pi)\\ &= \widehat{R}_x(\pi/2)\cdot\widehat{R}_x(-\pi/2)\cdot\widehat{R}_y(\pi)\\ &= \widehat{1}\cdot\widehat{R}_y(\pi)\\ &= \widehat{R}_y(\pi)\end{aligned}$$

The crucial step in the proof uses the sandwich relationship in Equation 7.15.

7.4 The matrix representations for spin-5/2 operators, in the basis $|I, M\rangle = \{|5/2, +5/2\rangle, |5/2, +3/2\rangle, |5/2, +1/2\rangle, |5/2, -1/2\rangle, |5/2, -3/2\rangle, |5/2, -5/2\rangle\}$ are as follows:

$$\hat{I}^{+} = \begin{pmatrix} 0 & \sqrt{5} & 0 & 0 & 0 & 0 \\ 0 & 0 & 2\sqrt{2} & 0 & 0 & 0 \\ 0 & 0 & 0 & 3 & 0 & 0 \\ 0 & 0 & 0 & 0 & 2\sqrt{2} & 0 \\ 0 & 0 & 0 & 0 & 0 & \sqrt{5} \\ 0 & 0 & 0 & 0 & 0 & 0 \end{pmatrix}$$

$$\hat{I}^{-} = \begin{pmatrix} 0 & 0 & 0 & 0 & 0 & 0 \\ \sqrt{5} & 0 & 0 & 0 & 0 & 0 \\ 0 & 2\sqrt{2} & 0 & 0 & 0 & 0 \\ 0 & 0 & 3 & 0 & 0 & 0 \\ 0 & 0 & 0 & 2\sqrt{2} & 0 & 0 \\ 0 & 0 & 0 & 0 & \sqrt{5} & 0 \end{pmatrix}$$

$$\hat{I}_y = \frac{1}{2\mathrm{i}} \begin{pmatrix} 0 & \sqrt{5} & 0 & 0 & 0 & 0 \\ -\sqrt{5} & 0 & 2\sqrt{2} & 0 & 0 & 0 \\ 0 & -2\sqrt{2} & 0 & 3 & 0 & 0 \\ 0 & 0 & -3 & 0 & 2\sqrt{2} & 0 \\ 0 & 0 & 0 & -2\sqrt{2} & 0 & \sqrt{5} \\ 0 & 0 & 0 & 0 & -\sqrt{5} & 0 \end{pmatrix}$$

$$\hat{I}_z = \begin{pmatrix} \frac{5}{2} & 0 & 0 & 0 & 0 & 0 \\ 0 & \frac{3}{2} & 0 & 0 & 0 & 0 \\ 0 & 0 & \frac{1}{2} & 0 & 0 & 0 \\ 0 & 0 & 0 & -\frac{1}{2} & 0 & 0 \\ 0 & 0 & 0 & 0 & -\frac{3}{2} & 0 \\ 0 & 0 & 0 & 0 & 0 & -\frac{5}{2} \end{pmatrix}$$

Chapter 8

8.1 (i) $B^0 = 1.174\,\mathrm{T}$; (ii) $\omega_{\mathrm{nut}}/2\pi = 21.29\,\mathrm{kHz}$; (iii) $\omega_{\mathrm{nut}}/2\pi = 17.38\,\mathrm{kHz}$; (iv) $B^0 = 11.593\,\mathrm{T}$; (v) $\omega_{\mathrm{nut}}/2\pi = 2.15\,\mathrm{kHz}$; (vi) $\omega_{\mathrm{nut}}/2\pi = 1.76\,\mathrm{kHz}$.

Chapter 9

9.1 (i) $b_{12}/2\pi = -15.012\,\mathrm{kHz}$; (ii) $b_{13}/2\pi = -15.012\,\mathrm{kHz}$; (iii) $d_{12}/2\pi = +7.506\,\mathrm{kHz}$; (iv) $d_{12}/2\pi = -9.382\,\mathrm{kHz}$; (v) $d_{12}/2\pi = -3.753\,\mathrm{kHz}$; $d_{13}/2\pi = -13.504\,\mathrm{kHz}$; $d_{23}/2\pi = +5.997\,\mathrm{kHz}$.

9.2 (ii) $d_{jk} = \int_0^\pi \mathrm{d}\Theta_{jk}\, \mathrm{p}(\Theta_{jk})\, b_{jk} \dfrac{1}{2}(3\cos^2\Theta_{jk} - 1)\, \sin\Theta_{jk} = 2b_{jk}/155$. If $r = 0.3\,\mathrm{nm}$, then $d_{jk}/2\pi = -57.4\,\mathrm{Hz}$.

Chapter 10

10.1 (i) The eigenvalue is $+\frac{1}{2}$. (ii) The state may be represented as an arrow in the zy plane subtending an angle θ with the z-axis. (iii) The required pulse has flip angle $(\pi/2 - \theta)$ and phase π.

10.2 (i) $\omega_{\mathrm{nut}}/2\pi = 10\,\mathrm{kHz}$. (ii) $25\,\mu\mathrm{s}$; (iii) π.

10.3 (i) $|\beta\rangle$.

(ii) $-1/2$.

10.4 (i) $\dfrac{1}{2}\begin{pmatrix} 1+\mathrm{i} \\ -1+\mathrm{i} \end{pmatrix}$.

(ii) $+1/2$.

10.5 $\tau_{\mathrm{p}} = 35.35\,\mu\mathrm{s}$.

Chapter 11

11.1 (i) $14.68\,\mathrm{T}$; (ii) $-625.1\,\mathrm{MHz}$; (iii) 12.6×10^{-6}.

11.2 (i) π; $-\mathbf{e}_z$.

(ii) $-0.309\mathbf{e}_y - 0.951\mathbf{e}_z$; 18°.

(iii) $-\mathbf{e}_z$.

(iv) $0.048\mathbf{e}_x - 0.008\mathbf{e}_y - 0.999\mathbf{e}_z$; 2.8°.

(v) See R. Freeman, *Spin Choreography. Basic Steps in High Resolution NMR*, Spektrum, Oxford, 1997.

Chapter 12

12.1 Peak 1: $T_1 \cong 2\,\mathrm{s}$; peak 2: $T_1 \cong 5\,\mathrm{s}$.

12.2 The signal phases are as follows:
(i) zero (the spin echo sequence refocuses the phase).
(ii) $-\gamma\Delta B x_0/v$
(iii) $\gamma\Delta B\tau + \gamma\Delta B x_0/v$
(iv) zero (the spin echo sequence refocuses the phase).

Chapter 13

13.1 A spin I has $2I+1$ energy levels, with M running from $-I$ to $+I$ in integer steps. There are, therefore, $I+\frac{1}{2}$ levels with positive M running from $+1/2$ to $+I$ in integer steps. The mean value of M for all positive-M levels, therefore, is $\frac{1}{2}(I+\frac{1}{2})$. This should be compared with the value of $1/2$ when no saturation is applied. The central-transition enhancement factor on satellite saturation, therefore, is $I+\frac{1}{2}$.

13.2 From Equation 7.30 the matrix element of $\hat{I}^+$ across the central transition is $\sqrt{I(I+1)-(\frac{1}{2})(-\frac{1}{2})} = I+\frac{1}{2}$. The central transition nutation enhancement on selective excitation, therefore, is $I+\frac{1}{2}$ (again!).

13.3 The matrix representation of a $(\pi/2)_x$ pulse is given in Section 7.9.1, and is equal to

$$\widehat{R}_x(\pi/2) = \frac{1}{2}\begin{pmatrix} 1 & -\mathrm{i}\sqrt{2} & -1 \\ -\mathrm{i}\sqrt{2} & 0 & -\mathrm{i}\sqrt{2} \\ -1 & -\mathrm{i}\sqrt{2} & 1 \end{pmatrix}$$

Matrix multiplications as in Equation 13.27 give

$$\widehat{R}_x(\pi/2)\begin{pmatrix} 0 & 0 & 0 \\ 1 & 0 & -1 \\ 0 & 0 & 0 \end{pmatrix}\widehat{R}_x(\pi/2)^\dagger = \mathrm{i}\sqrt{2}\begin{pmatrix} 1 & 0 & -1 \\ 0 & 0 & 0 \\ 1 & 0 & -1 \end{pmatrix}$$

$$\widehat{R}_x(\pi/2)\begin{pmatrix} 0 & -1 & 0 \\ 0 & 0 & 0 \\ 0 & 1 & 0 \end{pmatrix}\widehat{R}_x(\pi/2)^\dagger = \mathrm{i}\sqrt{2}\begin{pmatrix} 1 & 0 & 1 \\ 0 & 0 & 0 \\ -1 & 0 & -1 \end{pmatrix} \quad (4)$$

It follows that double-quantum coherences are excited, with amplitudes proportional to $2\mathrm{i}(\exp\{\mathrm{i}\frac{1}{4}\omega_{\mathrm{Q}}^{(1)}\tau\} - \exp\{-\mathrm{i}\frac{1}{4}\omega_{\mathrm{Q}}^{(1)}\tau\}) = \sin\frac{1}{4}\omega_{\mathrm{Q}}^{(1)}\tau$.

13.4 A nine-peak multiplet with intensities in the ratio 9:16:21:24:25:24:21:16:9.

Chapter 14

14.1 (i) 10.8 G corresponds to 1.08×10^{-3} T. This may be multiplied by the proton gyromagnetic ratio of 267.5×10^6 rad s^{-1} T^{-1} to obtain 288×10^3rad s^{-1} = 45.98 kHz.

(ii) The splitting between the strong 'perpendicular' peaks in the Pake doublet is $|3b/2|$, where b is the dipole–dipole coupling constant. Hence $|b/2\pi| = \frac{2}{3} \times 45.98\,\text{kHz} = 30.66\,\text{kHz}$. Solution of $|b| = (\mu_0/4\pi)\gamma^2\hbar r^{-3} = 2\pi \times 30.66 \times 10^3\,\text{rad}\,\text{s}^{-1}$ gives $r = 158\,\text{pm}$.

Chapter 15

15.1 (i)

$$\hat{\rho} = \frac{1}{4}\begin{pmatrix} 1 & 1 & 1 & 1 \\ 1 & 1 & 1 & 1 \\ 1 & 1 & 1 & 1 \\ 1 & 1 & 1 & 1 \end{pmatrix}$$

(ii)

$$\hat{\rho} = \begin{pmatrix} C^4 & C^3S & C^3S & C^2S^2 \\ C^3S & C^2S^2 & C^2S^2 & C^3S \\ C^3S & C^2S^2 & C^2S^2 & C^3S \\ C^2S^2 & CS^3 & CS^3 & S^4 \end{pmatrix}$$

where $C = \cos(\beta/2)$ and $S = \sin(\beta/2)$.

(iii)

$$\hat{\rho} = \begin{pmatrix} 1 - \frac{1}{2}\beta^2 & \frac{1}{2}\beta & \frac{1}{2}\beta & \frac{1}{4}\beta^2 \\ \frac{1}{2}\beta & \frac{1}{4}\beta^2 & \frac{1}{4}\beta^2 & 0 \\ \frac{1}{2}\beta & \frac{1}{4}\beta^2 & \frac{1}{4}\beta^2 & 0 \\ \frac{1}{4}\beta^2 & 0 & 0 & 0 \end{pmatrix}$$

Single-quantum coherences that share a state with the original population are excited to first order in β. Multiple-quantum coherences are excited to second order in β.

Chapter 16

16.1 (i) $\hat{\rho} = -\hat{I}_y \cos\Omega_S^0 t_1 - \left(2\hat{I}_x\hat{S}_x \cos\Omega_S^0\tau + 2\hat{I}_x\hat{S}_y \sin\Omega_S^0\tau\right)\sin\Omega_S^0 t_1$;
(iii) change the phase of the first pulse to $-y$.

16.2 (i)

$$\begin{aligned}\hat{\rho}_{④} = &-\hat{I}_{1x}\cos\Omega_1^0 t_1 \cos\pi J t_1 + 2\hat{I}_{1z}\hat{I}_{2y}\cos\Omega_1^0 t_1 \sin\pi J t_1 \\ &-\hat{I}_{1z}\sin\Omega_1^0 t_1 \cos\pi J t_1 - 2\hat{I}_{1x}\hat{I}_{2y}\sin\Omega_1^0 t_1 \sin\pi J t_1\end{aligned}$$

(ii) For a general value of t_1, all coherence orders $-2, -1, 0, 1$ and 2 are excited at time point ④.

(iii)

$$\hat{\rho}^{\cos}_{⑤} = -2\hat{I}_{1y}\hat{I}_{2z}\frac{1}{4}\left(\cos(\Omega_1^0 + \pi J)t_1 - \cos(\Omega_1^0 - \pi J)t_1\right)$$
$$-2\hat{I}_{1z}\hat{I}_{2y}\frac{1}{4}\left(\cos(\Omega_1^0 + \pi J)t_1 - \cos(\Omega_1^0 - \pi J)t_1\right)$$

(iv)

$$\hat{\rho}^{\sin}_{⑤} = -2\hat{I}_{1y}\hat{I}_{2z}\frac{1}{4}\left(\sin(\Omega_1^0 + \pi J)t_1 - \sin(\Omega_1^0 - \pi J)t_1\right)$$
$$-2\hat{I}_{1z}\hat{I}_{2y}\frac{1}{4}\left(\sin(\Omega_1^0 + \pi J)t_1 - \sin(\Omega_1^0 - \pi J)t_1\right)$$

(v) Both the diagonal-peak multiplets and the cross-peak multiplets are in antiphase absorption. Another advantage of 2QF-COSY is that signals from non-coupled spins-1/2 are suppressed, as in the INADEQUATE experiment. One drawback of 2QF-COSY is that one half of the signal amplitude is lost, compared with ordinary COSY.

Chapter 17

17.1 (i) Chemically and magnetically equivalent; (ii) chemically and magnetically inequivalent; (iii) chemically equivalent but magnetically inequivalent.

17.2 (i) A_2; (ii) AB; (iii) ABX; (iv) AA′BB′; (v) ABMX; (vi) AA′BB′X.

Chapter 18

18.1 (i) The final spin density operator is $\hat{\rho}_{⑤} \sim -\hat{S}_y \sin\theta + \ldots$. The optimal flip angle is $\theta = \pi/2$. The maximum signal enhancement is γ_I/γ_S.

(ii) The final spin density operator is $\hat{\rho}_{⑤} \sim -\hat{S}_y \sin 2\theta + \ldots$. The optimal flip angle is $\theta = \pi/4$. The maximum signal enhancement is γ_I/γ_S.

(iii) The final spin density operator is $\hat{\rho}_{⑤} \sim -3\hat{S}_y \cos^2\theta \sin\theta + \ldots$. The optimal flip angle is $\theta = \arccos\sqrt{2/3}$. The maximum signal enhancement is $1.15\gamma_I/\gamma_S$. Note that these results resemble those obtained for INEPT, but with the dependence on the pulse sequence delay τ replaced by a dependence on the flip angle θ.

Chapter 19

19.1 (i) $B^0 = 7.08\,\mathrm{T}$.

(ii) $B^0 = 17.8\,\mathrm{T}$.

(iii) $T = 283.5\,\text{K}$.

(iv) Between around $T = 210\,\text{K}$ and $280\,\text{K}$.

(v) Around $T = 660\,\text{K}$.

Chapter 20

20.1 (i) The plots of T_1 and T_2 against field are as follows:

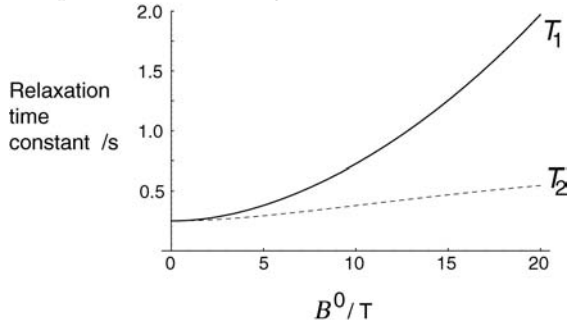

T_1 increases with field, since spin–lattice relaxation requires spectral density at the Larmor frequency ω^0 (and also twice the Larmor frequency). Spin–lattice relaxation is less effective at high field since the spectral density function decays with respect to frequency, and the Larmor frequency is higher at high field. Transverse relaxation, on the other hand, involves spectral densities at a selection of frequencies, including zero. The zero-frequency contribution to the transverse relaxation is field independent. As a result, the transverse relaxation time constant is relatively insensitive to field. (This applies to the case of homonuclear dipole–dipole relaxation, but not necessarily to other relaxation mechanisms, such as those involving the CSA).

(ii) The plots of R_{cross} and $R^{\text{T}}_{\text{cross}}$ against field are as follows:

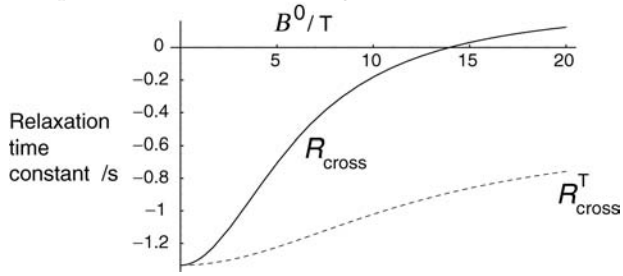

The ROESY experiment is expected to be superior at high field, since the transverse cross-relaxation rate constant remains large (and negative). The longitudinal cross-relaxation rate constant, involved in the NOESY experiment, becomes small (and positive) at high field.

Index

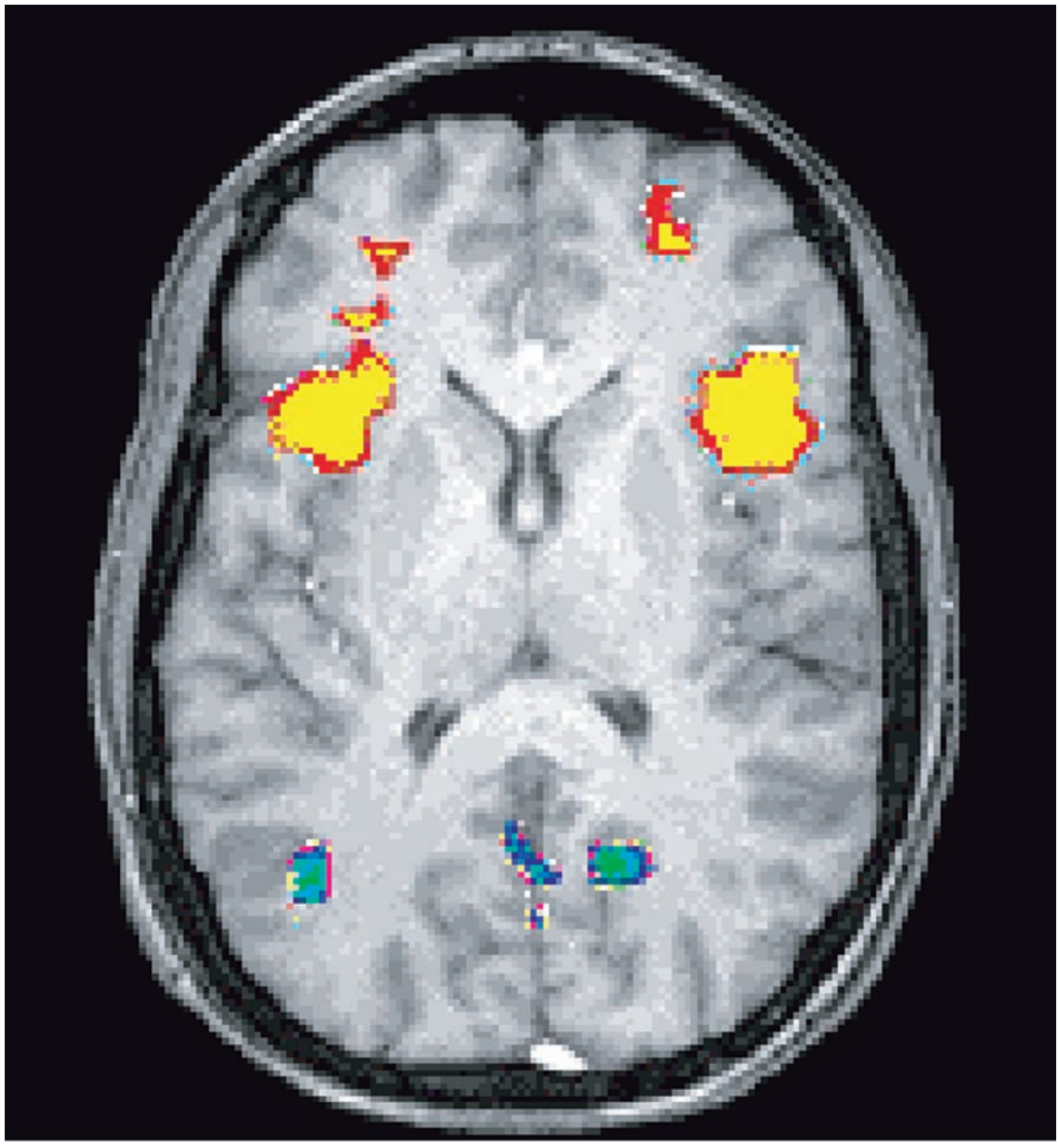

Plate 1 A functional NMR image. The grey image is a cross-section through the head of a person (the person may be thought of as lying down on their back, feet towards you). The grey-scale image shows the lobes of the brain. The yellow and red patches show activation of the prefrontal cortex after a face is removed from view, detected as small differences in the NMR signals. The blue patches denote diminished activation of these regions of the brain, under the same task. (From S. M. Courtney, L. G. Underleider, K. Keil and J. V. Haxby, *Nature* **386**, 608–611 (1997). Copyright, Macmillan Publishers Ltd.)

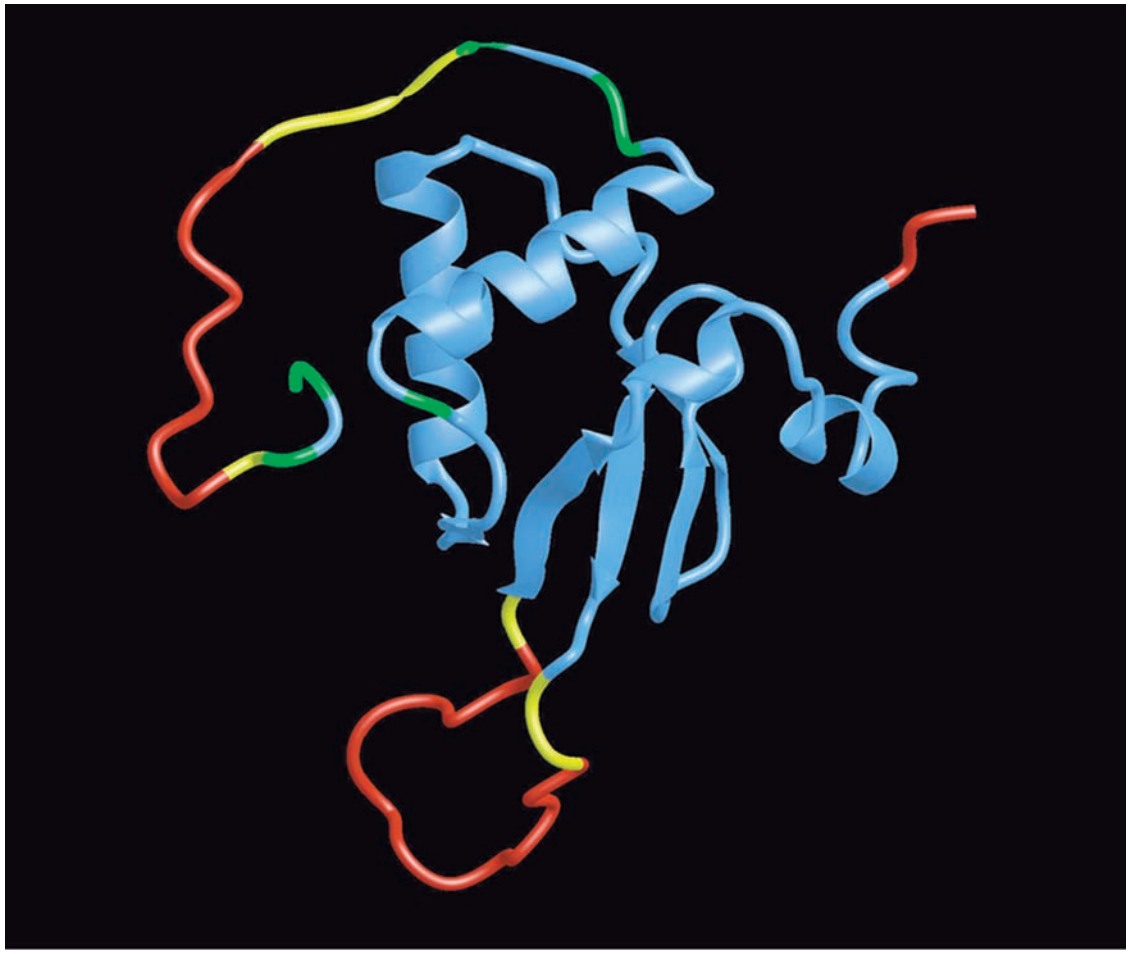

Plate 2 Backbone structure of a protein molecule in solution (residues 55–206 of the HIV-1 Nef protein), as determined by NMR. The structure is colour encoded to display the mobilities of different parts of the molecule, as revealed by ^{1}H–^{15}N NOE values (see Chapter 20). Blue: least mobile; red: most mobile. The N-terminal tail that anchors the protein to the membrane is disordered and not shown. (For details, see S. Grzesiek, A. Bax, J. Hu, J. Kaufman, I. Palmer, S. J. Stahl, N. Tjandra, and P. T. Wingfield, *Protein Science*, **6**, 1248–1263 (1997)). Thanks to Ad Bax for supplying this figure.

Plate 3 Three-dimensional NMR image of a human head, with layers of tissue computationally peeled off so that the brain is partially visible. The yellow spot shows the approximate location of neuronal activity in response to a sound. This spot was not obtained by functional NMR imaging, but by magnetoencephalography (analysis of the weak magnetic fields generated by electrical currents in the brain). The illustration was prepared by Mr Eero Salli. Thanks to Professor Hannu Aronen, Department of Radiology, and Dr Risto Ilmoniemi, BioMag Laboratory, Helsinki University Central Hospital, Finland, for permission to use this image.

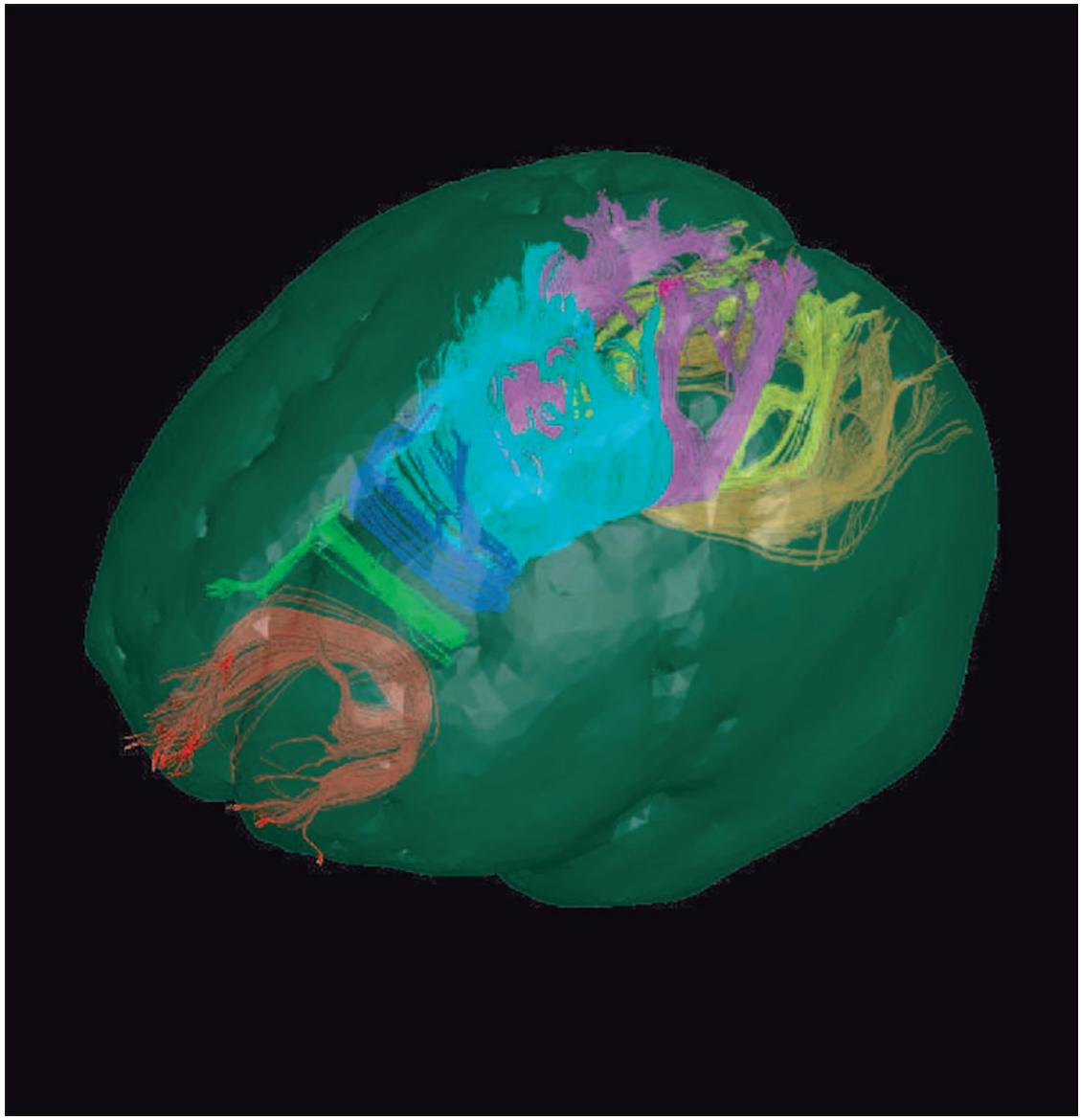

Plate 4 A three-dimensional rendering of the neural pathways connecting the two hemispheres of the human brain. These pathways were delineated using diffusion tensor MRI. The different colours indicate tracks connecting distinct brain regions. This figure was supplied by Roland Henry and SungWon Chung, Department of Radiology, University of California, San Francisco, USA.

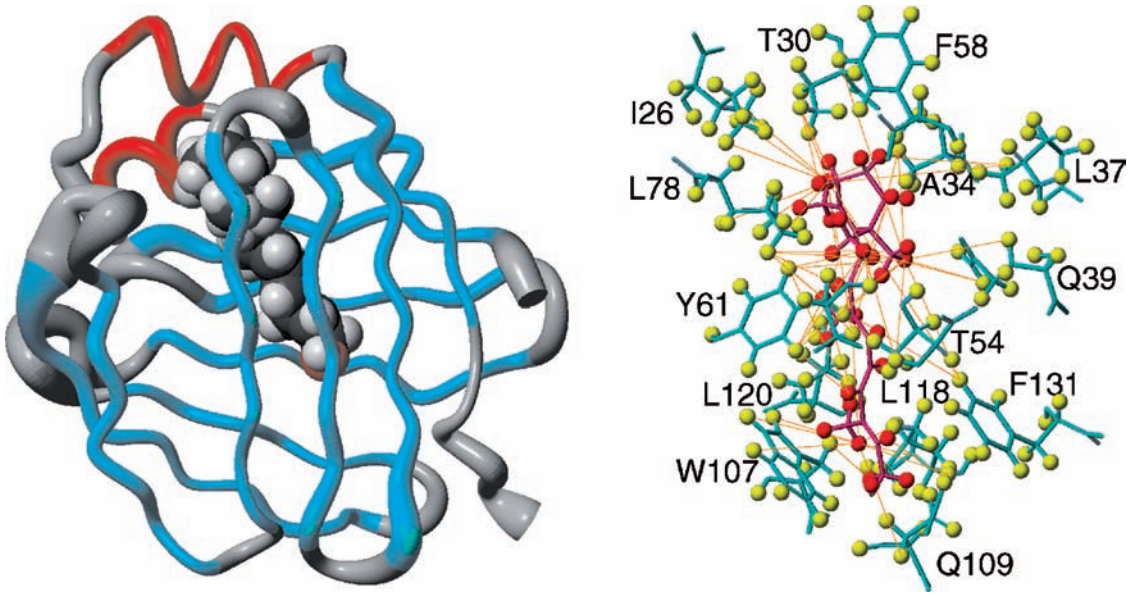

Plate 5 Experimental solution-state structure of a protein, solved by using NOESY distance constraints. The molecule is a 15 kDa protein called cellular retinol binding protein II. The structure was solved using a combination of double-quantum-filtered COSY, NOESY and TOCSY experiments, including three-dimensional combinations of these techniques. The final structure was derived employing 3980 NOESY distance constraints and displays a 10-stranded β-barrel motif. **(a)** The protein backbone, depicted as a sausage, enclosing the retinol ligand (space-filling model). **(b)** The retinol binding site and the retinol ligand (red). The NOESY distance constraints involving the protein protons (yellow) and the ligand protons are shown by lines. For full details, see J. Lu, C.-L. Lin, C. Tang, J. W. Ponder, J. L. F. Kao, D. P. Cistola; and E. Li, *J. Mol. Biol.*, **286**, 1179–1195 (1999) and the same authors in *J. Mol. Biol.*, **300**, 619–632 (2000). Thanks to J. Lu for preparing this figure.

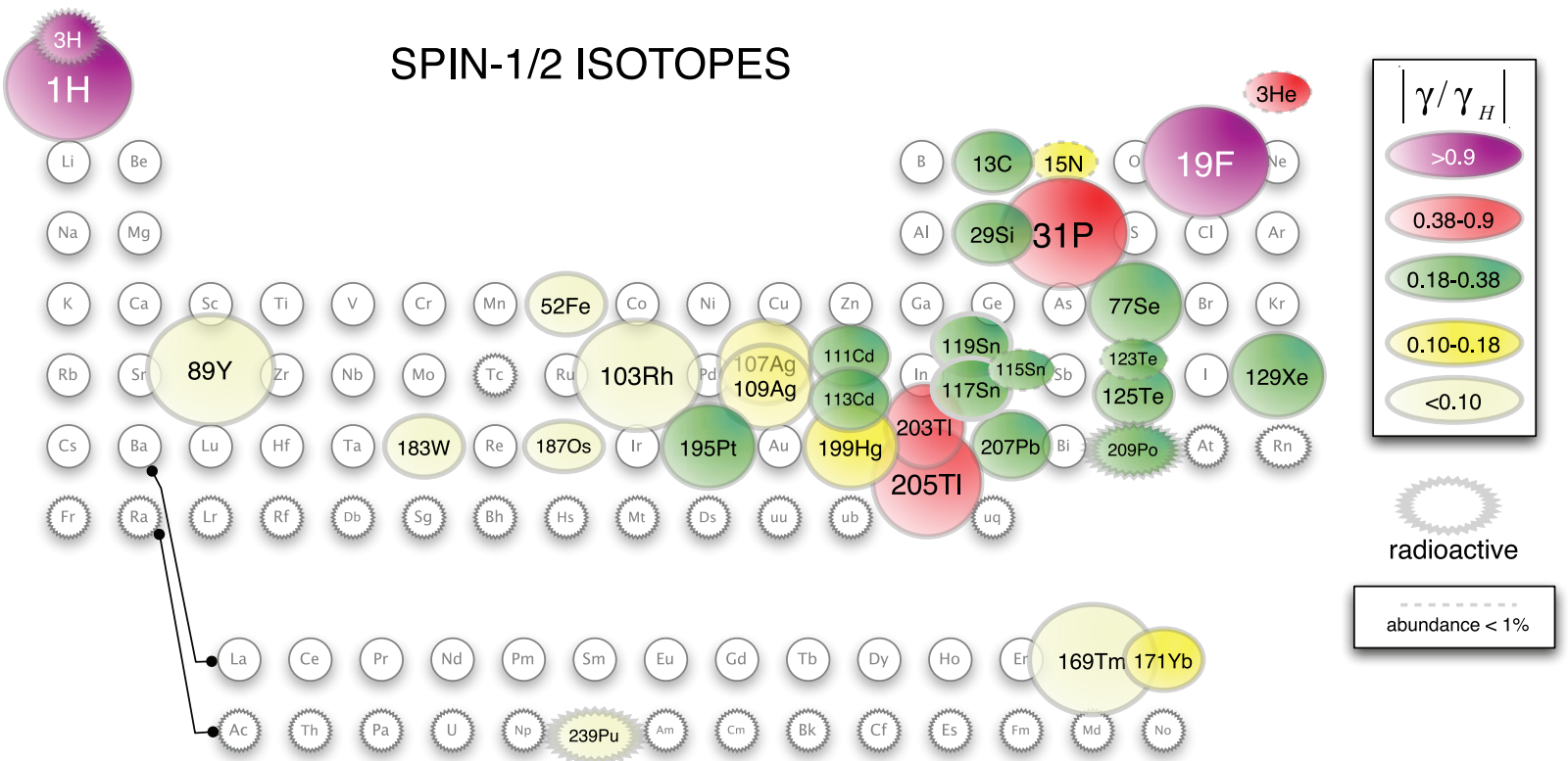

Plate A Distribution of spins-1/2 in the periodic table. In this and the following plates, the colours indicate the magnitude of the gyromagnetic ratio γ, relative to that of ^{1}H (see inset). The sizes of the symbols are related to the natural abundance of the isotopes, with a dotted border indicating a natural abundance of less than 1%.

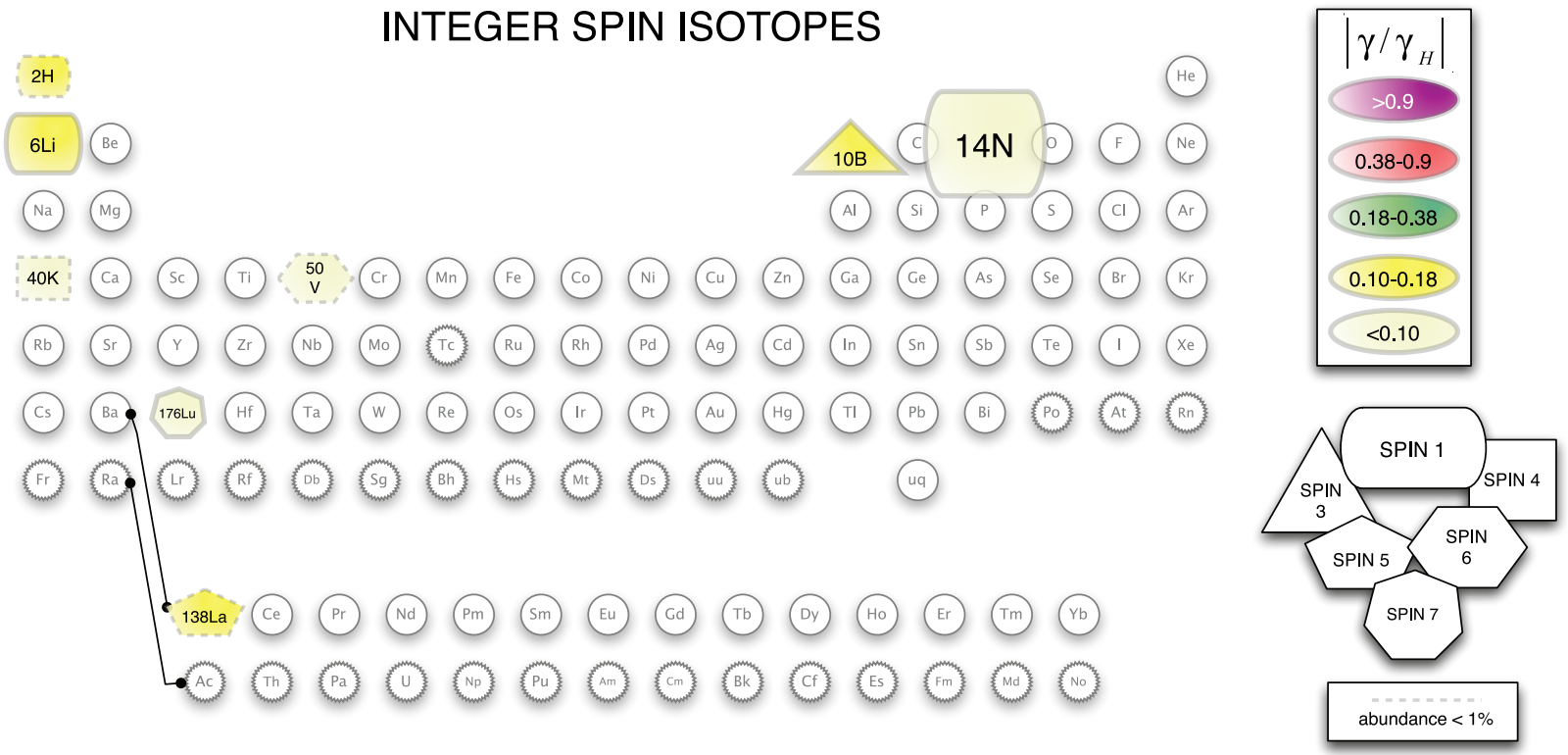

Plate B Distribution of integer spins in the periodic table. The symbol shape indicates the spin quantum number (see inset).

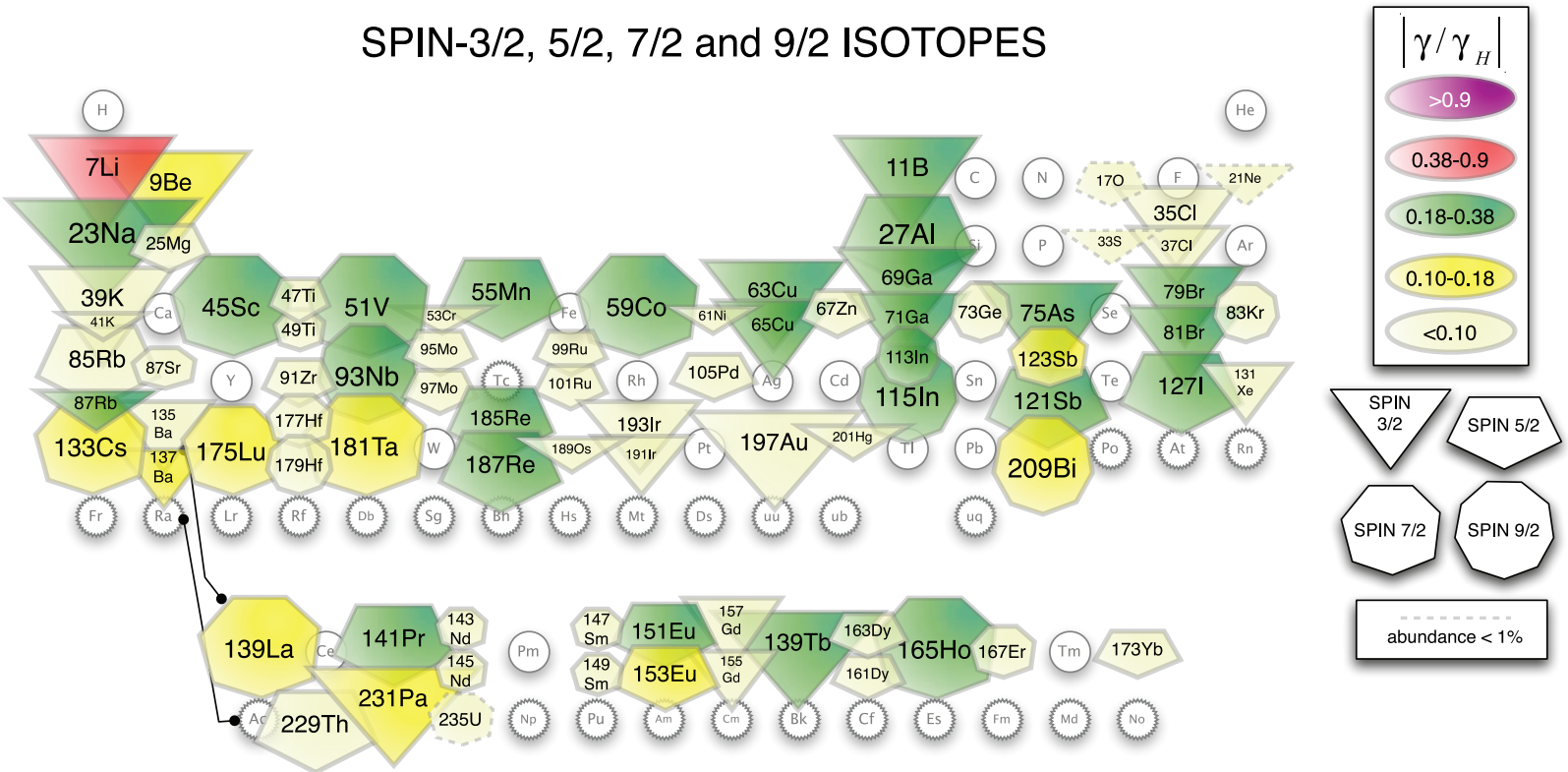

Plate C Distribution of half-integer spins with $I > 1$. The symbol shape indicates the spin quantum number (see inset).